UNIVERSITY OF BIRMINGHAM

TOWARDS A GENERALISATION OF THE RELATIONSHIP BETWEEN NOCTURNAL SURFACE AND CANOPY URBAN HEAT ISLANDS USING URBAN METEOROLOGICAL NETWORK

by

JIALI FENG

A thesis submitted to The University of Birmingham for the degree of

DOCTOR OF PHILOSOPHY

School of Geography, Earth and Environmental Sciences

The University of Birmingham, UK

September 2020

Abstract

The Urban Heat Island (UHI) as a result of urbanisation processes remains a compelling focus of urban climate research. With the advance of thermal remote sensing, surface urban heat island ($sUHI$) quantified by the land surface temperature from satellite observations becomes more prevalent in studying the UHI effects. The difference and the physical linkage between $sUHI$ and urban canopy air heat island ($aUHI$) measured by Urban Meteorological Network (UMN) intrigue the whole urban climate community. The complicated relationship between the intensity of $sUHI$ ($sUHII$) and $aUHI$ ($aUHII$) across cities limits the application of the thermal remote sensing in urban environment. This thesis explores the relationship between nocturnal $sUHII$ and $aUHII$ (the $sUHII$- $aUHII$ relationship) by applying a transferable method, using MODIS satellite and UMN in Oklahoma City, US and Birmingham, UK. Specific patterns of the $sUHII$- $aUHII$ relationship under different seasons, wind speed conditions and land characteristics are found in both cities. The comparisons between the two cities highlight the strong controls of the local climate and the configurations of the UMN on the differences of the $sUHII$- $aUHII$ relationship across cities, which are considerable factors in order to generalise this relationship globally.

Acknowledgements

There are a number of thanks due as I finish this thesis. I would like to express my gratitude to my supervisors: Dr. Xiaoming Cai and Professor Lee Chapman. They have been helpful and supportive of my research during the past four years. The weekly meeting with Xiaoming was an unforgettable experience for me to work more efficiently with plans. It was a pleasure to have monthly meeting with my supervisors to discuss my progress and exchange ideas with them. Their valuable feedbacks always kept me on track. The hands-off nature of their supervisions allows me to become a more mature independent researcher.

I would like to take this opportunity to thank all the reviewers contributed to the papers arising from this thesis. I have learnt a lot from them. Thanks is also due to my colleagues in office 412. I will never forget the days we spent in the office to work and play together. There are numerous others, too many to list, that I owe thanks to.

Finally, many thanks to my parents for supporting me to pursue my dream in the University of Birmingham. My husband Hanqin, thank you so much to stay with me and encourage me during this PhD!

Thanks to you all.

Publications arising from thesis

***Feng, J.L.**, Cai, X.M. and Chapman, L., 2019. Impact of atmospheric conditions and levels of urbanization on the relationship between nocturnal surface and urban canopy heat islands. Quarterly Journal of the Royal Meteorological Society, 145(724), pp.3284-3299. https://doi.org/10.1002/qj.3619.*

***Feng, J.L.**, Cai, X.M. and Chapman, L., 2020. A tale of two cities: The influence of urban meteorological network design on the nocturnal surface versus canopy heat island relationship in Oklahoma City, US and Birmingham, UK. International Journal of Climatology. https://doi.org/10.1002/joc.6697 (In press).*

Contents

List of Figures

Chapter 1:

Chapter 2:

Chapter 3:

Chapter 4:

Chapter 5:

List of Tables

Chapter 5:

List of Abbreviations

above ground level	a.g.l
Analysis of Covariance	ANCOVA
Air Temperature	T_a
Birmingham	BHAM
Boundary layer heat island	UHI_{UBL}
Birmingham Urban Climate Laboratory	BUCL
Canopy air Heat Island	$aUHI$
Canopy air Heat Island Intensity	$aUHII$
Central Business District	CBD
Correlation Coefficient	r
Coefficient of Determination	R^2
Dry Adiabatic Lapse Rate	DALR
Gradient Richardson Number	Ri
Kolmogorov-Smirnov	K-S
Inversed Distance Weighted	IDW
Local Climate Zone	LCZ
Low-level Jet	LLJ
Moderate Resolution Imaging Spectroradiometer	MODIS
Normalised Difference Vegetation Index	NDVI
Oklahoma City	OKC
Oklahoma Micronet	OKCNET
One-way Analysis of Variance	ANOVA
Principal Component Analysis	PCA
Pasquill-Gifford	P-G

Radiative transfer equation	RTE
Surface energy balance	SEB
Subsurface heat island	UHI_{Sub}
Surface Layer	SL
Satellite-sensed Land Surface Temperature	T_s
Surface Urban Heat Island	$sUHI$
Surface Urban Heat Island Intensity	$sUHII$
Thermal infrared	TIR
Urban Boundary Layer	UBL
Urban Canopy Layer	UCL
Urban Climate Zone	UCZ
Urban Heat Island	UHI
Urban Heat Island Intensity	UHII
Urban Meteorological Network	UMN
World Meteorological Organization	WMO

Chapter 1 Introduction

1.1 Research background

Over the past 200 years or so, the industrial revolution has continued to alter the surface properties of urban areas by the urbanisation process (Collier, 2006). It has been reported that the world's population living in urban areas has increased from around 2.5 billions in 1950 to 7.8 billion in 2002, which could be potentially reach 8.5 billions by 2030 (United Nations and Social Affairs, 2015). This rapid urbanisation process is inevitably influencing the urban weather and climate with potential impacts on human lives (Jin and Shepherd, 2005).

Urbanisation processes mainly impact upon the physical processes and dynamical structure particularly in the atmospheric surface layer that is roughly the lowest 10% of the atmospheric boundary layer (ABL), defined as the lowest part of atmosphere with the Earth's surface (Oke, 2002b). The complex structures and surface characteristics contribute to the different climate in urban environments, and as such, the atmosphere directly influenced by urban areas has its unique structure and is commonly called the urban boundary layer (UBL). One of the most well documented phenomena resulting from modifications to the urban climate is the Urban Heat Island (UHI) effect. The UHI is considered as an increasingly significant issue for inhabitants in cities where urban

temperatures become elevated as a result of anthropogenic modification of the atmospheric environment by urbanisation and industrialisation (Oke and Fuggle, 1972, Roth et al., 1989, Ren et al., 2011, Parlow et al., 2014).

A range of consequences for social economy, health and meteorology have been found to be associated with the intensification of UHI, such as atmospheric stability, modification of precipitation processes, air pollution dispersion, human comfort and morbidity and mortality (Oke, 2002a). However, its impacts can be either negative or positive, particular to the socio-economic and health aspects (Unger, 2004). This is largely due to the complicate urban environments that increase the diversity and uncertainties of the UHI effects in different cities. Correspondingly, recent research has developed strategies in order to utilise or mitigate its adverse effects (e.g. implementation of urban green infrastructure (Kong et al., 2014, Cavan et al., 2014)). It remains indispensable to gain further insight into the UHI by a more comprehensive understanding of the underlying physical processes in the UBL.

The scientific literature typically classifies the UHI into (i) canopy air urban heat island ($aUHI$), (ii) surface urban heat island ($sUHI$), (iii) boundary layer heat island (UHI_{UBL}) and subsurface heat island (UHI_{Sub}) (Oke, 1995). These four types of UHI have different their own physical representations as a result of different observational methods. The magnitude/intensity of $aUHI$ ($aUHII$) is quantified as the difference of the screen-level (usually 2 m above ground level) air temperature (T_a) between urban and rural (reference) stations. The $aUHII$ is of greater importance than the other measures of UHI because of its better representation of thermal comfort sensed by human, in close relationship with disease transmission and health risk (Koken et al., 2003, Tomlinson et al., 2011b). However, with the continual advances and development of satellite

techniques, research related to $sUHI$ commonly derived from satellite-sensed land surface temperature (T_s) has rapidly increased. The key advantage of using satellites over other methods is the spatial continuity of the data with relative high-spatial resolution (Anniballe et al., 2014). In contrast, the high-spatial resolution T_a data have historically been less available. This is largely because of the increased expense due to the requirement of observation apparatus regarding the configuration and maintenance of a dedicated urban weather station or, more recently, an urban meteorological network of stations (UMN) (Peng et al., 2011). The UHI_{UBL} is the difference of the air temperature above the UCL and that at similar altitude over the rural area. It is controlled by the energy balance at top of the roughness sublayer and the boundary layer. Temperature sensors mounted on aircraft, balloons or tall towers are needed to quantify the UHI_{UBL}. UHI_{Sub} is the difference of the temperature in the ground under the city and rural surface, generally measuring by the temperature sensors placed within the substrate. It is therefore driven by the subsurface energy balance differences between urban and rural (sub)surfaces. This thesis will only focus on the $aUHI$ and $sUHI$ which are the most commonly studied types in the scientific literature.

Table 1.1 adapted from Oke et al. (2017) describes the main differences between $aUHI$ and $sUHI$ that limit the application of the $sUHI$ as a surrogate of the $aUHI$. Specifically, urban surface is seen from a plan or bird's eye view from satellite. From this perspective, T_s (or the intensity of $sUHI$ [$sUHII$]) is estimated from the integrated radiance emitted from the surfaces that could be measured by satellite sensors. T_a (or $aUHII$) from the ground measurement is observed by a screen-measurement level; therefore, it largely depends on the processes within the urban canopy layer (a more comprehensive review regarding the $sUHI$ and $aUHI$ is provided in Chapter 2). Despite

significant scientific effort to study $sUHII$, three main questions (research gaps) regarding the application of T_s in urban environment raised by Roth et al. (1989) have not yet been fully solved, which includes:

(i) the explicit characteristics of the urban surface as viewed by thermal remote sensors;

(ii) the exact relationship between T_s and T_a in urban-atmosphere interface;

(iii) the relation between $sUHII$ and $aUHII$. These are the fundamental limitations of applying the thermal remote sensing in urban climate studies.

Along with these issues, the paucity of T_a data has proved to be the biggest limitations in studies investigating the relationship between $sUHII$ and $aUHII$ ($sUHII$-$aUHII$ relationship). However, a recent step-change in the availability of T_a data (thanks to an increase in UMNs now) means that there exists a new opportunity to extend previous investigations into the $sUHII$- $aUHII$ relationship and thus gain further knowledge of the physical interaction between surface and air atmosphere in urban climate research (Voogt and Oke, 2003). The whole analysis will focus on night-time period only. The reason for considering night-time period only is two-fold. Firstly, nocturnal UHI occurs more frequently than daytime UHI (Jauregui, 1997) and UHII was found to be higher than that during daytime (Kim and Baik, 2005, Lemonsu and Masson, 2002, Montávez et al., 2000, Kłysik and Fortuniak, 1999). Secondly, nocturnal UHII is not directly affected by solar radiation and the $sUHII$-$aUHII$ relationship becomes less complicated than the one at daytime. More importantly, better agreement between $sUHII$ and $aUHII$ has been found during night time by previous studies (Sun et al., 2015, Anniballe et al., 2014), providing more confidence to explore the nocturnal $sUHII$-$aUHII$ relationship. In this thesis, the recently available high-density UMNs in Oklahoma City, US (Oklahoma Micronet and

Mesonet network) (Basara et al., 2011) and Birmingham, UK (Birmingham Urban Climate Laboratory) (Warren et al., 2016) are used to explore the $sUHII$ - $aUHII$ relationship across cities, with considerations of different climate and configurations of UMN and the possibility of generalising this relationship globally. Overall, the newly available, high resolution, T_a data from UMNs provides the means to tackle the long-standing research gap that exists pertaining the relationship between T_s and T_a.

Table 1. 1 Summary of $sUHI$ and $aUHI$ in terms of their scale, causative thermal processes, observational method and the advantacges and disadvantages of the measurements (adapted from Oke et al. (2017)).

UHI Type	Scale	Processes	Measurement	Pros & Cons of the measurements
$sUHI$	Local	Surface energy balance	Satellite	• Spatial continuous data; • Free of charge • Lower temporal resolution
$aUHI$	Micro	Surface energy balance and energy balance of urban canopy layer air volume	Ground stations or UMN	• Limited number of stations • Uneven distribution • Large cost for configuration and maintenance • High temporal resolution

1.2 Study area

This thesis uses Birmingham, UK, and Oklahoma City (OKC), US, as case study areas, offering an opportunity to gain insights in two different environments. These two cities were primarily chosen due to the accessibility of UMN data that provides the opportunity for investigating the relationship between $sUHI$ and $aUHI$. Furthermore, these two cities offer a valuable chance to compare the $sUHII$-$aUHII$ relationship under various geographical and climatic background that plays an important role to the formation and development of UHI and will be further introduced as below.

Birmingham is the second largest city in UK with a population of about 1 million in 2011 (Birmingham City Council, 2013). It is a post-industrial city with an area of around 267.8 km^2 located on a fairly flat plateau in the West Midlands region of the UK (Figure 1.1). Birmingham is also the main city in the West Midlands conurbation that extends to approximately 901 km^2. General climate characteristics during the study period are summarised in Table 5.1. The climate type is humid subtropical with an annual mean temperature of around 9.10℃. The total amount of precipitation is about 660 mm with the mean relative humidity of 64%.

OKC (Figure 1.2) is one of the ten largest cities in the US and spans approximately 1610 km^2, with an estimated population of 562,343 2009. It is not a consolidated city where the urbanised area is around 630 km^2 embedded by a central business area of 20 km^2. OKC is situated at a reasonably high elevation with an average of 382 m on a flat plateau. According to Table 5.1, OKC belongs to the marine west coast climate with an average temperature of 20.54℃. Larger amount of total precipitation is recorded in OKC (928 mm) compared to Birmingham, but the RH is much lower in OKC (64%)

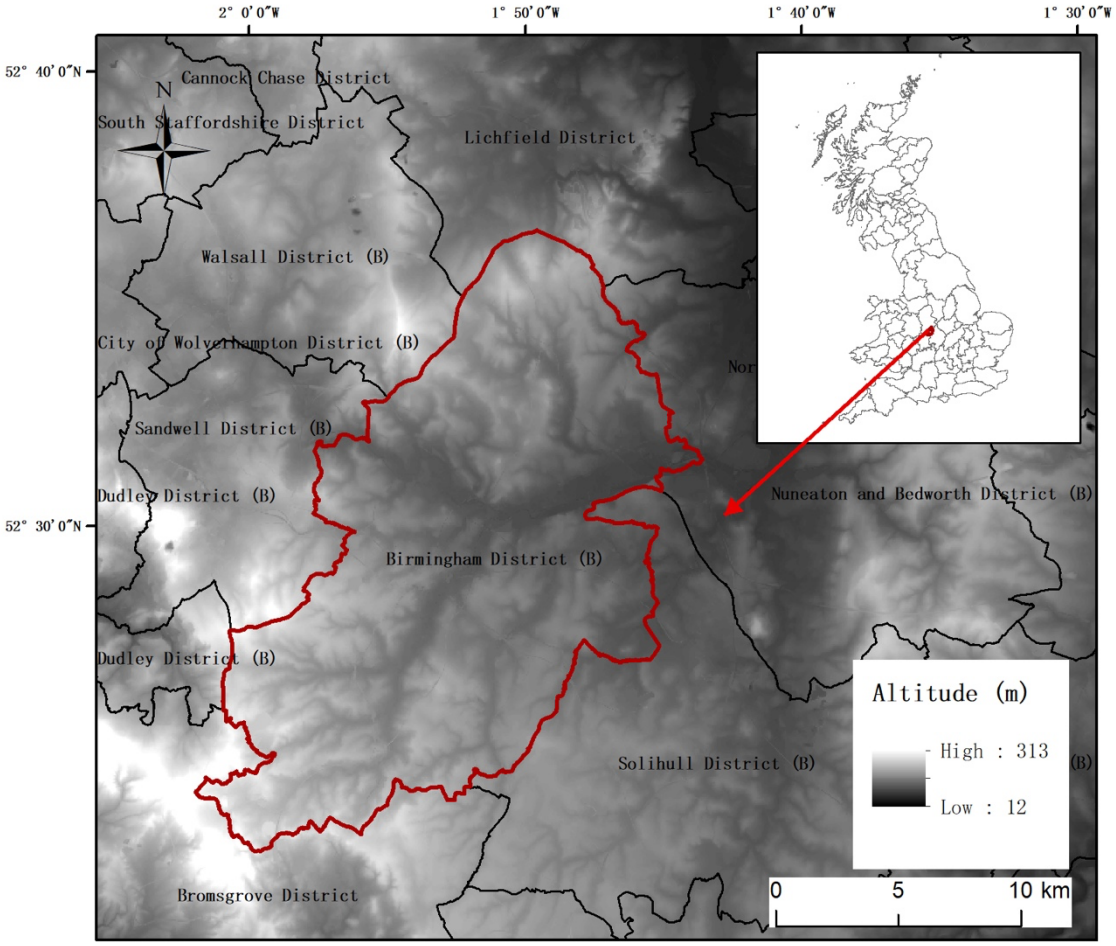

Figure 1. 1 Map of Birmingham within the UK with altitude information provided by Ordnance Survey (2014),

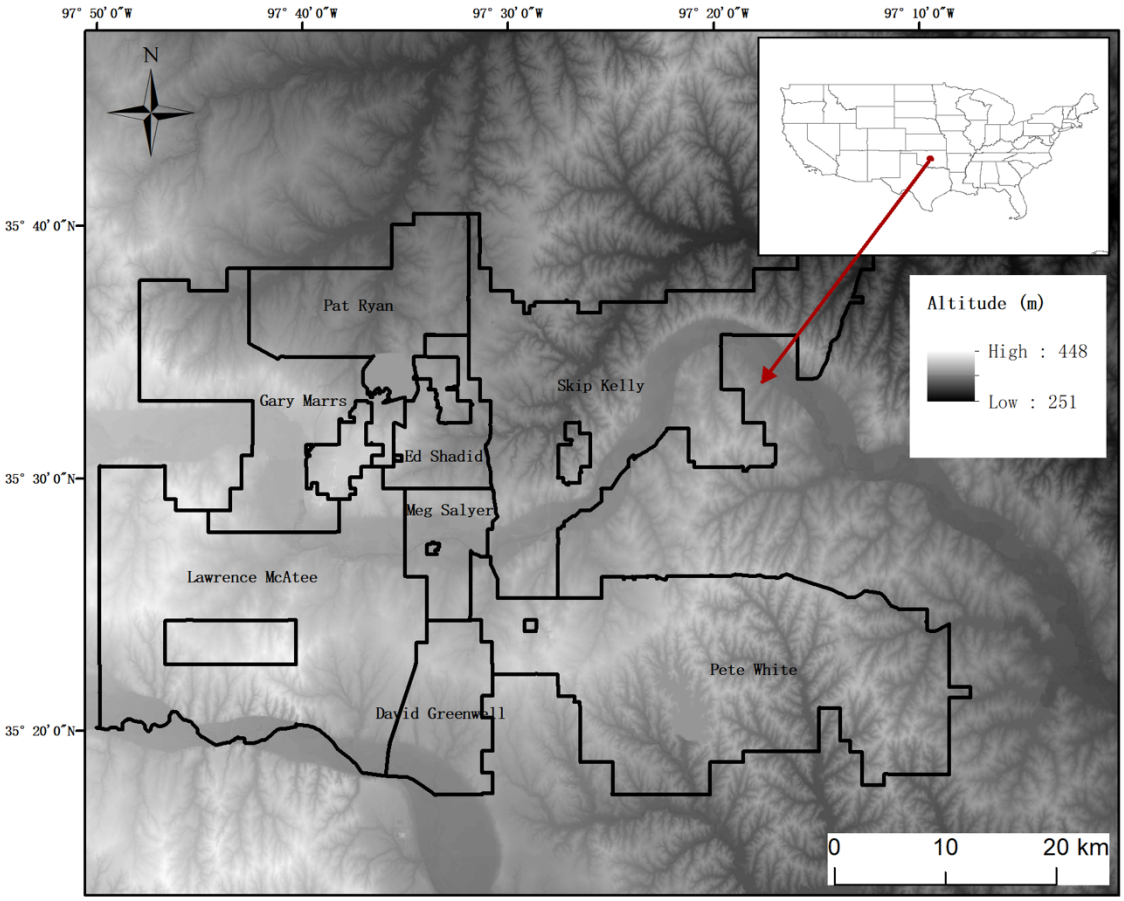

Figure 1. 2 Map of Oklahoma City within the USA with altitude information provided by Oklahoma City Council (2020).

1.3 Aim and objectives

Given the established research gaps and the newly available data in which to tackle it, the overall aim of this thesis is to investigate the relationship between nocturnal surface and urban canopy air heat island (the $sUHI$-$aUHI$ relationship) for individual cities and to examine the generalisation of the $sUHI$-$aUHI$ relationship across different cities. The aim of examining "generalisation" is mainly focused on comparing the outcome of the $sUHI$-$aUHI$ relationship from two different cities and identifying the conditions under which the relationship can be equally applied to the two cities. Specifically, the fulfilment of the aim is mainly based upon the following three steps. Firstly, the atmospheric variables that have significant impacts on both $sUHII$ and $aUHII$ need to be determined. Secondly, a method to quantify the $sUHII$-$aUHII$ relationship needs to be developed, and Birmingham is chosen as a case study to explore the characteristics of the $sUHII$-$aUHII$ relationship under certain meteorological conditions and the land surface characteristics. Thirdly, the method is applied to another city (OKC) under same conditions (meteorology and land surface characteristics) and then similarity or dissimilarity of the $sUHII$-$aUHII$ relationship across the two cities (Birmingham and OKC) will be carefully examined in order to seek the possibility of generalising the $sUHII$-$aUHII$ relationship and to further understand the impact of UMN configuration and local climate on the $sUHII$-$aUHII$ relationship.

In summary, there are four specific objectives that are consistent with the three steps discussed above for this thesis as below (note: detailed explanations regarding the four objectives are provided in Section 2.7):

(i) Investigate the atmospheric variables that have a strong link to the seasonal and spatial variations of nocturnal surface ($sUHII$) and urban canopy heat island intensity ($aUHII$) in OKC as a case study, which is achieved in Chapter 3.

(ii) Explore the effects of the atmospheric conditions and levels of urbanisation on the nocturnal $sUHI$-$aUHI$ relationship in Birmingham, UK in Chapter 4, to discover specific characteristics of this relationship with understanding of its corresponding physical processes, by developing a repeatable methodology that could be applied in another city (i.e. OKC).

(iii) Determine whether the specific characteristics discovered in (ii) are more broadly applicable and could be explained by the same physical processes in OKC in Chapter 5.

(iv) Discover the possibility of generalising the $sUHI$-$aUHI$ relationship by comparing it between OKC and Birmingham, with consideration of their local climate background and configurations of the UMNs in Chapter 5.

1.4 Structure of thesis

This introductory chapter has underlined the concepts and information related to research background for this thesis (Section 1.1), mainly incorporating types of UHI and the available observation methods: thermal remote sensing and urban meteorological network as well as primary differences between $aUHI$ and $sUHI$. This chapter is followed by the main literature review (Chapter 2) regarding the modelling of the nocturnal surface and canopy heat island which is relevant for the three main parts to this thesis (Chapters 3 - 5).

An illustrative framework (Figure 1.3) is provided to demonstrate how the four aims summarised in Section 1.3 to be achieved within the context of the thesis.

The response of the $sUHII$ and $aUHII$ to the atmospheric condition is firstly explored in OKC (Chapter 3). The atmospheric variables that have strong links to the UHI have been discovered. This chapter provides evidence regarding the consideration of the atmospheric condition in studying the nocturnal $sUHI$-$aUHI$ relationship. The atmospheric parameters used to represent the atmospheric condition are then considered, together with surface characteristics (levels of urbanisation) as key factors for building the nocturnal $sUHI$-$aUHI$ relationship in Birmingham (Chapter 4).

The repeatable methodology developed in Chapter 4 is then used for studying this relationship over OKC in Chapter 5. This enables comparisons of this relationship between OKC and Birmingham according to different climate background and settings / configurations of the UMNs.

The thesis concludes (Chapter 6) with a synthesis of the main chapters and critiques of the thesis alongside potential future perspectives.

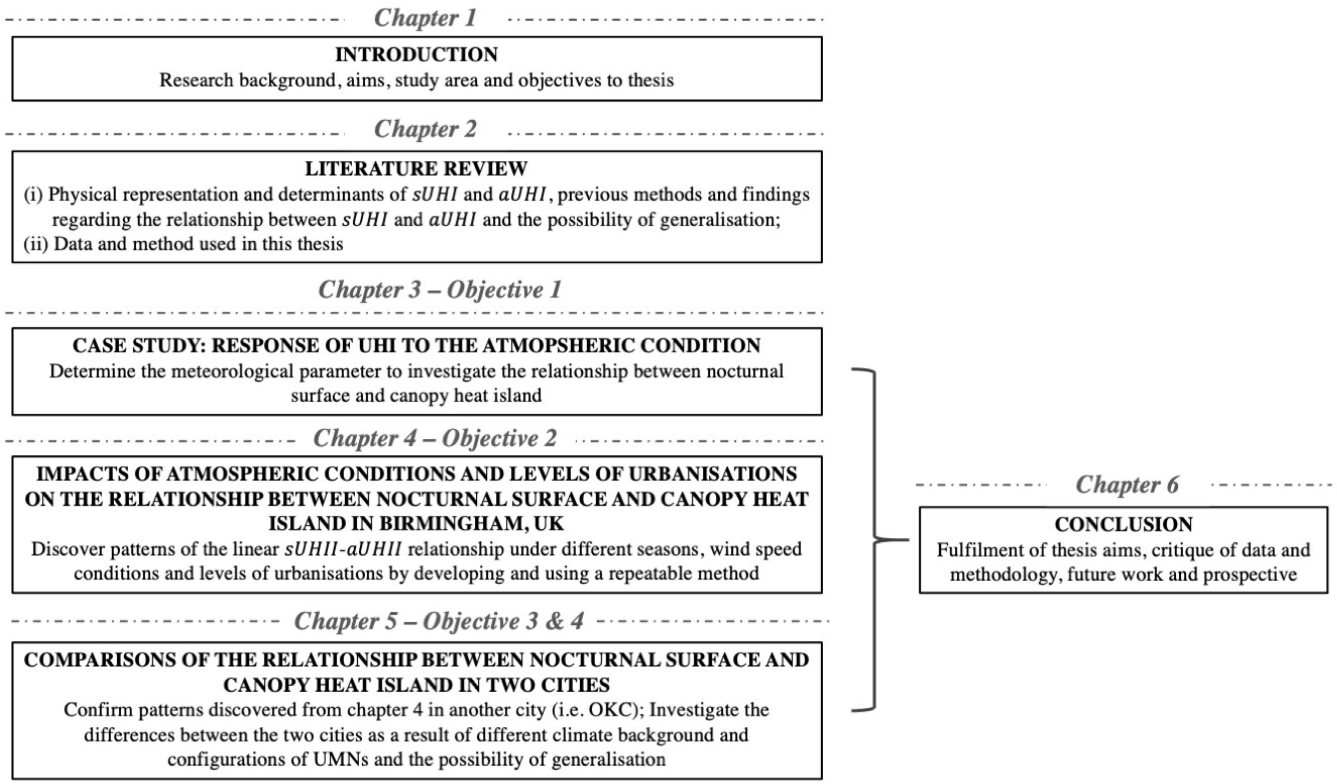

Figure 1. 3 Overview of thesis structure

Chapter 2 Literature review

This chapter offers a review on the physical processes and state-of-the-art of modelling of the relationship between surface and canopy air heat island during night-time, which are relevant for Chapters 3 - 5. The relationship between satellite-sensed land surface temperature and air temperature from ground observations are also discussed, which is strongly linked to the magnitude of urban heat island. At the end of this Chapter, the data and method used in this thesis are explicitly introduced. Please note that individual chapters (3 - 5) also offer short reviews of other relevant materials that are not fully covered by this Chapter.

2.1 Introduction

Traditionally, the intensity of UHI (UHII) is quantified by the urban-rural differences of the air temperature (T_a) observed from ground stations within the urban canopy layer (UCL) (i.e. $aUHII$, as introduced in Chapter 1). The advent of thermal remote sensing provides new avenues to observe the UHI by satellite instruments (i.e. $sUHI$, as introduced in Chapter 1) that could produce land surface temperature (T_s) with comparative high temporal resolution (e.g. four times daily from MODIS satellite). It is also a less costly way to acquire UHI information for any city when compared to the use of weather stations or indeed, an urban meteorological network (UMN) over urban areas.

T_s is connected with the T_a within the lowest parts of the urban atmosphere. This connection is of prime importance to urban climate (Gallo et al., 1995). Both T_s and T_a are the central meteorological parameters in modifying the surface energy balance (SEB) and therefore determine both $sUHII$ and $aUHII$ that affect the comfort of city dwellers (Arnfield, 2003). However, as discussed in Chapter 1, various physical mechanisms contributing to the dynamic of both $sUHII$ and $aUHII$ make it methodologically complicated to approximate the relation between the two parameters and therefore limit the application of satellite technology in the study of urban climatology (As a parameter, T_a has considerably more utility). It is expected that an increased exploration of the relationship between $sUHII$ and $aUHII$ (the $sUHII$-$aUHII$ relationship) will allow a better understanding of the surface-atmosphere interaction, and the application of satellite products, as well as the development of other temperature-related studies and applications such as numerical weather prediction, urban planning and management. Therefore, there remains a scientific need to better identify the causative factors influencing the spatial-

temporal patterns of both the $sUHI$ and $aUHI$ in order to develop a thorough understanding of their mechanisms and the relationship between them. In doing so, the satellite data could be more confidently used to as a surrogate to weather stations/UMNs for temperature-related studies in urban environment.

This review will firstly provide an introduction to $aUHI$ and $sUHI$, by emphasizing the SEB and influencing factors that largely control or affect their spatial or temporal characteristics. This is followed by the demonstrations of progresses that have been made in modelling the relationships between T_s and T_a (the T_s-T_a relationship) over different environments. It then reviews the progress made on the investigation of the $sUHII$-$aUHII$ relationship. It also makes comment on the modelling concerns and the possibility of generalisation of the $sUHII$-$aUHII$ relationship. Finally, informed by the literature review, the chapter concludes by introducing the data and methodology used in this project.

2.2 Surface energy balance and UHI

After sunset, UHI arises from the differences of the cooling rates between urban and rural areas that are inherently attributed to the alternation of SEB by urbanisations (Rizwan et al., 2008). The roles of T_s and T_a playing in the SEB provide the physical reasons for studying the T_s-T_a or $sUHII$-$aUHII$ relationships. Herein, this section will provide the general information of the surface energy balance and emphasize the roles of T_s or T_a in energy exchanges over urban and rural environment.

The surface radiant budget at any surface can be described as:

$$Q^* = K^* + L^* = K_\downarrow - K_\uparrow + L_\downarrow - L_\uparrow \qquad \text{Equation (2.1)}$$

where Q^*, K^* and L^* are the net allwave, shortwave and longwave radiation flux density (Wm^{-2}) with arrows of incoming (↓) and outgoing (↑) from surface, correspondingly. During night-time, there is no input of the solar radiation, therefore, the longwave radiative exchanges dominant in the surface radiant budget:

$$Q^* = L_{\downarrow} - L_{\uparrow} = L_{\downarrow} - [\varepsilon\sigma {T_0}^4 + (1-\varepsilon)L_{\downarrow}] \qquad \text{Equation (2.2)}$$

where ε is the average emissivity of surface (or emitting body) over longwave radiation bands, σ is the Stefan-Boltzmann constant ($\approx 5.67 \times 10^{-8}\ \mathrm{Wm}^{-2}\mathrm{K}^{-4}$), T_0 in Kelvin (K) is the absolute temperature of the surface. The ε indicates the radiative efficiency of the ground surface. The emitting body is a blackbody (a perfect emitter) if the ε equals to 1. However, most of the objects are imperfect emitters and emissivity values are spectrally dependent. Herein, the ε is assumed to be the average ε value over a suitable spectral range (i.e. longwave radiation bands herein). The $\varepsilon\sigma {T_0}^4$ therefore reflects the total energy flux density or emittance from the emitting body. The $(1-\varepsilon)L_{\downarrow}$ refers to the reflected longwave radiation that is primarily from the atmosphere during nights. Kirchhoff's law states that the emissivity of an object at a given wavelength equals its ability to absorb radiation at the same wavelength. Therefore, we could assume that the average emissivity value over the longwave radiation bands (ε) equals to the corresponding absorptivity (φ). Furthermore, the radiant energy conservation states that there are three fates of the radiation of a given wavelength when it encounters a medium: (1) absorbed by the medium determined by the absorptivity; (2) reflected by the medium determined by the reflectivity and (3) passing through the medium determined by the transmissivity. In general, the transmissivity of a solid and opaque surface is 0 and hence the reflectivity = 1 – absorptivity under the a given wavelength. Therefore, the reflected portion of the $L_{\downarrow}$

from ground surface over the longwave radiation bands can be estimated as $(1-\varepsilon)L_{\downarrow}$. T_s is estimated by the radiation emitted from ground surfaces by Stefan-Boltzmann law. It is evident that T_s is physically distinguished from T_0 with the latter close to the complete urban surface temperature that is the surface temperature considering the total active surface area and defined by Voogt and Oke (1997). As previously discussed, T_s is the estimated surface temperature taking into account the active surface sensed by the satellite. Thereby, to some extent, it still exerts controls on the surface radiant budget. As emissivity is between 0 – 1 (usually greater than 0.9 for land surfaces), the reflected longwave radiation (i.e. from atmosphere) is usually minor ($(1-\varepsilon)L_{\downarrow}$ from Equation 2.2) (Oke et al., 2017). According to the longwave radiation emitted from the atmosphere ($L_{\downarrow}$), researchers have attempted to estimate it from satellite instruments by applying empirical methods, e.g. by using temperature/humidity profile with cloud top heights (Darnell et al., 1986), relations to radiance from the top of the atmosphere in channels 4 and 5 of the AVHRR satellite (Meerkoetter and Grassl, 1984), or based on the relationship with surface meteorological parameters (i.e. relative humidity and ambient air temperature) (Masiri et al., 2017). However, the standard errors of the estimated $L_{\downarrow}$ are non-negligible (e.g. 10-25 W m^{-2} from the method proposed by Frouin et al. (1988)) and the technique used in the estimation has not been tested over urban areas from most of the studies (Pinker, 1990). Although the longwave fluxes could be observed from ground measurements (i.e. pyrgeometer), doing so incurs instrument and maintenance costs which are not commonly considered for collecting the irradiance data. Some efforts have been made to compare the $L_{\downarrow}$ between urban and rural environments from routine measurements (i.e. flux tower). It has been found that $L_{\downarrow}$ is generally larger in urban areas because of the warmer urban boundary layer resulted from the UHI effect. Studies show

that the UHI effect significantly triggers the convective processes over urban canopy and increase the amount of $L_{\downarrow}$ from atmosphere received by the urban surface (Estournel et al., 1983, Bergeron and Strachan, 2012, Oke et al., 2017). Although this is not the focus in this review, the estimation or observation of the $L_{\downarrow}$ are of great importance in constructing the $sUHI$-$aUHI$ relationship.

The surface energy balance may be written as:

$$Q^* = Q_H + Q_E + Q_G \qquad \text{Equation (2.3)}$$

where Q_H and Q_E are the turbulent heat fluxes of sensible heat and latent heat ($\mathrm{Wm^{-2}}$), respectively, and Q_G is the storage heat flux ($\mathrm{Wm^{-2}}$). By considering the 3-D energy conservation at larger scales, the surface energy balance for a volume is written as (Oke, 1988b):

$$Q^* + Q_F = Q_H + Q_E + \Delta Q_S + \Delta Q_A \qquad \text{Equation (2.4)}$$

where Q_F is the anthropogenic heat flux released within the volume due to human activities, ΔQ_S is the net heat storage variation by all elements in the volume and ΔQ_A is the net energy added or subtracted by wind advection which is usually ignored by assuming an extensive and relatively homogenous urban surface where the horizontal differences are negligible in practice field studies. However, the advection term should not be neglected particularly under high wind speed condition when the advection of rural air over the city becomes more influential. Herein, there is a direct link between surface and air temperature in the estimation of Q_H that is generally calculated based on the 'resistant' approach (i.e. aerodynamic resistance that is affected by wind speed, surface roughness and atmospheric stability (Oke et al., 2017)) due to the fact that it needs costly requirement of instrumentation and careful field implementation for data retrieval. Q_E is

defined by the energy used to vaporise the water mass (e.g. evaporation or condensation) and it is largely determined by the water availability. It can also affect surface and air temperatures indirectly. In theory, evaporation removes the energy from the surrounding environment, leading to the decrease of the surface and air temperature while condensation can bring the heat back and warm the surface and air layers. The calculation of these fluxes has been reviewed by Oke et al. (2017) and it will not be repeatedly introduced here. However, it is still noteworthy that the turbulent heat fluxes (Q_H and Q_E) are inherently controlled by the surface and the overlaying air layers, which provides theoretical evidence for building the T_s-T_a or $sUHII$-$aUHII$ relationships. Specifically, surface properties (e.g. vegetation and building materials) and atmospheric conditions (e.g. wind speed, wind direction, horizontal and vertical thermal structure and humidity variability or advection) are the most influential factors in controlling the temporal or spatial variations of energy fluxes. The heat storage change (ΔQ_S) is mainly controlled by the input of the heat outside (i.e. solar radiation) and inside (indoor human activities [i.e. cooking]) the volume, together with the thermal properties of the materials (e.g. heat capacity and thermal conductivity). It is intrinsically linked to the surface temperature and influences the air temperature ultimately. Regarding Q_F, heat converted from chemical and electrical energy and released to the atmosphere is the fundamental source, mainly resulting from human activities. It also has non-negligible effects on modulating the interaction between surface and air layers, such as the heat released from fuel, which has been found to be able to enhance the turbulent mixing and modify the UHI circulation particularly during night-time period (Chen et al., 2009).

In summary, the SEB is the principle of the near-surface thermal microclimate of a site and it is responsible for many urban climate effects (i.e. UHI), which is also

influenced by the status of the surface layer and surface properties (e.g. radiative, aerodynamic, thermal and moisture etc.). Therefore, it is pertinent to have a good understanding of the SEB before studying the UHI, although there are still many difficulties or uncertainties to apply the T_s in the SEB and to establish the association with T_a, particularly over urban areas.

2.3 Canopy heat island

2.3.1 Air temperature

Air temperature (T_a) is normally observed from temperature sensors at weather stations installed within the urban canopy layer over urban areas or surface layer over rural areas. T_a is fundamentally determined by the energy balance via radiation, conduction and convection in the air volume surrounding the site (Oke et al., 2017). T_a is also indirectly influenced by T_s with reference to turbulent heat fluxes between land surface and air as discussed in Section 2.2. Meteorological conditions (i.e. atmospheric stability), together with the surrounding environments of a site (i.e. site configuration and exposure) contribute to the cooling or warming of T_a at micro- or local scale. Specifically, the causative factors largely determine the size or shape of the source area and are responsible for the variations of T_a observed by sensors. In particular, temperature sensors are more sensitive to the turbulence status and therefore their exposure is termed as turbulent source area that is generally located upwind of the sensor.

2.3.2 Quantification of canopy air heat island

It is impossible to measure the urban effects on temperature by performing ideal experiments (Lowry, 1977). Nonetheless, efforts have been made to quantify the

difference to T_a caused by urbanisation, using a pair of weather stations in urban and non-urban areas (surrounding rural areas) (Kukla et al., 1986). $aUHII$ is then calculated as the difference in T_a between urban and rural sites. There are three fundamental concerns related to the calculation of the $aUHII$, including (i) the representativity / exposure of stations, (ii) the accuracy of the temperature sensors and (iii) the overall configuration of the UMN, which are explained in detail below.

(i) Site exposure

For cities having limited urban stations, the quantification of the $aUHI$ is often based on temperature obtained from a single urban station with comparisons to the reference to the closest rural station (Wilby et al., 2011). There are many site factors and criteria involved in the configuration of weather stations in any area (both urban and rural) (Lowry, 1977). Regarding the urban station, the process is particularly complicated (Oke, 1999) and there are limited options in most cities due to the difficulties of deployment and providing the maintenance in urban areas. Indeed, it can be difficult to assess the representation of the local thermal environment from urban stations due to its highly heterogeneous surface structure. Although concepts of Urban Climate Zone (Oke et al., 2006) or Local Climate Zone (Stewart and Oke, 2012) have been developed to classify urban areas into zones in terms of similar local environment (e.g. thermal and surface structure etc.), further analysis for examining the spatial variations of the $aUHII$ within the UCL is increasingly needed with the increasing prevalence of UMN deployments. Issues aren't limited to the urban reference temperature. Variations in rural temperature can also be caused by land cover differences (Oke, 1999), topography and heat advection from cities. For example, it was found that the rural thermal variability (amongst four rural sites over Oklahoma City, US) was maximised during the nocturnal period (Basara

et al., 2008), which is of vital importance for studying UHI. Fiebrich and Crawford (2001) has claimed that the rural temperature variability is principally induced by the vegetation variability across sites from Oklahoma Mesonet. Furthermore, topographic variability (i.e. elevation) can influence the wind from regional to local scale and increase the variance of the observed UHI, particularly for studies using the average temperature from all rural stations within a defined rural buffer surrounding the city (Hawkins et al., 2004). Although the rural reference site is assumed to be largely free from the urban climate effects, limited studies tried to concern or exclude the potential contamination of the urban heat. Bassett et al. (2016) firstly developed a comparatively simple method for estimating the averaged urban heat advection from UMN over a year period. The advected urban heat is still hard to be quantified at hourly or daily time scale and further analysis is needed. However, the possible impacts of the urban heat advection on the rural reference site need to be investigated by considering the background wind conditions. Otherwise it is biased for proclaiming the $aUHII$ by using single/multiple stations as the rural reference, particularly for comparisons across cities with various climate background (Brazel et al., 2000).

(ii) Instrument accuracy

The traditional method for calculating the magnitude/intensity of UHI (UHII) with respect to the observational temperature differences between urban and rural areas can inevitably introduce some uncertainties in the calculation. The errors (or accuracy) of the temperature sensors used in weather stations are usually better than 0.5℃, e.g. accuracy of ± 0.2℃ for the Met Officer MIDAS station network (Parton, 2015), $< \pm 0.24$℃ in average after calibrations for the Birmingham Urban Climate Laboratory network (BUCL) (Warren et al., 2016), ± 0.3℃ for the Oklahoma Micronet network (OKCNET) (Basara

et al., 2011) and ± 0.5℃ for temperature at 1.5 m above ground level (a.g.l) for Oklahoma Mesonet (McPherson et al., 2007) etc. The subtraction method would be likely to double the inaccuracies (in maximum) compared to the ones from temperature sensors in calculations of the UHII that is normally found to be a few degrees during night time (Kolokotroni and Giridharan, 2008, Gaffin et al., 2008, Smith et al., 2011, Chowienczyk et al., 2020). These errors are unavoidable from observational data; however, numerical models are promising in exploring the $aUHI$ to avoid these instrument-caused uncertainties.

(iii) Configuration of station network

Regarding the configuration of weather stations in cities, a dense weather station network (i.e. Urban Meteorological Network, UMN) is required because it is impossible for a small number of individual stations to resolve variations in meteorology at the city scale (Oke, 2007). A review of existing UMNs (Muller et al., 2013a) concluded that a standardised protocol was required due to the heterogeneous topography and morphology encountered in cities. Turbulence and obstacles existing in the UCL cause a large temperature variation between different urban sites and limits the source area for a sensor as well. As a result, different interpolation schemes are used to derive the spatial distribution of T_a or $aUHII$. However, all of the interpolation schemes are ultimately restricted by the number and location of the stations. In theory, such approximations cannot be used with confidence over urban areas due to its complex structure. Therefore, careful implementation of dense UMN is necessary for studying the spatial variations of the thermal pattern in cities. This could potentially be facilitated by the increasing use of low-cost of non-standard, yet fit for purpose, wireless temperature sensors are becoming a new method to retrieve T_a with a finer spatial resolution in cities (Warren et al., 2016).

2.3.3 Impact of weather and climate on $aUHII$

2.3.3.1 Atmospheric stability

The local weather conditions and the related physical mechanisms through which the development of the $aUHI$ is driven are well documented (Arnfield, 2003). The UHI is a result of the differences of the energy balance between urban and rural areas (Oke and Maxwell, 1975), with maximum UHI intensity (UHII) being recorded under clear and calm conditions. Hence, one of the causative factors in determining the development of the UHI is atmospheric state that is a response to the energy, mass and momentum exchanges in urban and its surrounding rural environments (Oke, 1982). When the atmosphere is unstable, as is often the case in urban atmosphere comparing to the rural background (Lee, 1979), the increased generation rate of the turbulence due to the warmer surface air temperature than the air above in an unstable atmosphere can affect the surface layer. This then becomes convective, well-mixed with small vertical gradients. In contrast, if the air temperature near the surface is colder than that directly above, the atmosphere becomes stable with a negative heat flux and turbulence is restrained and reduced, leading to the stratification with large vertical gradients (Bardal et al., 2018). The neutral atmosphere comes with nearly zero vertical heat flux, since then, vertical mixing in the atmosphere is no longer affected by the buoyancy forces (Emeis, 2018). The UHII is clearly influenced by atmospheric conditions and research related to UHI under varying conditions during the measurement period has previously led to inconclusive results (Krüger and Emmanuel, 2013). This has been tackled in previous studies by investigating the relationship between meteorological parameters and the $aUHI$, such as the synoptic situation or general weather conditions / mean sea level pressure (Morris and Simmonds, 2000, Kassomenos, 2003), cloud cover and background wind speed (Unger, 1996,

Figuerola and Mazzeo, 1998, Levermore et al., 2018), or thermal rural inversion (Basara et al., 2008, Hu et al., 2013, Lauwaet et al., 2016). However, there is scope to improve upon these approaches by using a classification scheme for overall atmospheric conditions, which could induce uncertainties of the true extent of the UHI (Krüger and Emmanuel, 2013).

2.3.3.2 Seasonal impact

Seasonal influences can further modulate the thermal differences (i.e. temporally and spatially) between urban and non-urban surfaces. Factors underpinning the seasonal variation of the development of UHI mainly include: (1) changes in the amount of solar radiation received from ground surface; (2) variations of the metabolic activity of vegetation (e.g. soil moisture); (3) precipitation; (4) release of anthropogenic heat and (5) snow cover. Specifically, solar input (including the length of day) is a surrogate of measuring heat storage (Q_G) within the urban elements and the amount of long-wave radiation ($L_{\uparrow}$) releasing from it during nights, resulted in the higher temperature in urban sites. Thereby, the greater $aUHII$ is usually observed during summer and spring seasons when the input of the solar radiation is larger. Meanwhile, these two seasons are considered as the growing seasons when the growth of the vegetation is more active, contributing to higher soil moisture and lower temperature in rural sites (Deilami et al., 2018). Several other meteorological patterns, predominantly in summer, are found to be the main driving factors for the maximum $aUHII$. For instance, the prevailing winds blowing from Lake Michigan lead to the greatest $aUHII$ during summer nights in Chicago (Ackerman, 1985). Chow and Roth (2006) found that higher $aUHII$ is prevalent during monsoon seasons (i.e. summer) in Singapore. In contrast, other found that the maximum $aUHII$ occurs in colder seasons (i.e. autumn and winter) because of the larger

controls on the $aUHII$ comparing to solar input, such as location, local climate and the anthropogenic heat released etc. (Kim and Baik, 2002).

Precipitation modulates the $aUHII$ through modifying the Bowen ratio (β) that is significant to surface climate represented as the ratio of the two turbulent heat fluxes (Q_H/Q_E) (Gu and Li, 2018). Some studies have demonstrated that the $aUHII$ is stronger in wetter climate because it enhances the rate of evapotranspiration over rural areas where the β becomes smaller, resulting in lower rural temperature particularly during the summer period with largest evapotranspiration rate (Li et al., 2016). However, infiltration is likely to be reduced with greater runoff in cities because of the nature of urban structure. In general, the role of precipitation in modulating the thermal anomaly is temporary and limited. Particularly, Zhao et al. (2014) identified that the nocturnal $aUHII$ was not correlated with the amount of precipitation at annual mean scales. Gu and Li (2018) highlighted that the role of precipitation in the development of the $aUHI$ was sensitive to locations (/climates) and seasons. The uncertainties remaining motivate further study related to the sensitivity of the UHI to precipitation.

In conclusion, seasonality brings marked changes to many aspects of a city and its surrounding rural areas, e.g. vegetation status, surface moisture and admittance even seasonal wind pattern, seasonal variations of precipitation etc. Therefore, cities are not in static status and season as a solely controlling variable might be too rough and simple to investigate the seasonal pattern of the $aUHI$.

2.3.4 Urban form controls on $aUHII$

Urban form predominantly controls the spatial thermal response (i.e. $aUHII$) which is generally reflected by the local orography, building structure, amounts of soil,

vegetation or green space, distributions of water bodies and the release of anthropogenic heat (Oke et al., 2017). The materials used for urban construction, such as asphalt, concrete and gravel change the thermal properties resulting in a greater heat capacity than vegetated or other natural surfaces in rural areas. As a consequence, urban elements absorb larger quantities of shortwave radiation that is then available to be released at night. The vegetated rural environment facilitates the evaporation process during the day, leading to the enhancement of the heat retention that reduce the heat from incoming solar radiation stored in and re-emitted from rural surfaces (Oke, 2002b). Meanwhile, urban structure with canyons and dense buildings reduce the efficiency for emitting longwave radiation from ground surfaces during night-time, contributing to weaker thermal cooling rate and the heat excess comparing to surrounding rural areas (Stone and Rodgers, 2001).

The heterogeneity of urban surfaces introduces nearly infinite spatial variations of the temperature or UHII across cities. Notwithstanding, scientists have endeavoured to investigate the spatial pattern of the $aUHII$ and its associations with all possible physical factors related to the urban form so that it can be estimated or modelled in terms of these influencing factors rather than using ground stations as many as possible. However, the limited number of the weather stations and the complex urban surfaces, leading to the sparse and uneven distributions of the stations' deployment, largely hinder the progress for investigating the spatial pattern of the $aUHI$. As mentioned previously, interpolation techniques, such as Kriging (Nguyen et al., 2015) and Inverse distance weighted (IDW) (Taskinen et al., 2003) etc., are generally used to compensate for these deficiencies by estimating the air temperature, in spite of the evidence showing that they are restricted to topography, land surface characteristics and seasonality (Cao et al., 2009, Kuzevicova et al., 2016). Satellite observations provide an alternative approach, and there are increasing

number of studies attempting to estimate the T_a from T_s in order to explore the spatial pattern of the $aUHI$, which will be further discussed in Section 2.6.

Many surface parameters are developed to represent the urban form and are generally found to be strongly associated with the $aUHII$ because of the decisive role of the three-dimensional (3-D) geometrical configuration in regulating the heat loss in cities (Unger et al., 2004), as previously mentioned. Amongst all the surface parameters summarised by Deilami et al. (2018), the ones closely representing street geometry are the primary concerns for determining the intra-urban variations of $aUHII$ or T_a inside a city (Unger, 2004). For example, the ratio of building height (H) to the street / canyon width or averaged space between buildings (W) demonstrates the density of the buildings with regards to their heights. Similarly, the sky view factor (SVF) indicates the radiation geometry of a given site by measuring the totally obstructed and free spaces (Oke, 1988a). Both are strongly correlated with the UHII because of their associations with the level of radiation loss and the efficiency of turbulent heat transfer surrounding the site (e.g. Reading, UK (Parry, 1987), Birmingham, UK (Johnson, 1985), Belo Horizonte, Brazil (dos Santos et al., 2003), Szeged, Hungary (Unger, 2004) etc). However, it remains more appropriate to focus on general characteristics or controls of the intra-urban thermal distribution instead of investigating the nearly infinite spatial differences of it in different locations within a city.

Different climate-based classification systems have been developed based on various land surface parameters for urban or rural sites at neighborhood-scale, mainly including the ones from Chandler (1965), Auer Jr (1978), Ellefsen (1991), Urban Climate Zone (UCZ) from Oke et al. (2006) and Local Climate Zone (LCZ) from Stewart and Oke (2012). LCZ is explicitly designed to classify heat island field sites, with considerations

of various surface properties including, but not limited to geometric and surface cover properties (e.g. SVF, aspect ratio, terrain roughness class), thermal, radiative and metabolic properties (e.g. albedo, admittance and anthropogenic heat output) (Stewart and Oke, 2012). As a result, numerous studies have attempted to conclude the general spatial patterns of the $aUHII$ according to LCZ classifications within or between cities (Yang et al., 2020, Chieppa et al., 2018, Kotharkar and Bagade, 2018). Nonetheless, intercomparisons of the $aUHII$ among cities still need to be treated with caution, considering the city-based climatic background that would result in dissimilarities of the $aUHII$ predicted from the same LCZ in different cities (Chieppa et al., 2018).

In addition, few previous studies pay attention to the impacts of weather / climate on the spatial pattern of the $aUHI$, despite the fact that studies tend to simplify the controls of $aUHI$ by choosing the calm, clear nights when turbulent mixing is weak and the atmospheric influences are considered to be minimised during different seasons. In doing so, thermal gradients become increasingly large in both horizontal and vertical across the city and prominently determined by the local urban environment (Takahashi, 1959, Taesler, 1980, Einarsson and Lowe, 1955, Jauregui, 1973). Some recent studies have made efforts in quantifying the magnitude of $aUHI$ induced by heat advection (UHA) from ground observations and numerical models (Bassett et al., 2016, Bassett et al., 2017, Heaviside et al., 2016). Lowry (Lowry, 1977) describes the constituents of a meteorological variable (i.e. temperature) at given time and location that is the results of mutual contributions from (i) macroclimate of the region (background), (ii) local landscape or topography and (iii) human activities and urban effects (i.e. UHI). The subtraction method for calculating the $aUHII$, to some extent, minimises the effect of regional climate. The UHII caused by the local landscape and urban-rural meteorological

difference might be submerged in the calculated $aUHII$. Therefore, further studies, which take these concerns into account, will need to be undertaken.

2.4 Surface urban heat island

2.4.1 Land surface temperature

2.4.1.1 MODIS Satellite instrument

There now exists a range of satellite instruments available to obtain T_s via thermal infrared (TIR) channels such as AVHRR, SEVIRI, ASTER, AATSR and MODIS (see Tomlinson et al. (2011a) for a comprehensive review). MODIS is a popular instrument for temperature-related studies (especially for delivering the time-series of temperatures), because of its global coverage, temporal and spatial resolution, and accessible surface products with moderate spatial resolution. Specifically, MODIS provides a daily maximum of four T_s products in a study area (Sohrabinia et al., 2015). Moreover, many MODIS products related to urban environmental studies are available, such as land surface albedo, emissivity, leaf area index (LAI), land cover, snow, cloud and aerosol characteristics. It provides more parameters to be considered for studying the T_s-T_a relationship (Jin and Shepherd, 2005).

2.4.1.2 Concerns regarding the application of T_s

There are two principal considerations for the application of the satellite-derived land surface temperature (T_s) from TIR data, discussed as below:

(i) Physical determinants

In contrast to the surface temperature observed from ground instruments, T_s is estimated by the measured radiation from Earth and its atmosphere viewed by the thermal

infrared sensors onboard satellites (Li et al., 2013). Fundamentally, satellites have a bird's eye view of ground surface from a sensor that receives the average radiative information from the surface for each pixel (after correcting the atmospheric effects). It is thus intrinsically determined by the SEB between the surface from every surface element and the overlying air temperature above it. Oke et al. (2017) summarised the five surface properties that exert exceptionally strong controls on the emitted longwave (including reflected or multiple reflected radiations) radiation from the land surface, including the geometric, radiative, thermal, moisture and aerodynamic properties. The geometric property is primarily considered for urban surfaces (i.e. urban form), as discussed in Section 2.3.4. For rural surfaces, it is reflected by the roughness length or the distribution of the vegetation (e.g. grass or trees). It fundamentally regulates the reflected longwave radiation among surface elements before re-emitting to the atmosphere during nights and is difficult to be quantified from ground observations, but progress been made through numerical simulation (Harman and Belcher, 2006). The radiative (i.e. albedo and emissivity) and thermal (i.e. thermal conductivity and heat capacity etc.) properties are mainly referred to the capacity of the land surface to reflect and absorb radiations, respectively, intrinsically governed by different types of land surfaces (e.g. materials used in artificial surfaces). Regarding the moisture property, it is less important in urban environment due to the limited latent heat from the non-vegetated areas. For vegetated areas or moist soil surfaces, T_s can decrease or increase by experiencing the evaporation or condensation processes, correspondingly, which affects the received radiance from satellite sensors ultimately. The aerodynamic property is recognised as the interference of the turbulence or wind flow by the land surface, basically attributed to the roughness length and structure of the surface elements. These five properties infinitely vary across

different locations, leading to the extremely complex of T_s, particularly between urban and rural environments.

(ii) Atmospheric, surface emissivity and cloud effects

The basic theoretical background with regards to the estimation of the T_s from the radiative transfer equation (RTE) has been detailed by Wan and Dozier (1989). However, the complexities and difficulties of atmospheric and surface emissivity corrections make the development of the T_s algorithm challenging. The atmospheric corrections include the correcting processes of radiance measured by sensors for the effects of atmospheric attenuation, emission and reflection (Li et al., 2013). It is difficult to implement mainly because it requires a large number of unknown parameters as inputs to the RTE, primarily including the absorption coefficient of atmospheric molecules (i.e. water vapour), scattering coefficient of aerosols and accurate atmospheric profiles (i.e. water vapour and temperature) (Perry and Moran, 1994). The surface emissivity correction requires the accurate surface emissivity for different land-surface materials that varies in different spectrums and viewing angles, in order to correct the reflected radiance received by sensors from surface. The surface emissivity data is normally derived from laboratory data. If atmospheric effect is not fully corrected, the surface emissivity at specific range of spectra derived from satellite could be different from the laboratory data (Rivard et al., 1993). Despite the difficulties in relation to the atmospheric and surface emissivity corrections, the algorithms developed to estimate T_s have been significantly improved over the past several decades. The single-channel and split window methods are the two commonly used algorithms to estimate T_s with known land surface emissivity data as pre-requisites (details can be found in Li et al. (2013)). The validation of the estimated T_s is normally via comparisons with the surface temperature derived from field measurements

that is the way to indirectly check the satisfaction of the algorithms and the corresponding atmospheric as well as surface emissivity corrections. Although the accuracy of the estimated T_s is normally better than a few degrees (e.g. 1 K from MODIS (Wan, 2008)), the validation sites are commonly chosen over large homogenous areas in order to configure the high-accuracy TIR radiometers at multiple locations (e.g. lakes and grasslands (Wang et al., 2004, Coll et al., 2005)). The atmospheric and surface emissivity effects are therefore known to be limited for both urban and vegetated (rural) areas, potentially leading to uncertainties in $sUHI$ studies.

One of the primary limitations for T_s derived from TIR bands is the influence of cloud. T_s from TIR is normally only available under clear-sky conditions as TIR does not penetrate cloud layers. However, calculations of T_s can be contaminated for the pixels covered by cirrus clouds since TIR can only partially penetrate cirrus layers (Li et al., 2013). Taken the MODIS T_s products as an example, although the T_s products were filtered by the cloud mask (the grid cell is cloud-free if it has the grid value for T_s), Wan (2008) found that cloud contamination still exists since the cloud-removing scheme insufficiently removes contaminated pixels under both light and modest cloudy conditions, especially in the high-altitude areas or areas with high reflectivity (i.e. deserts and snow covers). The contaminated pixels usually refer to the temperature at the top of clouds representing the extreme low values (Mutiibwa et al., 2015). For example, it has been found that the cloud-contaminated pixels from MODIS T_s product (V004) can reach 12 K lower than the non-contaminated ones over Lake Tahoe, US. Although new refinements have been applied in the MODIS T_s product in version 005 (V005), the validation study effectively still showed the impossibility to remove all cloud-

contaminated pixels over Lake Tahoe (Wan, 2008). Therefore, cautious need to be taken for pixels with extreme low values of T_s.

2.4.1.3 Characteristics of T_s over urban environment

(i) Heterogeneity of urban land surface

In urban areas, the characteristics of T_s become increasingly complex due to the stronger spatial variability of surface characteristics in cities than other natural areas. In general, variations of T_s primarily depend on daytime solar insolation and longwave radiation emission during night-time (Prigent et al., 2003). Spatial-continued variations of the emissivity or albedo caused by the heterogeneity of urban surface (i.e. the diverse land use types) affect the radiance for each pixel received by satellite imageries and increase the spatial variance of T_s. Specifically, the transformation of a surface component from soil to more asphalt and concrete contributes to the change of surface albedo and emissivity. The range of different materials of the buildings and road surfaces in cities result in the diversity of the thermal inertia and heat capacity. These would increase the variability of the radiation sensed by a satellite amongst urban pixels. Furthermore, variable amounts of vegetation (parks, grasses or trees) and water content (rivers or reservoirs) existing in cities result in different interaction processes between surface and air temperature during different seasons.

The impacts of the human activities on the urban SEB are termed as the Q_F which affects the net radiation balance in estimating the T_s. Although Q_F is generally considered to be small, numerous studies have attempted to quantify the Q_F in different cities. However, it is still difficult to fully characterise human activities in terms of temperature, due to the various sources of Q_F and the difficulties in quantifying them. In light of the aspects discussed above, the heterogeneity of the urban surface contributes to unique

spatial patterns of T_s for each city and make it harder for comparisons across different cities.

(ii) Three-dimensional (3-D) structure of city

The 3-D structure of urban elements induces temperature variability partially resulting from different local solar zenith angles and satellite zenith angles on facets, which leads to thermal anisotropy (Lagouarde et al., 2004). Using the MODIS T_s product as an example, (Wan, 2007) stated that the maximum of satellite zenith angle from nadir is $\pm 65°$ (Note: the negative sign means satellite viewing the grid from east). Previous studies showed that, although the anisotropy effect can be strong for the area with many tall buildings during daytime (Hu et al., 2016a), the thermal anisotropy is in generally negligible during night-time (Lagouarde et al., 2012). Lagouarde et al. (2012) estimated the urban anisotropy effect of around 1℃ based on the differences of surface temperature at between off-nadir and nadir from airborne observations obtained in the early or middle part of the night (3 nights in autumn and winter conditions) over the city center of Toulouse, France. The modelling approach from Lagouarde et al. (2012) also indicated that the thermal anisotropy effect could diminish rapidly following sunset and become negligible and almost azimuthally independent in the evening. Another study, carried out by Hu et al. (2016a) who estimated the anisotropy effect using the T_s from MODIS during warm months (May to September) for a 10-year period over Chicago and New York, also observed about 1℃ temperature bias due to the anisotropy effect at nights. They also found small variation of $sUHII$ as a function of satellite zenith angle that varied by city. Both studies are in highly urbanised areas and the effects should reduce further for less urbanised areas, however further research is required to investigate the spatial variation of the nocturnal anisotropic effect in urban areas, which remains of great importance in

the $sUHI$ studies. Areas covered by vegetation may raise more uncertainties because little is known about the thermal anisotropy caused by vegetation within urban areas (Dyce and Voogt, 2018).

2.4.2 Quantification of surface urban heat island

The quantification of $sUHII$ is the difference of the T_s between the urban and rural areas. The nature of observed T_s provides more options for choosing representative urban and rural background locations. There are mainly two approaches to calculate the $sUHII$ for a city from the literature and the key process is the way to define the pixels as urban and rural areas (or suburban), respectively. Some studies classified pixels as urban and rural areas for a city by using land-use type products or urban fraction data from satellite instrument or land classification from ordnance survey (Peng et al., 2011, Zhou et al., 2014, Schwarz et al., 2011, Clinton and Gong, 2013). In doing so, T_s for urban and rural areas are generally calculated as the average temperature from all urban and rural pixels correspondingly. This method thus depends on the accuracy of the underpinning land-use product or other data used to define urban and rural pixels. For example, Martilli et al. (2020) has pointed out that the SEDAC's Global Rural-Urban Mapping project (Schneider et al., 2009) is known for its overestimation of urban areas but it is still often used as reference to define urban and rural areas in the calculation of $sUHII$ by other studies (e.g. (Manoli et al., 2019)). Alternatively, single pixel (i.e. pixels closest to weather stations) (Schwarz et al., 2012, Tomlinson et al., 2012) or pixels within a buffer around a station or city centre are used to define the T_s from cities, particularly for studies attempting to examine the relationship between T_s and T_a or between $sUHII$ and $aUHII$. For example, urban T_s is averaged from the pixels within an interval of 30 m buffers

$(3 \times 3, 4 \times 4 \ldots 13 \times 13)$ in city centre (data: Landsat-8 OLI/TIRS with 30 m spatial resolution) to build up the relationship with impervious surface density and green space density (Estoque et al., 2017). Careful investigations of the cloud conditions from surface stations are needed because limited pixels are used which may increase the uncertainties of the estimated T_s.

2.4.3 Impact of weather or climate on $sUHII$

As per the $aUHI$, remarkably few studies have been undertaken to examining the weather influences on $sUHII$ (note: estimated from satellite observations). This is also one of the key research gaps identified in this thesis. A possible explanation for this might be that $sUHII$ is less affected by the weather but inherently determined by land surface characteristics, comparing to the $aUHII$. More importantly, the relatively low temporal resolution, together with the great chance of cloud effects limits the availability of the satellite observations, which inevitably restricts the corresponding research progress. Consequently, previous studies have been focusing on studying the seasonal variations of the $sUHII$. The underlying physical mechanisms of its seasonal patterns can be largely explained by the regional weather patterns or meteorological conditions (i.e. driven by the weather patterns) in surface layer, discussed as follows.

Regional weather patterns are generally season dependent, which becomes one of the driving factors modulating the seasonal patterns of the $sUHII$. It has been found that regional weather patterns can induce heatwaves because of the favourable high-pressure system dominating particularly during summer in some cities. For examples, a strong positive relation between heatwaves, caused by atmospheric blocking that is a large-scale atmospheric dynamic feature usually identified in the mid-troposphere, and $sUHII$ was

found during summer in south-eastern US (Dong et al., 2018). Likewise, the predominant anticyclonic weather system associated with the heatwave events during summer was found to govern the nocturnal $sUHII$ in Cluj-Napoca city, Romania (Herbel et al., 2018). In addition, the regional weather pattern determines the seasonal changes of the surface properties that is associated with the seasonal patterns of the $sUHII$. The surface properties are largely reflected by the ground heat fluxes (Q_G) and the soil moisture. Soil moisture is normally increased during the wet winters in many mid-latitude cities. It could induce a larger soil thermal admittance, leading to the weaker nocturnal surface cooling and reduce the $sUHII$ consequently (Oke et al., 2017). One such example is that the $sUHII$ (from Landsat 8 satellite) is found to be positively correlated with soil moisture, particularly during dry seasons (spring and winter) in Toluca, Mexico (Rivera et al., 2017). However, there is no consensus with respect to the seasonal patterns of the $sUHII$ that could vary in cities with different geographical locations. For instance, greater $sUHII$ in winter (comparing to summer) is found in Casablanca, Morocco, resulted from its geographical location at the coast that alters the local weather pattern by increasing the wind speed from strong see breeze during summer (Bahi et al., 2016b). In contrast, higher $sUHII$ are found during spring and summer in Brazil, explained by the cycle of precipitation and controls the robustness of the vegetation due to the weather patterns (Alves, 2016). Further research is needed in order to generalise or conclude the seasonal patterns of the $sUHII$ across cities, which is necessary for a better understanding of the physical mechanisms of it.

Regarding the influence of atmospheric conditions in surface layer on $sUHII$, cloud amount, input of solar radiation (from previous day), wind speed, relative humidity are the meteorological parameters primarily considered. As nearly all estimates of $sUHII$ are

under cloudless conditions, it is quite hard to explore the impact of cloud on the variation of $sUHII$. However, the UHI derived from surface temperature (e.g. from surface temperature sensors (Culbertson, 2001)) is supposed to be reduced in cloudy skies due to the greater loss of longwave radiation from surface during night-time. The input of previous-day solar radiation is directly related to the ground storage heat and the amount of emitted longwave radiation and therefore positively correlated with the $sUHII$. It is often highlighted by studies that found greater $sUHII$ during summer period (Ward et al., 2016) It has been acknowledged that the influence of wind speed on $sUHII$ has not been thoroughly scrutinised (Oke et al., 2017). However, some studies have attempted to explore the role of the rural background atmospheric stability in surface layer on the development of $sUHII$. The Pasquill-Gifford (P-G) stability classification scheme that considers wind speed, solar input, and cloud amount to define stability classes from unstable to neutral and stable (Pasquill and Smith, 1983) was typically used in these studies. Nocturnal $sUHII$ was found to be intensified when the stability class shifts towards stable with low wind speed and clear skies (Tomlinson et al., 2012, Azevedo et al., 2016). This is a consequential attempt for examining the impacts of atmospheric stability with consideration of readily retrieved atmospheric parameters on the $sUHII$, despite the fact that the studies mentioned above focused on summer period only with limited satellite dataand further study is needed. $sUHII$ is intended to be reduced with high humidity, owing to the weaker radiative cooling difference as a result of the smaller urban-rural differences of the humidity (Oke et al., 2017). Further research is needed for investigating the atmospheric impacts on the development of $sUHII$.

2.4.4 Urban form controls on $sUHII$

Contrary to the $aUHII$, the role of the urban structure on the intra-urban variance of the $sUHII$ is investigated much easily because of the spatially continuous data format of satellite products. Urban structure can be quantified or represented by more spatial or non-spatial continuous parameters, e.g. vegetation fraction, Normalised Difference Vegetation Index (NDVI), impervious surface area (ISA), building fraction (BF), map of anthropogenic heat release, SVF, H/W ratio etc. (Unger, 2004). The spatial pattern of the $sUHII$ is fundamentally determined by the urban-rural differences of the surface properties that control the SEB and the variations of T_s, as discussed in Section 2.4.1. Thus, parameters associated to the surface properties are supposed to have significant relationship with the $sUHII$. For instance, $sUHII$ demonstrates good agreement with the differences in vegetation fraction from MODIS products between urban and rural areas (Cui and De Foy, 2012). It is evident that the vegetation fraction is largely reflected the surface albedo, moisture and even ISA indirectly. $sUHI$ is also found to be significantly correlated with impervious surface area (%) and less correlated with NDBI (normalised difference built-up index) that is a rough measure of the BF in terms of differences of the surface reflection in middle and thermal infrared bands from satellite and it is season dependent (Rivera et al., 2017). Regarding the NDVI, $sUHII$ is negatively correlated with vegetation amount or the greenness that is usually represented by the NDVI product from satellite. It is evident that this correlation depends upon seasonality because of the seasonal-dependent latent heat processes dominantly affected by the vegetation and moisture (Yuan and Bauer, 2007). Although the potential seasonal influences are considered, contrasting relations between $sUHII$ and NDVI were stated from previous studies. It was found that this relationship is less significant during dry summer in semi-

arid city of Erbil, Iraq (Rasul et al., 2016), as a result of the decrease of NDVI that limits the range of one of the variables in the correlation analysis. However, $sUHII$ was inversely correlated with the NDVI during winter and it was largely attributed by the greater soil moisture in urban areas resulted from the irrigation of urban green space but lower soil moisture in rural areas where the agriculture is rain-fed rather than irrigated in Erbil. Likewise, many studies have made efforts to build up the relationship between SVF or H/W ratio to the $sUHII$ and Unger (2004) has reviewed most of these studies. The increasing release of the anthropogenic heat because of energy consumption (i.e. air conditioning and heaters), plays an important role for the intensification of $sUHII$ in different cities, such as Beijing, China (Yao et al., 2017) and Nagoya, Japan (Kato and Yamaguchi, 2005).

However, the same problem exists that the empirical relationships derived from the past literature vary time by time and city by city. This largely hinders the process of w generalising the intra-urban variation of the $sUHII$ globally. Here, the concept of LCZ has again helped to make further progress in this field where the intra-urban pattern of the $sUHII$ has been tried to be analysed by considering the LCZs across cities, similarly to the $aUHII$. It is generally found that $sUHII$ differs significantly between LCZs, which provides confidence in using LCZ to discriminate the intra-urban thermal differences quantified by T_s (Dian et al., 2020, Geletic et al., 2019). Seasonal factors are also considered in these studies due to the fact that local environment is seasonal-dependent. According to the intercomparison of the LCZ across different cities, few attempts have been made. Nonetheless, this intercomparison should not only consider the LCZ but also the regional/local climate background. Chieppa et al. (2018) highlighted that the LCZ systems do not predict the UHI equally in spite of comparing between cities with similar

background climates. Therefore, it is of critical importance to separate the local climate effect when doing an intercomparison of $sUHII$ across cities.

2.5 Modelling of the T_s-T_a relationship

A review of previous efforts in modelling the T_s-T_a relationship is now discussed. The reason for reviewing the T_s-T_a relationship from the literature is mainly because of the fact that the $sUHII$-$aUHII$ relationship is fundamentally determined by the linkage between T_s and T_a (from the definition). However, researchers have paid most attention to the T_s - T_a relationship by using empirical or physical modelling over different environments. It is thereby indispensable to summarise and criticise the methods and findings with respect to the T_s-T_a relationship before investigating the $sUHII$-$aUHII$ relationship. From the literature, the progress made to the relationship between surface (not from satellite) and air temperature starts from the similarity theory (Section 2.5.1), subsequently leading to empirical modelling regarding the T_s-T_a relationship (Section 2.5.2) and numerical models (Section 2.5.3) to simulate the air and surface temperature.

2.5.1 Surface layer similarity theory and parameterisation (MOST)

As regards the relationship between the surface temperature and the air temperature above the roughness elements in the atmospheric surface layer, applicability of the Monin-Obukhov similarity theory (MOST) has been well justified over smooth surfaces (Foken, 2006). MOST (Monin and Obukhov, 1954) is developed by A.S Monin and A.M. Obukhov based on the similarity of the dimensionless wind gradient ($\left(\frac{kz}{v_*}\right)\frac{\partial \bar{v}}{\partial \bar{z}}$) and temperature gradient ($\left(\frac{kz}{v_*}\right)\frac{\partial \bar{T}}{\partial \bar{z}}$) comparing to the dimensionless length scale (z/L) within

the inertial sublayer. Their relationships can be written with universal functions (φ_1 and φ_2) (Foken, 2006):

$$\left(\frac{kz}{v_*}\right)\frac{\partial \bar{v}}{\partial z} = \varphi_1(z/L) \qquad \text{Equation (2.5)}$$

$$\left(\frac{kz}{v_*}\right)\frac{\partial \bar{T}}{\partial z} = \varphi_2(z/L) \qquad \text{Equation (2.6)}$$

where k is the von Karman constant, z is height, v_* is friction velocity, $\bar{v}$ and $\bar{T}$ are mean velocity and temperature at specific z, respectively, and L is Obukhov length that is a function of v_*, g/T_0 (g: gravity acceleration, T_0: surface temperature [note: it is distinguished from the satellite-sensed land surface temperature]), two assumed constant variables – shear stress (as a function of air density [ρ], fluctuation of vertical [w'] and horizontal [v'] wind velocity) and $\overline{w'T'}$ (T': fluctuation of temperature), to describe the atmospheric turbulence and stability above the roughness sublayer. In addition, many different universal functions (φ_1 and φ_2) have been developed based on experiments in various locations, e.g. Businger et al. (1971) from 1968 KANSAS experiment (Izumi, 1971), which are introduced in Foken (2006).

As introduced above, MOST can address the vertical profile of T_a above small roughness surface (constant-flux layer), such as barren land, grassland over rural areas. As a result, many land surface schemes and models based on the MOST framework have been developed (Kimura, 1989). The MOST formulations in these studies are taken as a principle for the accuracy inspection due to the limitation for data acquisition prepared for land surface schemes. The Advanced Research Weather Research and Forecasting (WRF-ARW) mesoscale model has two surface layer parameterisations (MM5-similarity (Paulson, 1970) and Eta-similarity schemes (Janjic, 1996) based on MOST. Hari Prasad

et al. (2016) investigated the performance of these two surface-layer parameterisations with qualitative and quantitative comparisons of eight observation variables such as friction velocity, sensible and latent heat fluxes using eight-day data including four seasons over tropical sites in southeast India. In this study, MOST was taken as a fundamental theory in both mesoscale model and actual observation (Eddy correlation method). More typically, MOST is used to calculate sensible heat and momentum fluxes or drag coefficient etc. in terms of measured temperature and wind data by ground observations.

However, to apply MOST to link *urban canopy air temperatures* and *satellite products of land skin temperatures* for an urban surface is extremely difficult, despite MOST being well developed to study mean wind flow and temperature profile regarding to different heights within the inertial sublayer. Two issues relating to (i) satellite-sensed land surface temperature (T_s) and (ii) the applicability of MOST inside the UCL, might be the key concerns to apply MOST to study the T_s-T_a relationship over urban areas.

(i) The issue of satellite skin temperature (T_s)

There are two main issues regarding the application of the T_s in MOST, including (1) T_s is distinguished from the surface temperature used in MOST and (2) the accuracy of the T_s is insufficient and T_s is hard to be used to estimate the temperature profile in urban areas. These two issues are further discussed as follows:

Ideally, T_s may then be approximated as T_0 (surface temperature) in the MOST-derived temperature profile of T_a within the inertial sublayer (if exists, above the roughness sublayer), but this T_s over urban areas is still much different from the surface temperature that is described as the temperature at or near ground surface used in the

estimated temperature profile from MOST. As previously discussed, for an urban area, T_s is derived based on the combined radiation emissions from the top of ground materials (e.g. top of roof or tree, wall or ground surface etc.). It is therefore not perfectly used to represent the surface temperature in MOST over urban areas. This is one of the difficulties for applying MOST based on *satellite-sensed land surface temperature* over urban areas.

Furthermore, although T_s is widely used for some applications, the accuracy of T_s is still a concern for other applications, such as assessment of MOST, which involves the vertical temperature gradient (Equation (2.6)), $\frac{\partial T}{\partial z} \approx \frac{T_a(z)-T_s}{z}$, ideally requires a high accuracy of T_s due to the fact the vertical variation of the temperature near the urban ground surface, $T_a(z) - T_s$, is generally within one degree and occasionally a few degrees (Kanda et al., 2005, Kanda et al., 2006), even though the biases from cloud cover are not excluded (e.g. by selecting clear-sky conditions). As an example, a comparison with on-site longwave radiation data from the BUBBLE campaign at Basel showed that MODIS night-time radiation data had an error of 3-5%, which corresponds to an error of about 2.2-3.7 K for the T_s. Among multiple factors causing the errors, contamination from the atmospheric irradiance can be significant and inaccurate atmospheric corrections may lead to an error of a few degrees even for a simple land-use type such as bare soil (Dash et al., 2002). However, removal of the contamination via atmospheric correction is not a trivial task without simultaneous atmospheric profile measurements (Li et al., 2013). A very careful use of the NCEP profiles of humidity and temperature to correct MODIS Terra product for relatively homogeneous rural ground would still bear an error of ±1 K (Petitcolin and Vermote, 2002). Overall, the accuracy of the satellite products is another concern for using T_s to explore the MOST application.

(ii) The issue of applicability of MOST within the roughness sublayer or UCL

Even if the temperature data is accurately collected, it is common knowledge that MOST is only valid in inertial sublayer that is the upper part of surface layer (Lumley and Panofsky, 1964, Monin and Yaglom, 1999, Wyngaard, 2010). The lower limit of the inertial sublayer is typically two to five times the height of buildings, approximately 25 – 250 metres. The upper limit of it is usually taken as the 10% of the boundary-layer height. Over the homogenous land surface (e.g. rural areas), the horizontal variations and the vertical variations of turbulent fluxes are small (< 5%) in the inertial sublayer (Oke et al., 2017), therefore, it is also called the constant-flux layer as mentioned earlier in this section. In doing so, the logarithmic wind profile (Prandtl, 1925) that is one of the fundamental findings as a basis of MOST is applicable in the inertial sublayer. The logarithmic wind profile describes the semi-empirical relationship between the vertical distribution of wind speed and atmospheric stability in surface layer (Oke, 2002b). The height of the air temperature discussed herein is within the UCL (usually taken 2 m above ground level) that is the lowest part of the roughness sublayer where the logarithm wind profile is no longer valid. This is largely due to the fact that surface-wake generation and interactions are predominant, and the flow is extremely heterogenous attributed by the complicated geometric nature of the roughness elements over urban surfaces (Basu and Lacser, 2017). Even within the upper part of the roughness sublayer (above UCL), the effects of the roughness elements over ground surface (e.g. vegetated surface) on the applicability of the MOST cannot be neglected, which was firstly described in detail by Raupach et al. (1980) in a wind tunnel analysis. In summary, for urban area or vegetated areas, the roughness sublayer can be tens of meters thick and the inertial sublayer is often very shallow or not existent (Raupach et al., 1980). The temperature or wind profiles then

will not follow the ones stated in MOST anymore. Consequently, the application of MOST in the T_s-T_a relationship is hardly possible and to the best of our knowledge, no previous study is found with respect to this investigation.

2.5.2 Empirical modelling

In contrast to MOST, the empirical modelling approach based on regression techniques is more broadly applied in the investigation of the T_s-T_a relationship. Data required for this approach is more readily achievable and the results are more straightforward. It is evident that the T_s - T_a relationship becomes increasingly complicated from rural non-canopy, vegetation canopy and urban canopy environments, which will be further discussed respectively as below. It should be noted that there is no standard height for measuring the T_a over rural non-canopy and vegetation canopy environments. The height of the measurement depends on the purpose for each individual analysis.

2.5.2.1 Rural non-canopy environment

Rural non-canopy environment is herein referred to the land surface without vegetation (such as bare soil, sand, rock or ice) or the vegetated areas with average vegetation height lower than a weather station where T_a is measured (such as grasslands or shrublands). Strong correlation between the T_s from MODIS products and minimum T_a from 28 weather stations at nighttime was found over different ecosystems (from bare soil to forest) in Africa (Vancutsem et al., 2010). It was found that the differences between T_s and T_a (the T_s- T_a differences) were up to 6℃ over barren land compared with 0.6℃ over the vegetated areas. It should be noted that the transpiration of the existing vegetation often narrows the differences between surface and air temperatures. Moreover, the T_s- T_a

correlation is higher in bare soil and shrubland environment compared to grassland. Overall, the T_s- T_a relationship is much more straightforward with larger discrepancy but higher correlation over barren land environment. Nonetheless, there are few studies focused on the T_s- T_a relationship over barren land at micro-scale or pixel-scale because of the mature development of the MOST applied in bare soil or low vegetation environment.

2.5.2.2 Vegetation canopy environment

In the vegetation canopy environment (average height of vegetation taller than the screen height of weather stations), where T_a is referred to as understory temperature or under canopy temperature, the T_s-T_a relationship becomes complicated. Specifically, Hanes and Schwartz (2011) showed a non-linear relationship between the daily maximum T_s derived from MODIS and the daily maximum T_a derived from in situ observations at 1.5 m and 30 m levels above ground. The non-linear relationship was attributed to the seasonal variations in Chequamegon National forest, Wisconsin, USA. Moreover, the T_s-T_a discrepancy decreased with the increase of the vegetation density in this study. Laskin et al. (2016) improved the prediction of understory temperature (1 m above ground level) from MODIS T_s data over the forest areas in Alberta, Canada, particularly during daytime by using the top-ranked model based on the multivariate statistical approach. The predictors include more than 18 forest metrics derived from both conventional inventory and LiDAR data. Canopy closure and tree height data played an important role to estimate the understory temperature in this study. Similarly, Laskin et al. (2017) estimated the understory temperature using T_s products from MODIS by means of generalised linear models (T_s as predictor for estimating the T_a) over the same study area. They declared that there is no previous research on the estimation of understory temperature using

MODIS temperature products only. However, their studies still cannot draw a confirmed relationship over forest environments due to the lack of physical representations. In forest environments, T_s can be a combination of ground surface temperature and the surface temperature at the top of trees in sparse forest; thus T_s depends on the distributions and features of vegetation. Meanwhile, temperature differences between above and below canopy can reach $-10℃$ under stable conditions and the differences depend on forest stand type, canopy height and closure etc. (Flerchinger et al., 2015). In conclusion, the T_s-T_a relationship is more complex and it empirical relationship is more variant over different vegetated areas.

2.5.2.3 Urban canopy environment

The T_s-T_a relationship is even more complicated in urban canopy environments and more influencing factors need to be considered for empirical statistical modelling.

Previous studies focused on the T_s-T_a relationship are generally based on regression models over urban areas. For example, the night-time T_s-T_a relationship was documented with strong correlations (R^2) in linear regression models from some previous studies (Table 2.1): R^2 value of 0.60 was demonstrated based on the data from stations in Birmingham, UK over summer 2013 (Azevedo et al., 2016). Stronger relationship ($R^2 = 0.92$) between the T_s and the minimum T_a at night-time was found in Casablanca, Morocco, from 2011 to 2012 (Bahi et al., 2016a). The higher correlation of the T_s-T_a relationship is potentially due to the year-around data used by Bahi et al. (2016a), comparing to Azevedo et al. (2016) who considered summer cases only. In reality, a linear T_s-T_a relationship is likely to be significant with high R^2 values because of the large variability of regional-scale background temperature and/or seasonal signals (note: the

"regional-scale" here means the scales larger than the urban area of interest). Specifically, differences between T_s and T_a can be only few degrees comparing to the range of T_s and T_a across seasons during a year. This can result in a much greater magnitude than several degrees typically for $sUHII$ or for $aUHII$, taken as the surface and air temperature after removing the seasonal effects, to some extent. For example, Sheng et al. (2017) found the variation of the T_s - T_a range for a station i (T_s minus T_a , $\Delta T_{s-a}^{(i)}$) between $-1.12℃ \sim 12.92℃$ (14.04℃ differences in maximum) while the range of T_s and T_a are 30℃ and 31℃ respectively. Indeed, this large seasonal variation of temperature is the dominant signal in the T_s-T_a regression models of these previous studies, which can increase the R^2 values for these linear relationships.

Overall, the T_s-T_a relationship is still not fully understood and varies with locations and study periods, despite the significant correlation between these two temperatures found in the literature.

Table 2. 1 Selected previous studies on the T_s-T_a relationship in urban areas. NB: a.g.l, above ground level.

Study	Study area and period	T_s and T_a Data	Additional considered parameters	Temperature range (at night-time)	Derived R^2 (Nighttime)	Key findings
(Bahi et al., 2016b)	Casablanca, Morocco; 2011-2012	T_s: MODIS Terra (MOD11A1) T_a: 9 weather stations (2 m a.g.l)	Day length, seasons, day/night	Not available	T_s~$T_{a(min)}$: 0.92 T_s~$T_{a(max)}$: 0.83	(a) Significant T_s-T_a correlation at nighttime; (b) Stronger relationship by separating data in summer and winter
(Azevedo et al., 2016)	Birmingham, UK; Summer (June, July, August), 2013	T_s: MODIS Aqua (MYD11A1) T_a: BUCL: 82 air temperature sensors and 25 automatic weather stations (3 m a.g.l)	Day/night, land use types	T_a: 11℃ ~ 14℃ T_s : 8℃ ~ 12℃ $\Delta T_{s-a}^{(i)}$: − 0.7℃ ~ 3.2℃	T_s~T_a: 0.6 T_s~T_a : 0.8 ~ 0.99 $(single\ station)$	(a) Strong relationships in both day and night at neighbourhood scale but negligible relationship at city scale; (b) Stronger relationship at nighttime; (c) T_s and T_a are more dependent on land surface characteristics and advection, respectively
(Tomlinson et al., 2012)	Birmingham, UK; Summer (June, July, August), 2010	T_s: MODIS Aqua (MYD11A1) T_a: 28 sites with two iButtons for each site	Land cover data from MODIS	T_a: 12℃ ~ 22℃ T_s : 9℃ ~ 12℃ $\Delta T_{s-a}^{(i)}$: 1.67℃ ~ 6.39℃	T_s~T_a : 0.51 ~ 0.95 $(single\ station)$	(a) No clear relationship at city scale; (b) Strong relationship at neighbourhood scale and the relationship varied between each station

Numerous studies have focused on the influences induced by advection (Nichol et al., 2009, Bassett et al., 2016, Bassett et al., 2017, Shiflett et al., 2017) atmospheric stability (Azevedo et al., 2016), land use types (Tomlinson et al., 2012, Xu and Liu, 2015), and seasonal variation (Sheng et al., 2017, Bahi et al., 2016a) during daytime and night-time conditions. It is expected that the T_s-T_a relationship is more significant during night-time due to the negligible impacts from solar radiation in urban environments (Sheng et al., 2017). Moreover, this study showed that T_a is more affected by different land covers at night and the correlation between T_s and T_a is improved during night-time when microscale advection is reduced. Likewise, Tomlinson et al. (2012) also presented the T_s-T_a relationship using Aqua MODIS observations and paired iButton air temperature loggers from 28 sites, with consideration of land use types across the city of Birmingham, UK. The impact of atmospheric stability on the UHI development was highlighted in their study. Azevedo et al. (2016) investigated the T_s-T_a relationship from Aqua MODIS and a UMN for both daytime and night-time in Birmingham, UK. In this study, higher correlations were found at night-time. However, the relationship became negligible at the neighborhood scale (when the focus shifted to each weather station rather than the whole city). It was thereby suggested that the T_s-T_a relationship varies spatially over urban areas (e.g. different LCZs). Meanwhile, this study pointed out that the T_s and T_a are more dependent on land surface characteristics and advection respectively.

Limited studies have investigated the impacts of different seasons on the T_s-T_a relationship in urban environment. Stronger T_s-T_a relationship was found in summer and winter in Casablanca, Morocco (Bahi et al., 2016a), while the weaker relationship was found during hot seasons in four cities, Zhejiang province, China (Sheng et al., 2017). Overall, the literature provides convincing findings regarding the causative factors

affecting the T_s-T_a relationship, which is of vital importance to future research. However, less clear interpretation (e.g. physical explanations) existed in the discussed studies, and the complicated urban environments and limited studies induce different results and the ambiguous T_s-T_a relationship in different cities.

Consideration of the SEB is a typical representation of the physical processes for surface-air temperature modelling over urban environments. For instance, Hou et al. (2013) proposed a model for estimating T_a based on the SEB and applied the approach in Beijing, China, where the model estimation of mean temperature had an error of 2.2℃ at midnight. This model used the following data: T_s from Landsat TM, the aerodynamic resistance from the roughness length data, the Bowen coefficient from NDVI, normalised difference water index (NDWI), and the Q_H from MODIS. Likewise, Sun et al. (2005) calculated the T_a based on SEB using the T_s from MODIS, vegetation index and a resistance over the north China Plain. Comparing all the studies without the consideration of physical processes, the methods used are generally universal and have the potential to be implemented elsewhere where in situ observations exist.

In summary, the T_s-T_a relationship becomes more complex and uncertain for urban areas. Previous studies focused on the rural non-canopy and vegetation canopy environments have made a contribution to the understanding of the T_s-T_a relationship in urban environments, in according to the development of the data retrieval and analysis methods and additional considerations of different influencing factors. However, the empirical statistical approach is yet to derive a satisfactory T_s-T_a relationship at this stage although there is a lack of representation of physical mechanism for land-atmosphere interaction. However, there is no doubt that the T_s-T_a correlation is clearly presented by

this method based on multiple specific equations to derive T_a from T_s. Therefore, the empirical statistical approach may still be adopted to demonstrate the characteristics of the T_s-T_a relationship on the case-by-case basis. More importantly, the large range of the daily or seasonal variation of temperature present studies from investigating the real differences between the T_s and T_a that can be submerged in it. Further research is needed to minimise this effect in the T_s - T_a relationship, e.g. investigating $sUHII$ - $aUHII$ relationship instead which will be further discussed in Section 2.6.

2.5.3 Numerical modelling

The interactions between the land surface and atmosphere inside the UBL is ultimately non-linear and means that the T_s-T_a relationship will never be fully explained by empirical statistical methods. Numerical modelling provides an alternative process-based approach on the basis of MOST and SEB parameterisations for the atmospheric boundary layer, possibly coupled with flow dynamics (Best et al., 2006). The energy transfer via heat fluxes between surface and atmosphere by incorporating temperatures (modelled surface and air temperature) can be estimated in numerical models. It would therefore be beneficial to provide evidence relating to the physical processes when studying the T_s-T_a relationship.

Numerical models generally incorporate both atmospheric models and urban canopy models (UCM) over urban areas. As many of the atmospheric models do not have enough spatial resolution to account for the change of dynamics and thermodynamics by urban structures (Boybeyi, 2000) urban canopy schemes (i.e. UCM) have been developed to approximate the impacts from urban elements. In general, an atmospheric model can provide the upper boundary conditions (such as air temperature, humidity and wind

velocity) to urban schemes in the UCL. Meanwhile, urban schemes can provide the turbulent heat, momentum, moisture fluxes within the UCL to atmospheric models. To a large extent, UCMs are used to explicitly provide detailed information of urban morphology and energy exchanges within UCL, and to be connected to an atmospheric model to represent the interaction between land surface and atmosphere in urban environments. Various parameterisations of urban environments can be grouped into two primary categories (Grimmond et al., 2010)— single layer urban canopy model (SLUCM) and multi-layer urban canopy model (MLUCM). In general, SLUCM has the advantage of simplicity and transferability whereas MLUCM has the detail to represent the urban heterogeneities even at street level.

However, numerical models are not designed to unravel the T_s - T_a relationship because of the distinct definitions of the modelled air ($T_{a,m}$) and surface temperature ($T_{s,m}$) from the observations (i.e. T_s and T_a). Using SLUCM (Masson, 2000) as an example, T_s can be different from $T_{s,m}$ because T_s is taken as the integrated temperature from all the urban components (such as roof, road, and wall) as well as non-urban components (such as vegetation and bare land) in each grid cell. In order to compare with the T_s, it is necessary to incorporate the contributions from non-urban components. The calculated $T_{s,m}$ considers a simpler constitution of the urban elements in a grid. For example, $T_{s,m}$ is an integrated temperature according to the percentage of urban (considering surface temperatures of wall, roof and ground which are modelled as prognostic variables based on energy balance equations) and non-urban areas. $T_{a,m}$ in SLUCMs is a diagnostic variable calculated based on $T_{s,m}$, representing the average air temperature of the urban surface, with consideration of the total heat flux and interaction with atmospheric model. Consequently, there should be a difference between the T_a and

$T_{a,m}$ since T_a is the air temperature at a specific height (i.e. 2 m a.g.l) whereas $T_{a,m}$ represents the canyon-averaged temperature. Therefore, a case can be made that numerical models are best used as a secondary method to provide physical evidences to study the empirical T_s-T_a relationship.

2.6 Modelling of the $sUHII$-$aUHII$ relationship

As discussed in Section 2.5.2.3, linear models based on the T_s and T_a are insufficient to reveal the 'true' T_s-T_a relationship and of limited use to estimate $aUHII$ from T_s.The smaller variability of the differences between T_s and T_a due to different atmospheric conditions or land surface properties would be submerged in the seasonal variability (or regional-scale background temperature variability) and the physical processes determining the T_s-T_a relationship would become unclear and difficult to investigate. In contrast, a direct investigation of the $sUHII$-$aUHII$ relationship is expected to minimise the impact of background temperature variability and/or seasonal signals, which are subsequently cancelled out in their definitions (i.e. temperature differences between urban and rural areas). Meanwhile, the exploration of the $sUHII$-$aUHII$ relationship is more directly linked to the urban effects on the local climate. More importantly, the generalisation of the $sUHII$-$aUHII$ relationship would become more promising across different cities.

Table 2.2 lists the previous studies that focused on the comparison of the differences between $sUHII$ and $aUHII$ or building the $sUHII$ - $aUHII$ relationship based on regression models during the night-time period. Due to the ad-hoc distribution of weather stations over urban areas, screen-level T_a was estimated based on satellite and other auxiliary data directly to generate $aUHII$ and compare its magnitude (seasonal or

monthly) and spatial distribution with $sUHII$ from most of the previous studies. For example, Li and Zha (2019) compared the spatial patterns between the $aUHII$ and $sUHII$ at national scale (32 cities in China) using estimated T_a data obtained via a random forest regression model with consideration of T_s from MODIS and other parameters (e.g. night-time lights, enhanced vegetation index, digital elevation model data etc.). Likewise, $aUHII$ data were generated to compare with $sUHII$ based on the estimated T_a from MODIS land surface temperature products by using linear regression models (Sun et al., 2015) or from the radiance and reflectance products from MODIS (Anniballe et al., 2014). These studies have generally reported a similar spatial pattern between $sUHII$ and $aUHII$ with relative high correlation; for example, a R^2 of 0.81 was found from 32 cities in China (Li and Zha, 2019). However, as mentioned previously, the strong correlation between T_s and T_a could be attributed to the large variation of background temperature. $aUHII$ estimated from the empirical relationship between T_s and T_a is lack of confidence to further compare with $sUHII$. In contrast, an exploration of the $sUHII$ - $aUHII$ relationship based on T_a directly derived from weather stations or UMNs is suggested to provide more accurate information about this relationship and the differences between the surface and the canopy layers.

Regarding temporal variations, comparisons between $sUHII$ and $aUHII$ are mostly based on mean values, e.g. seasonal mean and annual mean (Hu et al., 2019, Li and Zha, 2019). These studies generally make a conclusion of the good agreement between $sUHII$ and $aUHII$. Notwithstanding, the averaged comparison can potentially smooth the noise and reduce the disparity between two variables. Alternatively, a direct comparison (e.g. time by time, pixels to stations) present an alternative means to showcase the true differences between $sUHII$ and $aUHII$ despite the dependence on the availability of the

satellite observations. A comparison of the spatial pattern is normally based on the interpolation of the ground observation (i.e. $aUHII$) or spatial mean of both $sUHII$ and $aUHII$ in specific days (Rivera et al., 2017, Anniballe et al., 2014, Chow et al., 1994), as a result of limited urban stations in most of the cities. Likewise, it may induce uncertainties and the true relationship may become compromised by using interpolation or averaged methods.

In summary, research with regard to the modelling of the $sUHII$- $aUHII$ relationship is typically based on empirical models from the literature. As no two cities are alike, it is more appropriate to build up this relationship city by city, which is useful and necessary to understand the characteristics of UHI for each city. In doing so, the influences of the causative factors (e.g. meteorological factors and land surface properties) on $sUHII$- $aUHII$ relationship need to be investigated fundamentally by case studies in cities with good observational data from UMNs (e.g. Birmingham, UK and Oklahoma City, US). The comparisons of this relationship are then conducted with consideration of the diverse local climate and response to the causative factors from the previous step across different cities.

Table 2. 2 Selected previous studies related to the comparisons between $sUHII$ and $aUHII$ during night-time.

Study area	Study period	Temperature Data	Method used to compare $sUHII$ to $aUHII$	Considered parameters	Key findings
Three cities in China (Hu et al., 2019)	2003-2016	T_s: MYD11A2 and MOD11A2 T_a: 8 stations in Beijing; 7 stations in Shanghai; 4 stations in Guangzhou	Magnitude comparison (annual mean, without separating daytime or night-time cases)	Season; Humidity; Precipitation	--
32 Cities in China (Li and Zha, 2019)	2009	T_s: MYD11A2 T_a: estimated from the random forest regression model by considering the following parameters: enhanced vegetation index (EVI), night-time lights, land-use types, digital elevation model (DEM) and T_s	Spatial pattern comparison by considering spatial mean UHI	Season	(i) LRM ($aUHII = 0.52 * sUHII + 0.03$) of annual mean $aUHII$ on $sUHII$ with R^2 of 0.81 at national scale (based on the data from all 32 cities) (ii) Lower correlation between $aUHII$ and $sUHII$ in summer compared other seasons as a result of larger stored heat flux during summer period
Toluca, Mexico (Rivera et al., 2017)	2014	T_s: Landsat 8 (4 images) T_a: 11 stations	Magnitude and spatial pattern comparisons	Season (dry and wet)	$sUHII$ and $aUHII$ are well correlated with soil moisture, particularly during dry seasons (spring and winter)
Birmingham, UK (Azevedo et al., 2016)	June, July and August in 2013	T_s: MYD11A1 T_a: UMN: 82 air temperature sensors and 25 weather stations	Comparison of the Spatial distributions between the mean $sUHII$ and mean $aUHII$ under different atmospheric stabilities	Atmospheric stability based on Pasquill-Gifford classification	(i) Both $sUHII$ and $aUHII$ are both stronger under stable conditions

					(ii) Similar spatial patterns between the $sUHII$ and $aUHII$ are found
Beijing, China (Sun et al., 2015)	2009-2010	T_s: MOD11A1 and MYD11A1 T_a: estimated from T_s based on linear regression model (T_a = a*MOD11A1+b*MYD11A1+c, where a, b, c are the corresponding regression coefficients)	(i) Spatial distribution based on one-day data (ii) Temporal variation comparisons based on the daily average UHI across whole year	season	(i) No significant seasonal differences between the $sUHII$ and $aUHII$ (ii) Similar spatial patterns between the $sUHII$ and $aUHII$ are found
Milan, Italy (Anniballe et al., 2014)	June to September between the years 2007 and 2010	T_s: MOD11A1 and MYD11A1 T_a: estimated from the level 1B MODIS radiance and reflectance products	(i) Spatial distribution comparisons between the mean $sUHII$ and mean $aUHII$ by using Gaussian surface (ii) Comparison of the relationship with the normalised difference vegetation index (NDVI) between $aUHII$ and $sUHII$	NDVI	(i) $aUHII$ has similar features to $sUHII$, e.g. similar magnitude and orientation (ii) Correlation coefficient between $sUHII$ and $NDVI$ is stronger than the one between $aUHII$ and NDVI based on the mean values of the UHII ($sUHII$ and $aUHII$) during summer 2008
Birmingham, UK (Zhang et al., 2014)	2002 – 2007	T_s: MYD11A1 T_a: single urban and rural station	(i) Comparisons of the monthly mean value of $aUHII$ with $sUHII$ (ii) LRM of $aUHII$ to $sUHII$ based on all data (all stations)	(i) Classify UHI based on lamb weather types (ii) Season	(i) Seasonal variations of the magnitude of $aUHII$ and $sUHII$ are not significant (ii) LRM: $aUHII = 0.55 * sUHII + 1.75$, R^2=0.18

Mexico city, Mexico (Cui and De Foy, 2012)	2006	T_s: MYD11A2 and MOD11A2 T_a: single urban and rural station	Temporal (monthly) comparison	Wet and dry seasons	(i) Similar seasonal trend of $aUHII$ and $sUHII$ is observed; (ii) $aUHII$ is more affected by atmospheric stability while $sUHII$ is strongely detetmined by the vegetation cover and daytime insolation
Milan, Italy (Pichierri et al., 2012)	2007-2010	*Ts:* estimated based on the multiple linear regressions between Ta and radiance/reflectance products from MODIS (MOD021KM/MYD021KM) *Ta:* 6 weather stations (3 urban and 3 rural stations)	Temporal (daily) comparisons between the $sUHII$ and $aUHII$ on 25/07/2010	--	Daily patterns of $sUHII$ and $aUHII$ are consistent to each other
Shanghai, China (Chow et al., 1994)	20:00PM, 1984	T_s: MYD11A2 T_a: Single paired of urban and rural station	Spatial pattern comparison in specific days	--	$aUHII$ is spatially relate to $sUHII$

2.7 Data and methods

The ambition of generalising the $sUHII$ - $aUHII$ relationship across cities (or globally) will result in a better understanding of the UHI. It will further facilitate the development of approaches to study and utilise this heat effect to improve human's life in urban environment for every city. As previously mentioned in Section 1.3, the process for this goal fundamentally includes: (i) define the influencing factors of the UHI ($sUHII$ and $aUHII$) and their corresponding physical mechanisms; (ii) explore the characteristics (i.e. temporal or spatial) of the $sUHII$ - $aUHII$ relationship with considerations of the influencing factors from (i) in some case studies; (iii) Compare and generalise peculiar characteristics of the $sUHII$-$aUHII$ relationship between two cities and attribute the differences to the climatic and urban structures of these two cities, which provides evidence or guidance for further comparisons until the goal has been achieved. This three-step is implemented in Chapters 3-5 and follows the workflow in Figure 1.3 in order to achieve the aim in this thesis, which will be further introduced as follows.

This literature review has demonstrated the comprehensive nature in which the key factors controlling the $sUHII$ and $aUHII$ have been studied (Oke, 1982, Arnfield, 2003, Voogt and Oke, 2003, Rizwan et al., 2008, Mirzaei and Haghighat, 2010). Therefore, there exists sufficient support by efforts from previous research for the first step regarding the generalisation of the $sUHII$-$aUHII$ relationship. Specifically, atmospheric condition and land surface properties are the key factors that more evidently impact upon the physical linkage between surface and air layers from the literature. Lots of atmospheric variables can be used to represent the atmospheric condition and it is dispensable to evaluate the impacts of these variables on the development of UHI. Regarding the land

surface properties, UCZ or LCZ typologies are now mature enough to universally classify the urban areas into different climate zones. However, a paucity of meteorological data per climate zone remains a major limitation in terms of further classification. As such, at the initial stage of the generalisation process, it appears sensible to simplify this step into suburban / urban. In addition, there are some requirements regarding the satellite products used to estimate the $sUHII$. It is better to choose the satellite with comparatively high temporal and moderate spatial resolution in order to compare with $aUHII$ calculated based on the T_a data from UMNs, e.g. MODIS satellite.

Regarding the second stage of the generalisation process, several concerns need to be carefully considered. Firstly, an appropriate method to study the $sUHII$ - $aUHII$ relationship needs to be selected. Numerical and empirical models have been shown to be the two main approaches for studying this relationship. Numerical models are preferable to provide the evidence for energy transfer in the processes of the surface-air interaction. However, it is not desirable to build up the $sUHII$-$aUHII$ relationship by using the modelled air and surface temperatures. The primary concern is about the accuracy of such models and limited confidence due to limited observations. In contrast, empirical methods are based directly on the observations which are readily to be applied. Although the derived relationship or values are subjective to location and time, without providing relevant physical processes, the stratifications of the data and the intercomparisons of the derived relationship under specific conditions defined by physical parameters are also promising for generalising the $sUHII$-$aUHII$ relationship. There is also an additional need to develop a statistical method with regard to the comparisons of the $sUHII$-$aUHII$ relationship under specific conditions (i.e. atmospheric

stability and land surface properties). It needs to be easily transferable to other cities in order to accomplish the generalisation in the third stage.

For the third, intercomparison stage, the local climate effects on the UHI become one of the biggest challenges in generalising the $sUHII$-$aUHII$ relationships. This is difficult to isolate using statistical methods but sensitivity tests using numerical models might be a prudent approach. Otherwise, comparisons under specific atmospheric conditions are needed to minimise these effects. Furthermore, the different settings of the weather stations or UMNs are also largely responsible for the differences of the $sUHII$-$aUHII$ relationships across cities because of its impacts on the data sample (i.e. T_a and T_s). However, these impacts are still unclear and future work is required to establish these fundamental knowledges in order to achieve the generalisation of the $sUHII$-$aUHII$ relationships globally.

Overall, as highlighted, the paucity of measurements in urban areas remains a major issue in developing a universal approach. It is clear from the literature review, that the greatest recent advances in the area have occurred due to the increasing use of UMNs in deriving insights. As such, this thesis will focus on data from two UMNs. In the following sections, general descriptions of the ground observations (the two UMNs) are firstly introduced, following by the satellite data used in this thesis, data processing and the computation of $sUHII$ and $aUHII$.

2.7.1 Ground observations

2.7.1.1 Birmingham

The ground observations are retrieved from the Birmingham Urban Climate Lab (BUCL) and Met Office during the period from 01/06/2013 to 31/08/2014 (due to the

data availability) over Birmingham. Part of BUCL included an installation of 24 automatic weather stations with sensors at 3 m a.g.l across the whole city (more details in Chapman et al. (2015)). These 24 Vaisala WXT520 weather stations measure seven atmospheric variables including air temperature, precipitation, wind speed and wind direction etc. with average spacing of 3 km and a high-quality control. These seven variables are sampled every 15 seconds and an average produced each minute (Warren et al., 2016). Two additional UK Met Office weather stations complement the network (Paradise Circus and Coleshill stations), with temperature data from Paradise Circus station being particularly useful due to its location in the middle of the central business district (shown in Figure 2.1). The temperature and wind are hourly measured at 1.25 m and 10 m a.g.l at Met office sites, respectively. Overall, the temperature data from 20 BUCL weather stations are used (4 stations are excluded because they are sited outside the city and over more vegetated areas) located within the city limits and the one station from UK Met Office over urban areas. The Coleshill station (Figure 2.2) is located outside the city, and as per other UHI studies (Tomlinson et al., 2012, Azevedo et al., 2016) in Birmingham and it is chosen to be the rural reference site (or urban background) for temperature, wind speed, relative humidity, daily accumulated solar radiation and cloud data in this thesis.

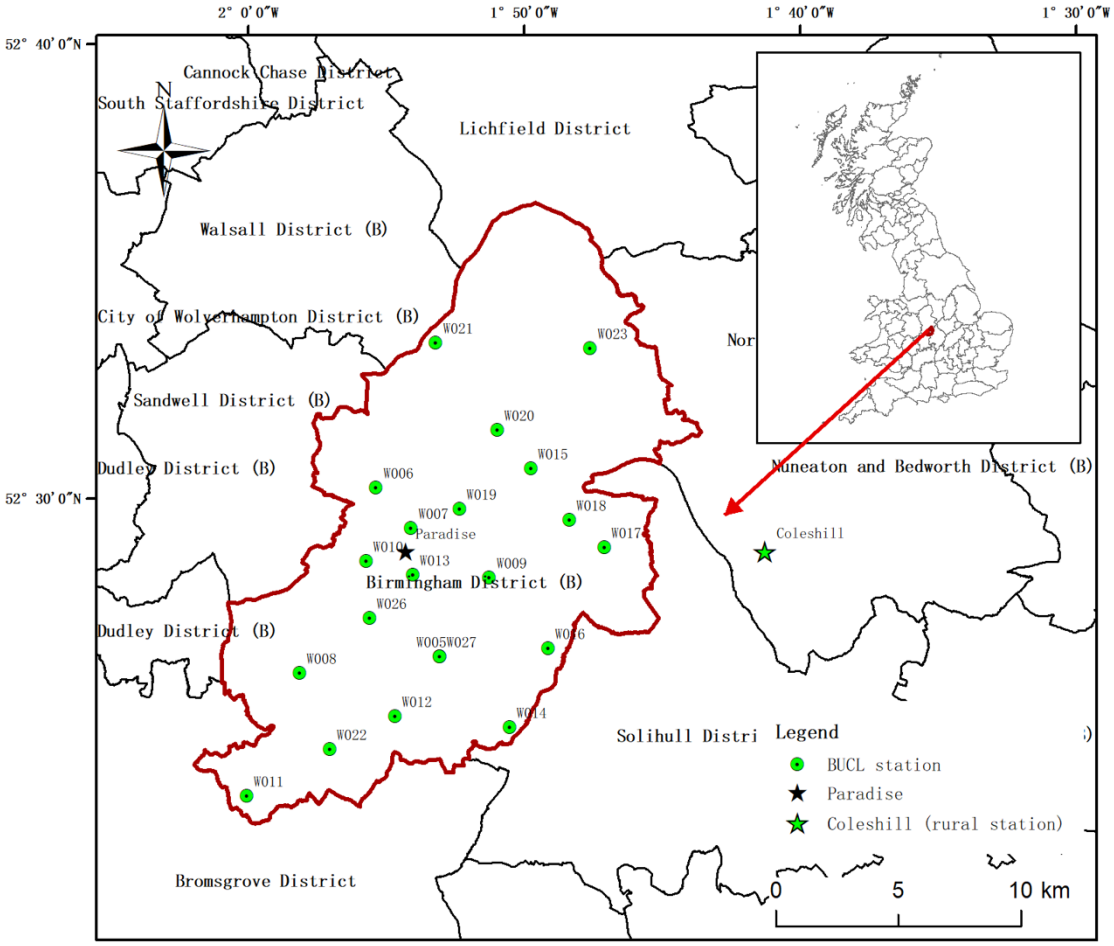

Figure 2. 1 Location of BUCL stations(source of boundary data: Ordnance Survey (2014))

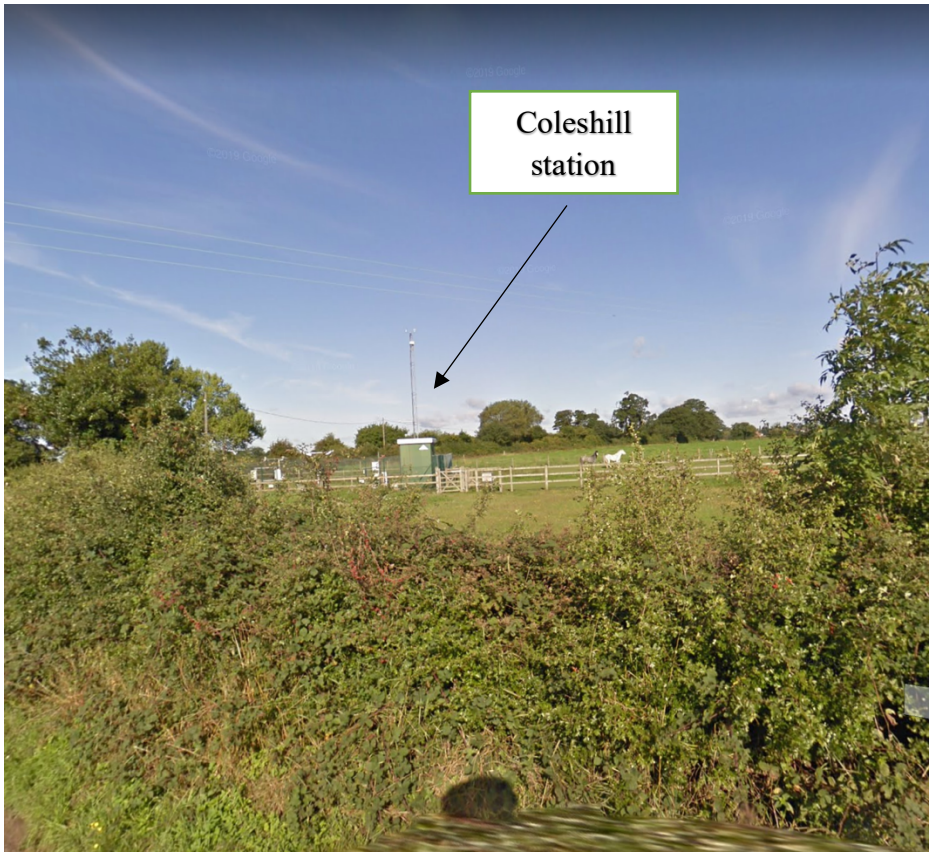

Figure 2. 2 Location of Coleshill station from Google street map

2.7.1.2 Oklahoma City

The air temperature data over urban areas are derived from the Oklahoma City Micronet (OKCNET) which was deployed since 2008 to provide high-quality atmospheric observations in near real-time in OKC. This dense network consists of 36 robust automatic weather stations (using the WXT510 sensors) mounted on traffic signals at a height of 9 m, with an average spacing of about 3 km across OKC metropolitan area. Site selections are constrained by the OKC WIFI access points and data are measured at minute resolution. Due to the data availability, 33 stations shown in Figure 2.3 are chosen to represent the urban thermal conditions over OKC during the period from 01/01/2009 to 31/12/2010.

Regarding the urban background reference, SPENCER station, part of the Oklahoma Mesonet network, which serves as the dense network for monitoring the surface-layer meteorological condition at mesoscale across the state, is considered as rural reference to provide the background temperature, wind and humidity conditions that are measured at an interval of 5 minutes over OKC. It is located within a fenced 100 m^2 plot of land close to the rural area but within the city limits (Figure 2.4). Temperature and wind are measured at two different height levels – temperature at 1.5m and 9 m, wind at 2 and 10 m. Other sensors (e.g. humidity, pressure, solar radiation etc.) are mounted on or near a 10 m tower (Basara et al., 2011).

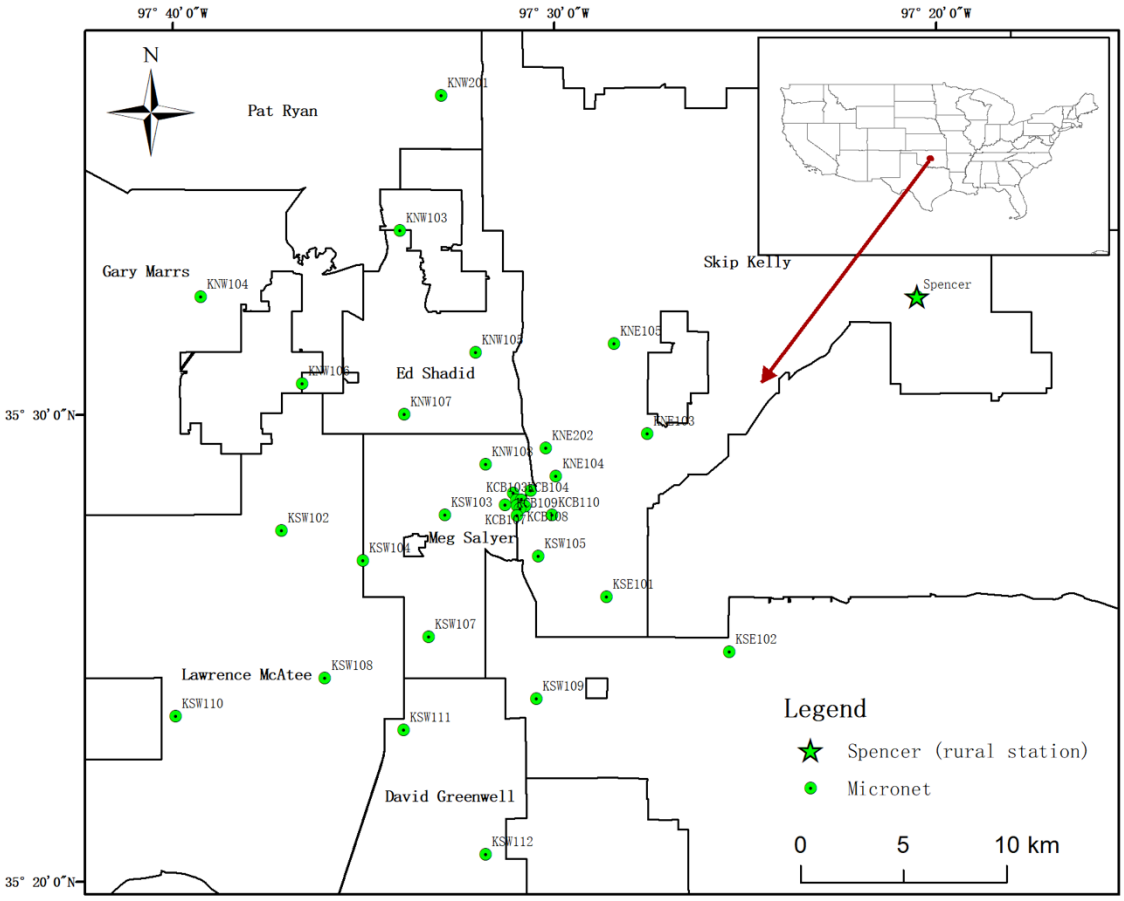

Figure 2. 3 The location of OKCNET stations

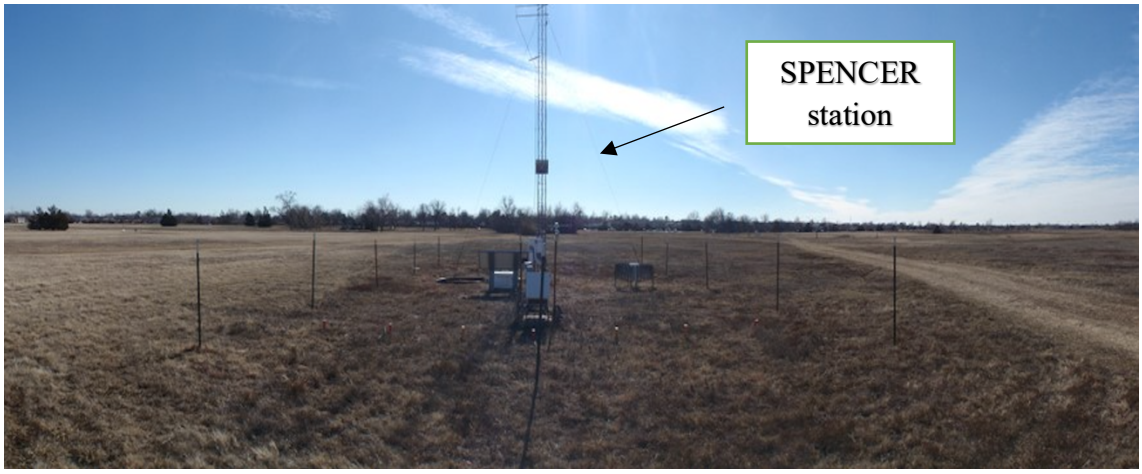

Figure 2. 4 Location of Spencer station (available from http://www.mesonet.org/index.php/sites/site_description)

2.7.2 Satellite observations

The following satellite products from Moderate Resolution Imaging Spectroradiometer (MODIS) are used in this project (all available from: https://modis.gsfc.nasa.gov/data/), which are processed in ArcGIS 10.4.1 and the projection is converted from the Sinusoidal projection to WGS 1984 Web Mercator Auxiliary Sphere over OKC and to British National Grid over Birmingham respectively.

I. Yearly land cover types product (MCD12Q1) with approximate 500-m spatial resolution

II. Night-time daily land surface temperature (T_s) products in version 5 (V005) from MODIS onboard Aqua (MYD11A1) and Terra (MOD11A1) satellites with approximate 1-km spatial resolution (926.63 m);

III. Normalised Difference Vegetation Index (NDVI) from the vegetation index product from MODIS onboard Aqua (MYD13A2) and Terra (MOD13A2) satellites;

According to the land cover types product, it is derived in the year of 2010 over OKC and in the year of 2014 over Birmingham, in order to present the land surface characteristics across these two cities.

The T_s dataset is developed based on the generalised split-window algorithm from the two thermal infrared bands of MODIS (bands 31: $10.78 - 11.28\,\mu m$ and 32: $11.77 - 12.27\,\mu m$) (technical details for the MODIS product can be found in Wan (2007)). The MYD11A1 and MOD11A1 are stored in a hierarchical data format (HDF) including 12 scientific datasets such as day and night-time T_s, satellite overpassing time and view zenith angle etc (Wan, 2006). Although they are pre-filtered by the cloud mask (the pixel is cloud-free if it has the grid value for T_s), Wan (2008) stated that cloud contamination still exists in the V005 products since the cloud-removing scheme is unable to remove the contaminated pixels under light and moderate cloud conditions. The contaminated pixels usually refer to the extreme low temperature at the top of clouds (Mutiibwa et al., 2015). Therefore, the selection of the satellite data is restricted to images with no missing value or extreme T_s value over the study areas. Moreover, cloud cover data measured from ground observations (cloud data derived at Coleshill station in Birmingham and at four Oklahoma ASOS stations [available from: https://mesonet.agron.iastate.edu/]) have been utilised to double-check the cloud conditions and further quality control the satellite data.

NDVI products from MODIS are retrieved to approximate levels of greenspace in the vicinity of each station, which has been widely used in previous studies (Montandon and Small, 2008, Li and Liu, 2008, Grover and Singh, 2015). NDVI is one of the subdatasets of the MODIS vegetation indices product (MYD13A2 and MYD13A2) with 1 km spatial resolution and 16-day temporal resolution. The calculation of the NDVI is

based on a filter with consideration of cloud cover and viewing geometry etc. which enables to retrieve the NDVI with good quality (Van Leeuwen et al., 1999). It is noted that a simple linear averaging method is used to generate daily NDVI data by using the two 16-day NDVI products as they contain an 8-day overlap.

Likewise, the satellite data (T_s and NDVI) are derived from 01/01/2009 to 31/12/2010 over OKC and from 31/06/2013 to 31/09/2014 over Birmingham. Table 2.3 provides a summary of the available satellite data of T_s across the two cities. Data from Aqua and Terra satellites are combined for the analysis due to the limited sample size, which is further discussed in Section 2.7.3.

Table 2. 3 Summary of the available satellite imageries and sample size across OKC and Birmingham. NB: total sample size from all stations is based on the availability of T_s and T_a from each station.

City	Study period	Available imagery from Aqua Satellite	Available imagery from Terra Satellite	Total sample size from all stations (Combine two satellites)
OKC	01/01/2009 - 31/12/2010	52	83	4034
Birmingham	31/06/2013 - 31/08/2014	63	88	2316

2.7.3 Data processing

This section will introduce the pre-processing of the T_s and T_a data and the way to compute the $sUHII$ and $aUHII$. There are two primary concerns that need to be considered for comparing or investigate the relationship between the $sUHII$ and $aUHII$, including the temporal and spatial consistency between T_s and T_a, which will be discussed in the following two sections, respectively.

2.7.3.1 Temporal consistency between T_s and T_a

There are two available daily night-time observations (T_s) from MODIS with approximate overpass times of 01:30 (Aqua satellite, from north to south) and 22:30 (Terra satellite, from south to north) local solar time across the equator. However, the overpassing time does vary day by day and their achieves can be accessed at *https://www.ssec.wisc.edu/datacenter/*. The differences between actual overpassing time and the approximate equatorial overpassing time for OKC and Birmingham are compared (Figure 2.5). As the mean differences are about within an hour for both satellites, the overpassing time of Aqua and Terra satellites are assumed to be the same as the ones crossing the equator and the variations of the real overpassing time are not considered in this project. As introduced in Section 2.7.1, the T_a is collected at every 1-minute from OKCNET and is sampled at every 15 sceonds from BUCL. On the basis of the small difference between local solar time and local time over the two cities, the T_a dataset in this study is calculated as the hourly average values of the T_a (01:00 - 02:00 for Aqua and 22:00 - 23:00 for Terra satellite) to achieve the temporal consistency between satellite and ground measurements.

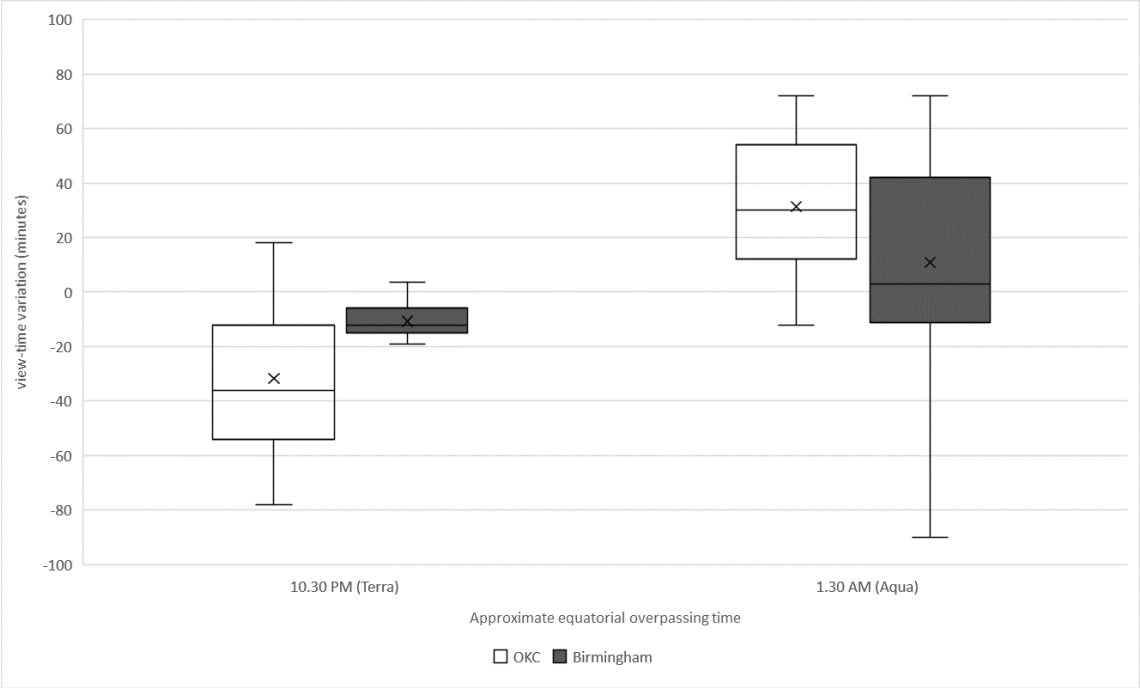

Figure 2. 5 Differences between the actual overpassing time and the approximate equatorial overpassing time for Aqua (~01.30 AM) and Terra (~10.30 PM) satellites over two cities, where the cross symbols are the corresponding mean differences

As previously mentioned, the differences of the T_s observed from Aqua and Terra satellites or the T_a collected from ground measurements are not considered in this project, which are combined to increase the sample size. There are two types of evidence supporting this combination. Firstly, the corresponding linear relationships between T_s and T_a at the acquisition time of Aqua and Terra satellites are similar over OKC：

$Aqua: T_a = 0.89 * T_s + 5.05, R^2 = 0.97, N = 1569;$

$Terra: T_a = 0.86 * T_s + 6.56, R^2 = 0.95, N = 2465;$

and Birmingham:

$Aqua: T_a = 0.93 * T_s + 2.17, R^2 = 0.95, N = 957;$

$Terra: T_a = 0.90 * T_s + 1.83, R^2 = 0.97, N = 1359;$

Although there are about 1.5 K differences (indicated by intercept values in regression model) between estimated T_a from Aqua and Terra satellites, the subtraction method for quantifying the UHI (temperature differences between urban and rural sites) will further minimise the differences between the two satellite. It therefore provides confidence to combine the data from these two satellites for the further analysis. Indeed, the overpassing time of Aqua and Terra satellite is approximately three hours apart, which could potentially cause the different UHII (both air and surface) particularly during summer period. However, previous research found that the $aUHII$ will increase rapidly during the early evening transition period that has been found to be 19:00-20:00 in OKC during April 2009 – October 2010 (Hu et al., 2016b). After that, $aUHII$ will stay at a roughly constant level throughout the night until early the next morning. Therefore, data was combined from both Aqua and Terra satellites to increase the sample size.

2.7.3.2. Spatial consistency between T_s and T_a

It is difficult to achieve the spatial consistency between point-derived T_a and pixel-averaged T_s, especially over urban areas where the terrain is complex (Oke, 1988a). In-situ sensed T_a is strongly associated with the turbulent source area, whereas remote-sensing T_s is mainly determined by the radiation source areas (Oke et al., 2017). The turbulent source area of T_a cannot be defined confidently using a traditional approach (e.g. a footprint model (Kent et al., 2017)) because the measurement height is within the urban canopy layer. Although the turbulence source area can be local, the selection of the sites considered their representativeness (as best as can be achieved in the heterogenous urban area) of microclimatic environments of the area on a neighbourhood scale ($\lesssim$ 1 km), which is about the spatial resolution of the satellite data of T_s. Some previous studies have

investigated the spatial variability of T_a by comparing the correlations between T_a and T_s estimated from different "window sizes". However, the most appropriate spatial scales of T_a varied in different study areas. For example, 200 m, 450 m and 700 m were found to be the most appropriate spatial scale of T_a for urban, suburban and rural areas respectively, in Hong Kong, China (Nichol and Wong, 2008). Although spatial variability is not a key aim in this project, a simple correction based upon Inverse Distance Weighting (IDW) is applied to achieve the spatial consistency between T_s and T_a.

The IDW interpolation has been widely adopted to estimate the spatial distribution of some variables such as rainfall (Teegavarapu and Chandramouli, 2005) and temperature (Greenberg et al., 2011) etc. based on the data at some given points (e.g. weather station). Herein, a 500-metre radius buffer is created for each weather station. The T_s values of the pixels overlapping with the buffer are then adopted to calculate the T_s value at the weather station using the following formulas:

$$\lambda_m = \frac{\frac{1}{d_m}}{\sum_{m=1}^{n} \frac{1}{d_m}} \quad \text{Equation (2.5)}$$

$$T_s = \sum_{m=1}^{n} \lambda_m \cdot T_{sm} \quad \text{Equation (2.6)}$$

where m is the index of the pixel overlapping with the buffer for the weather station, d_m is the distance between the centre of the m-th pixel and the station, λ_m is the weighting coefficient for the m-th pixel, T_{sm} is the land surface temperature for the m-th pixel. Figure 2.6 gives an example to estimate the T_s in a weather station (W026) of BUCL based on the above scheme.

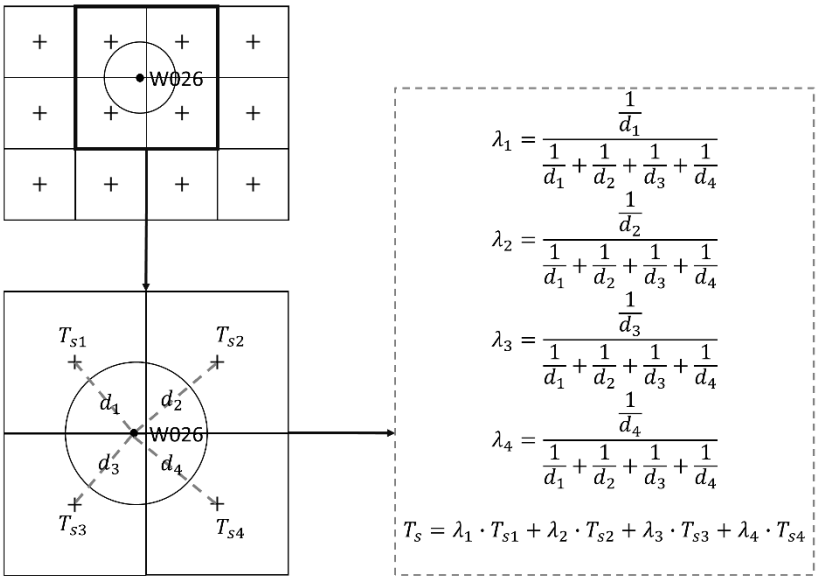

Figure 2. 6 An example for calculation of T_s for a specific station (W026), where the circle represents the 500-m buffer, the cross symbols are the centre of each pixel from satellite imagery, black point is the weather station from BUCL in Birmingham (W026).

2.7.4 Quantification of surface and canopy heat island

$aUHII/sUHII$ is defined as the difference between the temperature from a weather station/pixel located in urban area ($T_a^{(i)}$ or $T_s^{(i)}$) and the temperature from a rural station/pixel ($T_a^{(r)}$ or $T_s^{(r)}$):

$$sUHII = \Delta T_s^{(i)} = T_s^{(i)} - T_s^{(r)} \quad \text{Equation (2.7)}$$

$$aUHII = \Delta T_a^{(i)} = T_a^{(i)} - T_a^{(r)} \quad \text{Equation (2.8)}$$

Here, i represents weather station index in urban areas and r is for the rural station in the study area (Coleshill or Spencer station in Birmingham and OKC respectively). The surrounding environment of the two rural stations have been introduced in Section 2.7.1. $aUHII$ has been found to be sensitive to the wind advection (Bassett et al., 2016), therefore, the rural sites should be chosen with consideration of the prevalent wind

direction. Southernly winds are predominant during the study period over the two cities, while the two rural stations are located in the east of the city centres. Thus, the heat advection from city to the rural stations is taken to be negligible in this thesis. The number and location of stations chosen to be configured in a UMN are meant to be confidently showcase the temperature variation of a city. Data from all stations are then used to formulate the regression models under different conditions. In addition, it could increase the sample size to make the results more reliable.

2.8 Conclusion

This review has given an overview of $sUHI$ and $aUHI$ with respect to their own characteristics, surface-layer and urban canopy processes that impacts upon the UHII, and previous literature regarding attempts of establishing the T_s-T_a and $sUHII$-$aUHII$ relationship. It is clear that the current research has been surrounding of these relationships (i.e. the T_s - T_a and $sUHII$ - $aUHII$ relationship) by using empirical modelling and these relationships vary city by city. There is a significant research gap relating to the characteristics of the $sUHII$-$aUHII$ relationship with consideration of the potential influencing factors. However, as shown in the choice of methods for this thesis, it is now possible to acquire the high-resolution data for both T_s and T_a which could significantly advance our understanding of this relationship. Alongside this, the above review highlights the needs and difficulties to achieve the generalisation of the $sUHII$-$aUHII$ relationship globally.

2.9 Summary

This review clearly illustrates the causative factors (e.g. climate or meteorological factors and surface characteristics) influencing the sUHII-aUHII relationship during

nights. Also, the majority of the approaches used to study this relationship have been summarised and discussed, including their advantages and application limits. This review has important implications for the data analysis in this thesis, because the key element of the thesis is to discover specific characteristics of the sUHII - aUHII relationship in Birmingham, UK (Chapter 4) and compare it to those in Oklahoma City, US (Chapter 5). Both cities have well developed UMNs and thus provide an excellent opportunity to progress this research in two areas of different geography.

Chapter 3 Characterising the Nocturnal Surface and Canopy Heat Islands in Oklahoma City, US according to the Atmospheric Condition

This chapter aims to explore the potential impacts of the atmospheric condition on the magnitude of the surface urban heat island (sUHII) and canopy heat island (aUHII) during night-time. Results from this chapter are used to underpin later analyses in this thesis which investigate the variations of the relationship between sUHII and aUHII under different atmospheric conditions and levels of urbanisation in Chapter 4 and Chapter 5.

3.1 Introduction

The process of urbanisation has inadvertently modified the urban climate. Impacts such as the Urban Heat Island (UHI) well documented in the scientific literature (Stewart, 2011). The importance of the UHI effects on human's lives and the future urban design strategies has been increasingly recognised. There is growing evidence showing that the UHI effect has the potential to intensify extreme climatic events (Patz et al., 2005). For instance, heatwave events could intensity the UHI and increase the heat health risk in cities, resulting in excess deaths (Meehl and Tebaldi, 2004, Gosling et al., 2009, Tomlinson et al., 2011b). There is therefore a continued need to further understand and manage the UHI effect (De Wilde and Coley, 2012).

As discussed in Chapter 2, one of the determinant factors influencing the development of the UHI is the atmospheric stability / state. Stability is used to qualitatively describe the property of the atmosphere based on the controls of the acceleration of the vertical motion of an air parcel (Mohan and Siddiqui, 1998). When the atmosphere is unstable, the acceleration is positive and turbulence increases. It becomes zero in neutral (deceleration) and negative in stable atmosphere (turbulence suppressed). There are seven major stability schemes used to classify the atmospheric stability (details of the definition and calculation of each scheme can be found in Mohan and Siddiqui (1998)): (a) Pasquill-Gifford (P-G) stability system, (b) standard deviation of the horizontal wind direction fluctuation method, (c) temperature gradient method, (d) Gradient Richardson method (Ri), (e) Bulk Richardson number method, (f) Moni-Obukhov length method, and (g) wind speed ratio method. Previous studies have tried to assess the effectiveness of these schemes ((b) to (g)) by comparing with the P-G scheme.

Result indicates the better agreement between the three schemes (including (d), (e) and (f)) and the P-G scheme. However, to the best of our knowledge, there is no study trying to assess their effectiveness based on classifying the characteristics of the UHI. The choice of a particular scheme potentially impacts on the final outcome of the analysis of UHI and a comparative study to find out the key meteorological variables as representation of the atmospheric condition that significantly affects the UHI is needed.

UHI studies of, the relationship with atmospheric stability, mainly use one of the following two methods: (i) synoptic weather type (Kolokotsa et al., 2009, Zhang et al., 2014) and (ii) P-G stability system (Tomlinson et al., 2012, Krüger and Emmanuel, 2013, Azevedo et al., 2016, Drach et al., 2018). The synoptic weather system method is largely dependent on the variations of the surface pressure (i.e. Anticyclonic or Cyclonic) with considerations of wind direction (i.e. southeasterly, southerly, northerly, westerly, southweaterly, northweaterly, easterly, and northeasterly), such as the Lamb weather types (Lamb and HH, 1972). Studies highlighted the strong relationship between the intensity of the UHI (UHII) and anticyclonic conditions. As an alternative, the P-G system is widely used because of its simplicity. It is based on the local surface meteorological conditions, with considerations of insolation and surface wind speed for daytime scenarios and cloud cover and surface wind speed for night-time cases (Turner, 1970). Subsequently, each case is classified into different stability classes which include A-C, D and E-G that represents unstable, neutral and stable conditions respectively (see Table 3.1 for night-time cases).

Table 3. 1 Pasquill-Gifford stability classes during night-time (adapted from Pasquill and Smith (1983) and Chapman et al. (2001))

Surface wind speed measured at 10 m a.g.l (m/s)	Pasquill-Gifford stability class	
	>= 4/8 oktas cloud	<4/8 oktas cloud

<2	G	G
2-3	E	F
3-5	D	E
>5	D	D

Although the P-G system is designed to describe dispersion conditions and never intended to be used as a "stand-alone" system to measure stability (Kahl and Chapman, 2018), it has been shown that the P-G scheme can be confidently used for characterising the temporal variations of the canopy air heat island ($aUHI$) from ground observations and the surface urban heat island ($sUHI$) (Azevedo et al., 2016). As discussed above, there exists many potential variants / improvements to the P-G stability scheme which could provide more quantitative detail on the nature of the atmospheric stability (e.g. the six schemes [b-g]). In order to test the utility of adding additional complexity to the established, but simplistic, P-G scheme, it is necessary to conduct a comparison amongst parameters, including Ri, vertical temperature and wind gradient and parameters used to define P-G scheme in this study (thoroughly introduced in Section 3.2.4), to characterise the UHI. Ri is chosen mainly because previous research disclosed that it gave more reasonable comparisons than the rest of the parameters mentioned above when comparing with the P-G scheme regarding the classification of atmospheric stability (Mohan and Siddiqui, 1998). The considerations of the wind speed and temperature gradients (at two different heights) are largely due to the fact that they can be simply used as estimates of wind generated turbulence and thermal-damping capacity of the turbulence, correspondingly. The other reason is that these two parameters are the determinants of the Ri and it is worth to explore their controls on Ri.

Overall, the aim of this chapter is to find the key meteorological variable affecting the UHI by assessing the effectiveness of the P-G classification scheme and comparing it to four other parameters related to atmospheric condition. This will be achieved by (i)

examining whether the robustness of the P-G classification scheme varies across seasons for characterising the daily mean $aUHII$ and $sUHII$ and determine the key variable impacting upon the UHI; and (ii) exploring the potential impacts of the key variable on the spatial variations of both nocturnal $aUHII$ and $sUHII$ over Oklahoma City (OKC), US, by using both a dense Urban Meteorological Network (UMN) and land surface temperature products from MODIS satellites.

3.2 Methods

3.2.1 Study area

OKC is the study area (Figure 3.1) used in this analysis, as introduced in Chapter 2. It provides a unique opportunity in which to conduct this study due to unique observation instrumentation that enables the measurement of temperature at two different heights at multiple locations across the city (i.e. the suburban areas beyond the CBD are also considered). Previous research into the $sUHI$ in OKC has been limited, while several studies have investigated the magnitude and spatial patterns of the $aUHI$ estimated from the UMNs. For example, the JU2003 (Joint Urban 2003 field experiment) used 13 PWIDS (Portable Weather and Information Display Systems) and 33 HOBO temperature data loggers deployed in and near the CBD to measure the temperatures at 2 m and 9 m a.g.l, respectively between 28 June and 31 July 2003. In this study, Basara et al. (2008) found that the urban environment is consistently warmer than the surrounding rural areas at both the 2- and 9-m heights at night (over 1.5℃ at 9 m and 2℃ at 2 m) whilst an urban cool island was also found during afternoon period over CBD in OKC. A large intra-urban variability in temperature between the urban sites was also found by Basara et al. (2008), compared to the greater spaced rural sites.

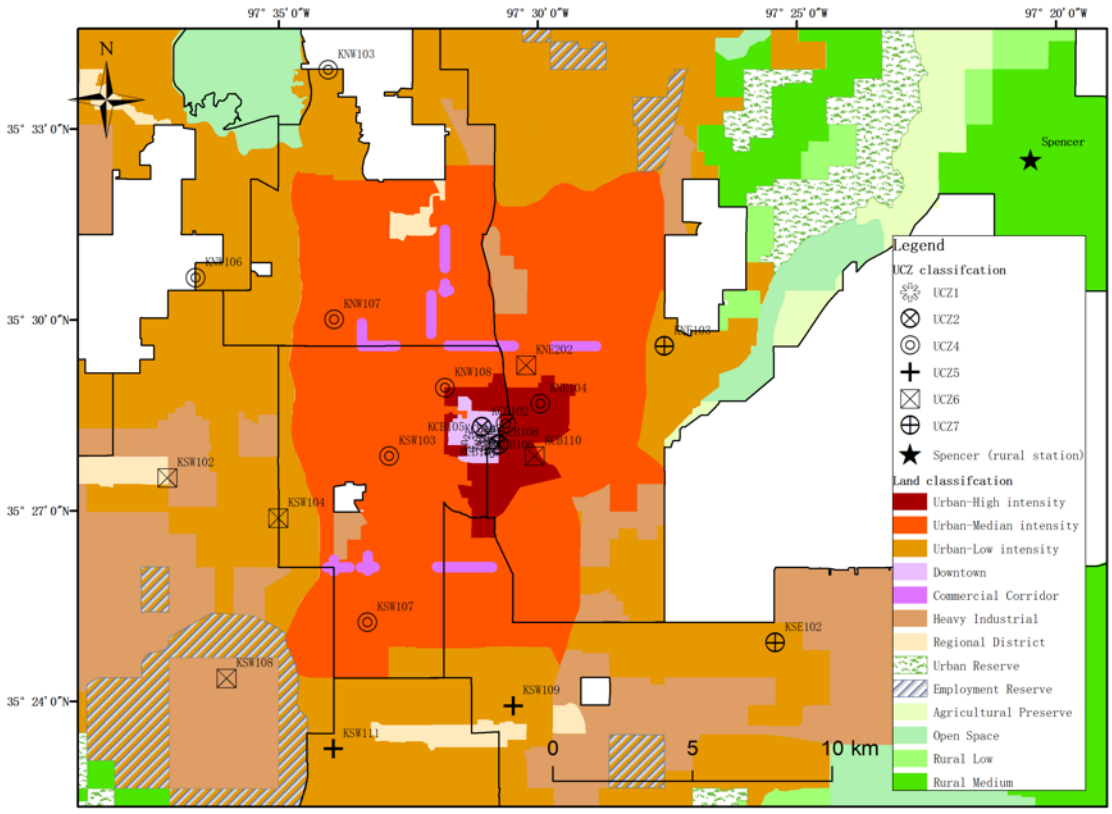

Figure 3. 1 UCZ classification for urban stations used in this study. Note: the land classification shown in the map is from Oklahoma City Council (2020)

3.2.2 Canopy air urban heat island

The definition of canopy air heat island intensity ($aUHII$) is as per Chapter 2. To be consistent with the site classification scheme applied in this analysis (introduced in Section 3.2.5), urban ground observations from the 26 stations and a rural station (Spencer station) shown in Figure 3.1 are used to calculate the $aUHII$ during the period from 01/01/2009 to 31/12/2010. In order to achieve the temporal consistency between ground and satellite observations, T_a measured only during 22:00-23:00 and 01:00-02:00 are considered for the $aUHII$ computation, as introduced in Chapter 2.

3.2.3 Surface urban heat island

The calculation of the nocturnal surface heat island intensity ($sUHII$) uses the same method as introduced in Chapter 2, using the daily land surface temperature (T_s) products (MOD11A1 and MYD11A1) from MODIS aboard the Terra and Aqua satellites. The pre-processing with respect to the spatial consistency between the T_s and T_a follows the method introduced in Chapter 2, simply described as follows. T_s pixels within the 500-m buffer centred on each of the 26 stations are considered for the computation of the $sUHII$ during the same period in which the $aUHII$ is calculated, by applying the Inversed Distance Weighted (IDW) to get an average T_s corresponding to each station. In addition, data processing related to the computation of the $sUHII$, such as quality control of cloud contamination and the combination of both Terra and Aqua satellites etc., is referred to the introduction in Chapter 2 and will not be repeatedly mentioned here.

3.2.4 Atmospheric stability and corresponding meteorological variable

3.2.4.1 Previous studies in OKC

Some previous studies in OKC have tried to consider the impacts of the atmospheric stability on the development of the UHI (i.e. $aUHI$) over OKC. For example, Hu et al. (2013) observed a strong relationship between the strength of nocturnal Low-level jets (LLJs) and the UHI derived from ground observations (2 m and 9 m a.g.l). The increased surface wind speed caused by the LLJs that induces more intense turbulent mixing and reduced atmospheric stability in the nocturnal boundary layer contribute to the weaker $aUHII$. Later, Hu et al. (2016b) found large spatial variability of the nocturnal UHI over OKC between April 2009 and October 2010. This study used Ri, estimated by the temperature differences (9 m and 1.5 m a.g.l), and wind speed differences (10 m and 2 m

a.g.l) at two levels from seven rural sites. It found that Ri could become larger than 0.20 that is considered quite stable condition in average during night-time (Banta et al., 2003, Galperin et al., 2007), which could largely explain the existence of the nocturnal UHI over OKC. Correlation between the nocturnal UHII and temperature inversion at the seven rural sites was also investigated in their study, which was as strong as the one with the wind speed at the same rural sites. The nocturnal UHII is positively and negatively correlated to the rural temperature inversion and wind speed, respectively, while these two parameters (temperature inversion and wind speed) are the determinants of the atmospheric stability (i.e Ri). It is thereby suggested the great influences of both background temperature gradient and wind speed on the determination of the atmospheric stability and the development of the UHI over OKC.

3.2.4.2 Pasquill-Gifford (P-G) stability classification scheme

(i) Classification Approach

The Pasquill-Gifford (P-G) stability classification scheme (Pasquill and Smith, 1983) will be used to classify the satellite images into D (Neutral), E (Slightly Stable), F (Moderately Stable) and G (Extremely stable) classes in this analysis (Table 3.1). As introduced in Chapter 2, a quality control of the cloud conditions is applied by checking the ground observations and assuring that all of the images are collected under clear-sky conditions. Regional wind speed (WS_{10m}, 10 m a.g.l) measured at Spencer station (shown in Figure 3.1) during 22:00 - 23:00 and 01:00 – 02:00 for Terra and Aqua satellites respectively is therefore the only parameter that considers for the P-G classification.

(ii) Image availability

The total number of available images is 130 in this analysis with 26 paired groups of UHII (i.e. $sUHII$ and $aUHII$) for each image. These cases are classified into class D, E, F and G, approximately accounting for 17%, 40%, 43% and 10% correspondingly. The outstanding percentage of the nights under slightly (E) or moderately (F) stable conditions is consistent with Tomlinson et al. (2012) who explored the $sUHII$ during summer months between 2003 and 2009 over Birmingham, UK.

Figure 3.2 provides a summary of the available images for each stability class during four seasons. The less availability of images in winter are a result of cloud influence, therefore, data during winter are not considered in the following analysis. Regarding autumn and spring, hereafter known as the transition seasons, the similar trend of the averaged background temperature under each stability class from them (Table 3.2) gives confidence to combine them to increase the sample size and reliability of the analysis in the following analysis. Therefore, to explore whether the robustness of the P-G classification scheme for characterising the $sUHII$ and $aUHII$ varies across seasons, responses of the UHII ($sUHII$ and $aUHII$) to the atmospheric stability between summer and transition seasons are compared.

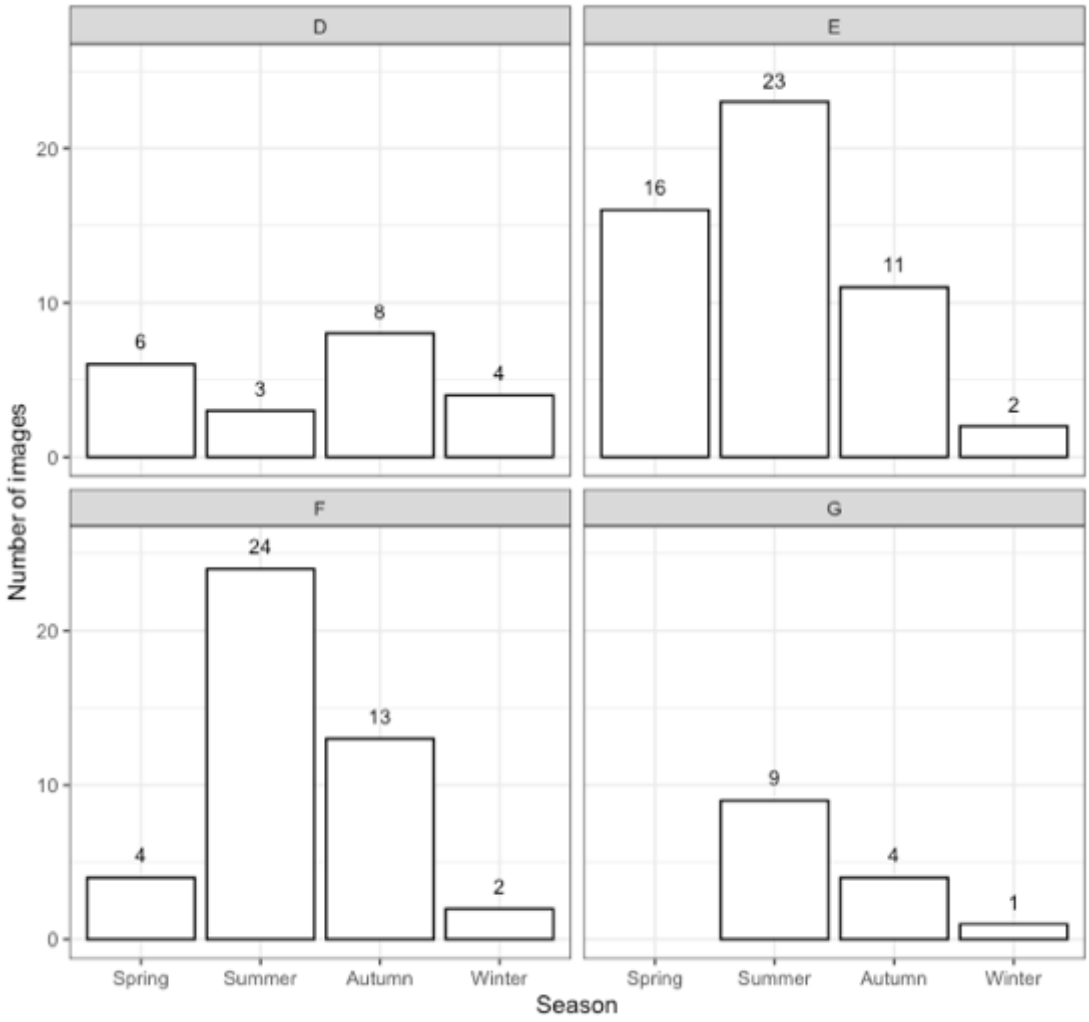

Figure 3. 2 Frequency of the images classified by the Pasquill-Gifford stability class

Table 3. 2 Average background air temperature (℃) under four stability classes in four seasons

Season	Average background air temperature under four stability classes			
	D	E	F	G
Spring	17.28	18.20	14.51	--
Summer	27.10	26.75	26.66	26.05
Autumn	17.59	19.10	18.40	15.85
Winter	5.29	3.54	9.67	3.19

3.2.4.3 Assessment of the Pasquill-Gifford (P-G) stability classification scheme

Four meteorological parameters based on the observations from Spencer station are chosen to compare with the key parameters (WS_{10m}) used to determine the P-G scheme,

by conducting the correlation analysis with both $sUHII$ and $aUHII$ respectively. Specifically, all of the four parameters can directly or indirectly reflect the atmospheric stability and were taken as variations of the P-G system to compare with the P-G scheme (Mohan and Siddiqui, 1998), which include: (i) P-G classification based on WS measured at 2 m a.g.l (WS_{2m}); (ii) Gradient Richardson number (Ri) calculated based on two height levels of temperature and wind speed measurements (Stull and Ahrens, 1995):

$$Ri = \frac{g[(T_{9m} - T_{1.5m})/\Delta z_T + \Gamma_d]\Delta z_u{}^2}{T_{1.5m}(WS_{10m} - WS_{2m})^2} \quad \text{Equation (3.1)}$$

where $g \approx 9.8\, ms^{-2}$ is the acceleration due to gravity, $\Gamma_d = 0.01℃\, m^{-1}$ is the dry adiabatic lapse rate (DALR), T_{9m} and $T_{1.5m}$ in Kelvin (K) are the air temperature measured at 9 m and 1.5 m a.g.l respectively, WS_{10m} and WS_{2m} in m/s are the wind speed measured at 10 m and 2 m a.g.l correspondingly, $\Delta z_T = 7.5m$ and $\Delta z_U = 8.0m$ are the height differences between the two levels of the temperatures and wind speeds measurements respectively; (iii) the wind speed gradient (∇WS, $\nabla WS = (WS_{10m} - WS_{2m})/\Delta z_U$) and (iiii) the temperature gradient (∇T, $\nabla T = (T_{9m} - T_{1.5m})/\Delta z_T$). The reasons for choosing these four parameters are summarised in Section 3.1.

3.2.5 Site classification

To investigate the response of the spatial pattern of UHI to the atmospheric condition, stations/pixels are grouped by different Urban Climate Zones (UCZ) (Oke et al., 2006). UCZ is principally determined by three parameters: roughness class, aspect ratio and fraction of impermeable surface (more details in Oke et al. (2006)). It aims at classifying a city into districts with similar modifying characteristics for the local climate. OKCNET has previously been classified by Schroeder et al. (2010) but significant challenges were

found for the classifications of some of the stations located within the areas from urban to suburban or from suburban to rural. To overcome this, only 26 clearly defined stations from the OKCNET are selected in this analysis (see Figure 3.1 and Table 3.2). Table 3.3 also presents additional information for each UCZ, including (i) the averaged Normalised Difference Vegetation Index (NDVI) from MODIS vegetation indices products (MOD13A2 and MYD13A2) during the study period and (ii) the averaged building fraction from the building footprints data in the year of 2010 (Oklahoma City Council, 2010). In general, the NDVI and building fraction follows the UCZ system, such as the greatest NDVI at UCZ7 and largest building fraction at UCZ1.

Table 3. 3 Information related to UCZ classification

UCZ	Number of stations	Averaged NDVI (within 500-m buffer)	Averaged Building fraction (within 500-m buffer)	General definition of UCZ from (Oke et al., 2006)			
				Description	Roughness class	Aspect ratio	Fraction of impermeable surface
UCZ1	5	0.227	0.293	*Intensely developed urban with detached close-set high-rise buildings with cladding*	8	> 2	> 90
UCZ2	2	0.239	0.275	*Intensely developed high density urban with 2 – 5 storey, attached or very close-set buildings often of brick or stone*	7	1.0 - 2.5	> 85
UCZ4	8	0.333	0.158	*Highly developed, low or medium density urban with large low buildings & paved parking, e.g. shopping mall, warehouses*	5	0.05 - 0.2	70 - 95
UCZ5	2	0.389	0.117	*Medium development, low density suburban with 1 or 2 storey houses, e.g. suburban housing*	6	0.2 - 0.6	35 - 65
UCZ6	5	0.393	0.08	*Mixed use with large buildings in open landscape, e.g. institutions such as hospital, university, airport*	5	0.1 - 0.5	< 40
UCZ7	4	0.47	0.107	*Semi-rural development, scattered houses in natural or agricultural area*	4	> 0.05	< 10

Additional information related to stations classified by each UCZ:* ***UCZ1**: KCB103, KCB104, KCB105, KCB106, KCB108;* ***UCZ2****: KCB102, KCB107;* ***UCZ4****: KCB101, KNE104, KNW103, KNW106, KNW107, KNW108, KSW103, KSW107;* ***UCZ5****: KSW109, KSW111;* ***UCZ6****: KCB110, KNE202, KSW102, KSW104, KSW108;* ***UCZ7****: KNE103, KNW104, KSE102, KSW110.*

3.3 Examining the relation between meteorological variables and UHI

As mentioned in Section 3.2.4.2, the four parameters (WS_{2m}, Ri, ∇WS and ∇T) with underlying linkage to the atmospheric stability were compared with the WS_{10m} which is the decisive parameter for the P-G scheme. A correlation analysis with the averaged $sUHII$ ($\overline{sUHII}$) (Figure 3.3a) and $aUHII$ ($\overline{aUHII}$) (Figure 3.3b) demonstrates that WS_{10m} has the strongest associations with both the $\overline{sUHII}$ (coefficient correlation [r] of -0.50) and $\overline{aUHII}$ ($r = -0.57$), indicating the reliability of background wind speed condition at 10 m a.g.l (WS_{10m}) as a representative of atmospheric condition to study the UHI.

Ri should theoretically provide more robust means to identify the state of the atmosphere, when compared to the P-G scheme based on cloud and wind data which does not incorporate the dynamics of the surface layer, although it is elegant in its simplicity and useful in the absence of ground measurements (Gupta and Sastri, 1990). However, Ri performs unsatisfactorily in the relationship with the UHII ($r = 0.23$ with $\overline{sUHII}$ and $r = 0.24$ with $\overline{aUHII}$). The increase of the Ri occurs with the greater ratio of ∇T to ∇WS that is a measure of the dynamic stability through the ratio of buoyant production to mechanical production of turbulence near the rural ground surface (Mohan and Siddiqui, 1998, Stull, 2012). Near ground surface, turbulence is the pivotal factor controlling the vertical exchange of momentum and heat fluxes and its intensity is estimated by the ∇WS. A strong rural thermal inversion quantified by the ∇T implies the strong stable stratification that can result in the suppression of the turbulent motion and reducing the turbulent fluxes. This reduction of the fluxes contributes to the shallower, but more stable,

surface boundary layer that could accommodate very low temperatures over rural areas during clear skies (Poulos and Burns, 2003), leading to the magnification of the $aUHII$ (Hu et al., 2013).

One of the likely causes for Ri not performing as well as expected is the accuracy of the temperature and wind speed instruments. Accuracy, commonly known as systematic error, is defined as the capability of the instrument to measure the accurate value (or closeness to this value) while precision is the observational errors that is a random error and not related to the instrument itself (Cork et al., 1983). Previous studies have shown that Ri can be extremely sensitive to small variations in temperature and particularly in wind speed due to the greater control of it in the definition (see Equation 3.1) (Golder, 1972, Bardal et al., 2018). Indeed, the increased scatter between WS_{10m} and Ri (Figure 3.4a), compared to the one between WS_{10m} and ∇T (Figure 3.4b), suggest that the uncertainties triggered by the wind/temperature measurements potentially result in the poor performance of Ri. For example, Golder (1972) draw attention to the errors in the instruments of wind and temperature at two levels which could create errors in the calculation of the Ri, thereby, temperature and wind speed sensors are recommended to be mounted so far apart so that the temperature/wind speed gradient will be dominating over the uncertainty. Likewise, the comparisons between the Ri measuring by different heights of the sensors and the one observed by eddy covariance method at two coastal sites outlined the importance of choosing the measurement height that should be made with sufficient vertical separation to reduce the inaccuracies from the wind speed and temperature instruments (Bardal et al., 2018). The conclusion is that wind measured at single level is not only more pragmatic (and common) but also sufficient to describe the atmospheric condition for characterising the UHI (i.e. as a key parameter for classifying

the atmospheric stability in the P-G stability system). Using this finding as a basis for further analyses, this chapter continues by investigating seasonal impacts of background wind speed condition on seasonal and spatial variations of UHII.

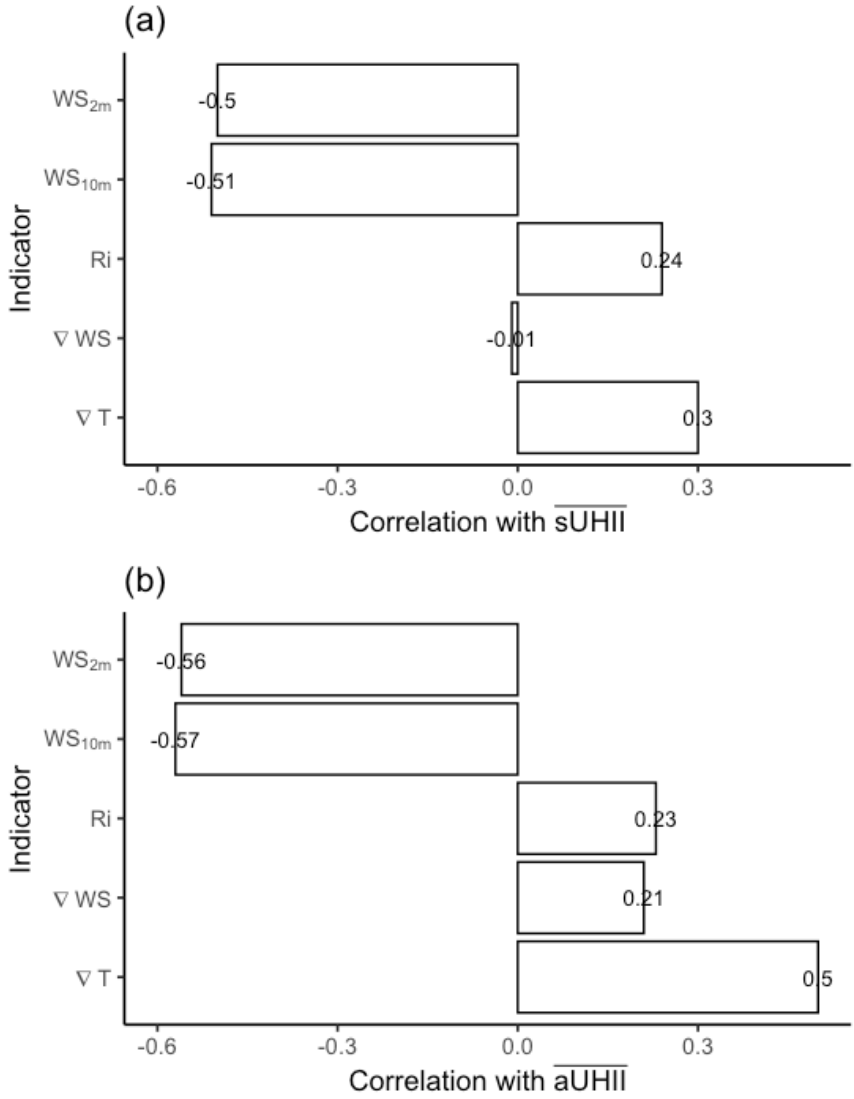

Figure 3. 3 Correlation coefficients (r) between five meteorological parameters and (a) $\overline{sUHII}$ and (b) $\overline{aUHII}$

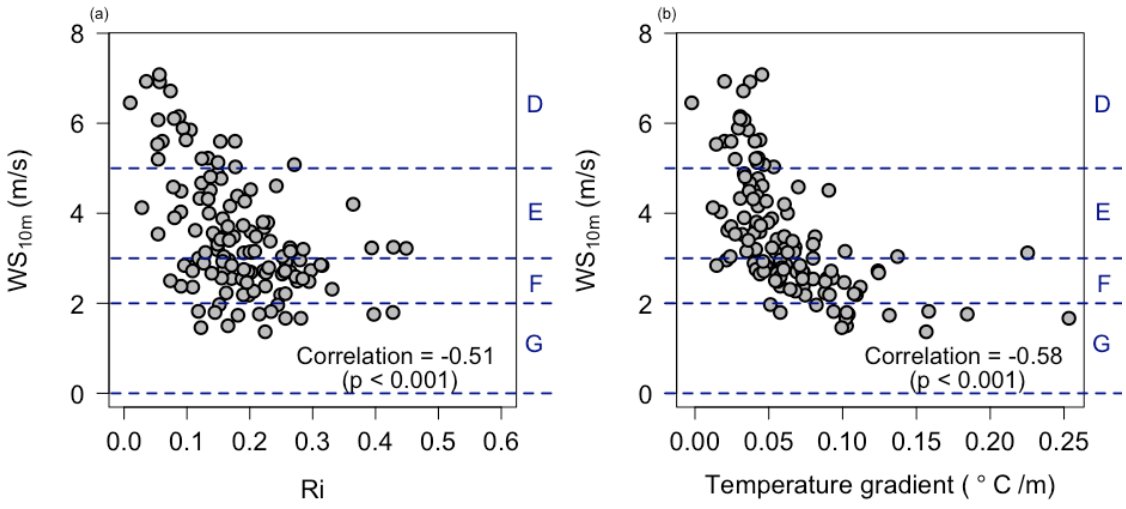

Figure 3. 4 Scatterplot between (a) WS_{10m} and Ri and (b) WS_{10m} and ∇T, where the dashed lines represent the threshold of WS_{10m} for the PG classes

3.4 Seasonal variations of the UHII and atmospheric condition

3.4.1 General results

According to the analysis in Section 3.3, background wind speed at 10m a.g.l (WS_{10m}) is found to be the meteorological parameter highly correlated to the UHI. Meanwhile, it is also the determinant to classify the atmospheric stability in the P-G scheme. This section will then assess the impacts of the WS_{10m} on the seasonal patterns of the UHII by applying the P-G classification scheme.

Without considering seasonal differences, the daily magnitude of the pixel-averaged $sUHII$ (Figure 3.5a) and station-averaged $aUHII$ (Figure 3.5b) for different P-G stability classes present a significant increase in the UHII as atmospheric stability increases. These responses of both the $sUHII$ and $aUHII$ to the WS_{10m} generally corroborate previous work in Birmingham, UK (Tomlinson et al., 2012, Azevedo et al., 2016).

The differences between the UHII (i.e. $sUHII$ and $aUHII$) under the four stability classes are statistically significant, supported by a one-way analysis of variance (ANOVA) test for independent samples together with the *post-hoc* Tukey tests. It shows that significant differences in the $sUHII$ ($F = 12.342, p < 0.001$) and $aUHII$ ($F = 24.561, p < 0.001$) exist at least between two scenarios (D-E, D-F, D-G, E-F, E-G, or G-F) at 0.001 confidence level. These significant differences of both $sUHII$ and $aUHII$ under different WS_{10m} conditions indicate that the WS_{10m} generally performs well for characterising the UHII during night-time.

The P-G classification scheme can effectively be considered as an estimator of a simplified bulk Richardson number by considering only one WS measurement (Larsen and Gryning, 1986, Arya, 2001). The increase of the stability implies the decrease of WS_{10m} that is found to be crucial for modulating the spatial pattern and the magnitude of the thermal features that would be advected downwind of the source areas (Oke, 1982) and affect the $aUHII$ ultimately (Morris et al., 2001). Results herein also highlight the consistent impacts of WS_{10m} on modulating the magnitude of the $sUHII$ that is reduced under higher WS conditions, which was also found over Birmingham, UK (Tomlinson et al., 2012). Indeed, Lee (1979) discovered the existence of a "critical" background WS over urban areas, below which the city atmosphere becomes more unstable, compared to the rural atmospheric stability. Therefore, the increase of the $sUHII$ under more stable rural atmospheric conditions could be explained by the more unstable city atmosphere that allows a greater momentum heat flux to the surface and increase the surface temperature over urban areas. In addition, the more steady increment of the mean $aUHII$ under more stable conditions, reflected by the red points in Figure 3.5, gives evidence that the $aUHII$ is more affected by the WS_{10m}, comparing to the $sUHII$ that is possibly

affected by the differences of other influential factors (e.g. seasonal differences of the input of solar radiation and anthropogenic heat etc.), together with the cloud and wind conditions under different P-G classes, becoming less stable or "linear" with increasing atmospheric stability.

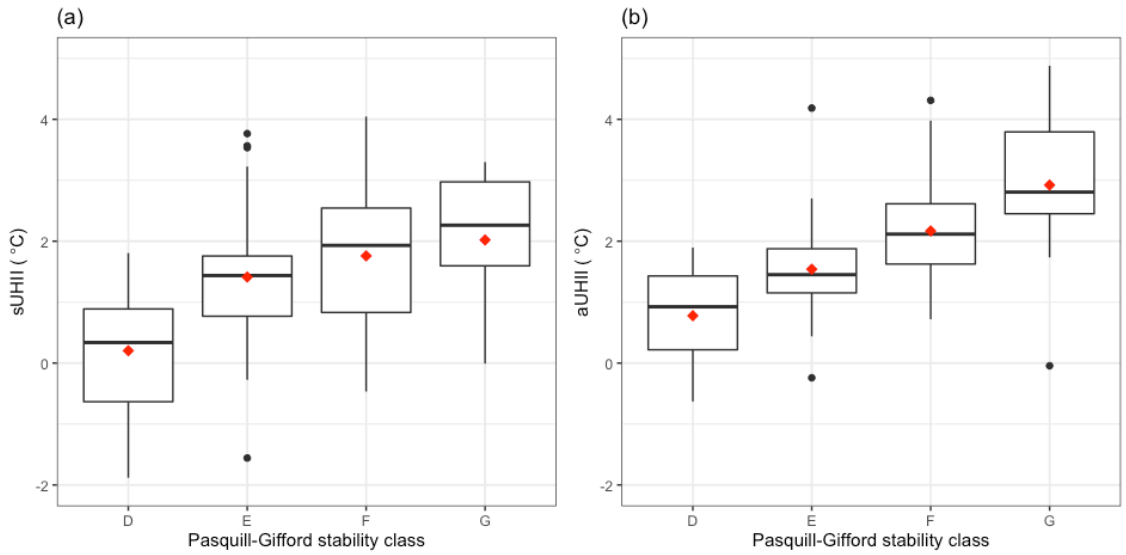

Figure 3. 5 Boxplots of daily (a) pixel-averaged sUHII and (b) station-averaged aUHII magnitude for different atmospheric stabilities, where the red points are the mean values of the UHII correspondingly

3.4.2 Seasonal differences

It is evident that the responses of both $aUHII$ (Figure 3.6a) and $sUHII$ (Figure 3.6b) to WS_{10m} differ under summer and transition seasons. Specifically, the increments of the mean UHII (i.e. $aUHII$ and $sUHII$: Figure 3.6) when the stability shifts towards stable are more substantial during summer, particularly from E to G. However, the limited number of available images possibly contributes to the misleading results under class D, where the mean UHII are similar to the ones under class E during summer. More importantly, the irregular variation of the $sUHII$ that tends to be weaker under more stable and neutral conditions during transition seasons from Figure 3.6b, indicating that

the WS_{10m} generally has less of a role to play with the $sUHII$ in these conditions, compared to the $aUHII$. This rather contradictory result may be due to $sUHII$ being more affected by other causative factors particularly during transition seasons. One potential factor is the background temperature that could indirectly reflect the daily input of the solar radiation into the urban environment. This has been found to be linked to the seasonal variations of the $sUHII$ (from MODIS) from previous studies (Zhou et al., 2013, Zhou et al., 2016). Zhou et al. (2016) also discovered that the seasonal variations of the $sUHII$ are less evident when the input of the shortwave radiation into the urban system is controlled to be constant throughout the year from a modelling analysis. It is thereby suggested that land surface temperature follows the astronomical seasons mainly driven by solar radiation, where as the $aUHII$ is more influenced by the meteorological conditions corresponding to the regional climate (Zhou et al., 2013). Therefore, the larger variations of the background temperature under different stability classes during the transition seasons (Table 3.3) could have a greater impact on the development of the $sUHII$, leading to the inconsistent variation of the $sUHII$ shown in Figure 3.6 and the poorer performance of the WS_{10m} in characterising the $sUHII$. Figure 3.7 provides statistical evidence by showing the variations of the background air temperature during the transition seasons. On averaged, the change of the mean temperature (red dots in Figure 3.7) is consistent with the change of the $sUHII$ (Figure 3.6) during the transition seasons, where both the background temperature and $sUHII$ increase from class D to E before slightly decreasing from E to G.

In addition, the results (Figure 3.6c) demonstrate that the differences between $aUHII$ and $sUHII$ ($\Delta UHII$, $aUHII$ minus $sUHII$) are less affected by the WS_{10m} during summer, where the averaged $\Delta UHII$ is nearly constant (≈ 0°C) from class D to F. It is

suggested that the impacts of the WS_{10m} are more consistent on $sUHII$ and $aUHII$ particularly under neutral condition when the influences of the WS_{10m} more evidently affect the UHII, comparing to other causative factors.

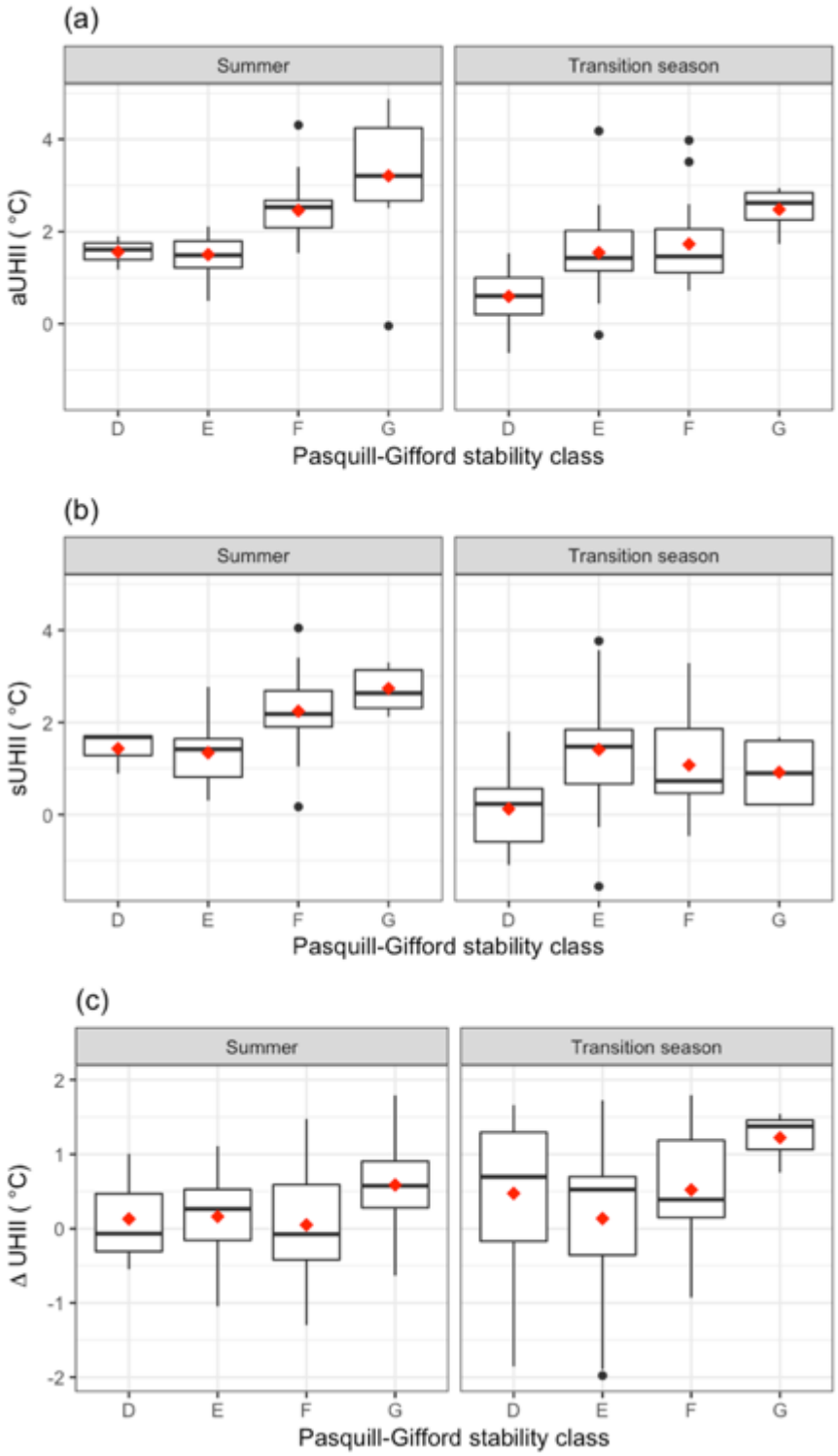

Figure 3.6 Boxplots of daily mean (a) aUHII, (b) sUHII and (c) ΔUHII (=aUHII - sUHII) under summer and transition seasons where the available images are: Summer: D(3), E(23), F(24), G(9); Transition seasons: D(14), E(27), F(17), G(4); and each image considers aUHII and sUHII from 26 stations

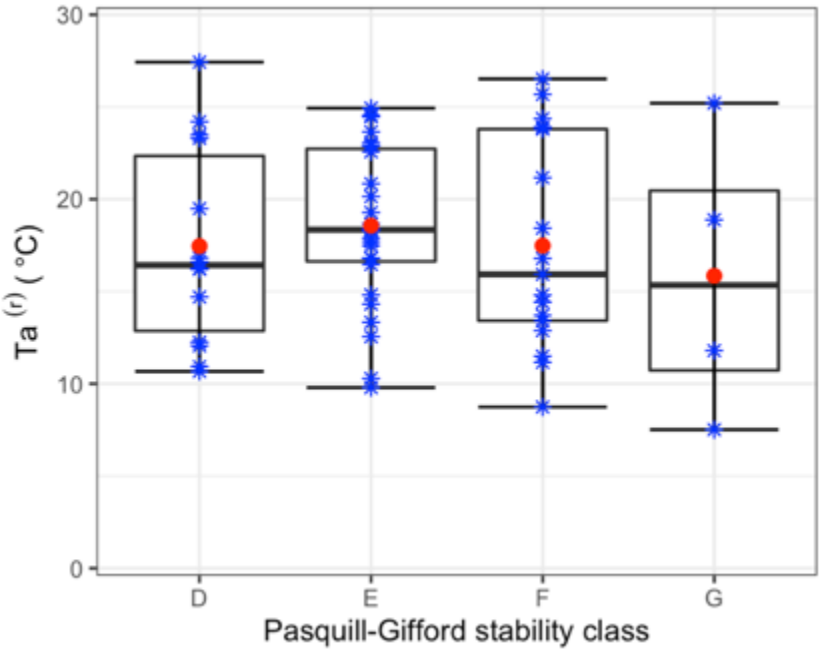

Figure 3. 7 Background air temperature ($T_a^{(r)}$) under the four stability classes during transition seasons

3.5 Spatial variations of the UHII and atmospheric condition

To investigate whether the spatial patterns of UHII are influenced by the WS_{10m}, the variations of the daily mean $aUHII$ and $sUHII$ across the six UCZs under four stability classes during summer and transition seasons are presented in Figure 3.8. The inter-UCZ UHII are clearly differentiated and universally follow the UCZ typology, where the most urbanised sites (UCZ1 and UCZ2) present the greatest nocturnal UHII. Contrary to expectations, both $aUHII$ and $sUHII$ from UCZ6 are greater than the ones from UCZ5 under most of the cases (Figure 3.8). Stations classified as UCZ5 are more urbanised, have a lower NDVI and greater building fraction (Table 3.3), compared to UCZ6. The reason for this unexpected contrasting magnitude of UCZ5 and UCZ6 is not clear but could possibly be explained by the geographical location of UCZ5 and UCZ6 in OKC. Referring to Figure 3.1, it is evident that stations classified as UCZ5 are located in the

south of UCZ6 and the central business district (CBD) in OKC. As a southerly wind is dominant over the study period, the advection effect from the southerly wind, together with the greater distance to the CBD, is likely to generate these surprising results that the UHII from UCZ5 is lower than the ones from UCZ6. (Note: the prevalence of Low-Level Jets (LLJs) which have been previously found to have significant impacts on the $aUHII$ in OKC: (Hu et al., 2013). Similar results (greater $aUHII$ from UCZ5 than UCZ6) were also found by Hu et al. (2016b) in OKC and in Jihon, France (Richard et al., 2018). Unfortunately, neither study provides explanation or further investigation. However, there is similar issue related to the station locations regarding the analysis of Richard et al. (2018), where some of the stations assigned as UCZ6 are closer to the city centre. This finding raises intriguing questions regarding the necessary considerations of advection (i.e. wind direction) and location of the stations in UMNs (i.e. distance to city centre) for a typology (i.e. UCZ) to classify the urban stations. Specifically, urban heat advection effects to the downwind areas from city centre have been shown to be non-negligible by using observational (Bassett et al., 2016) or numerical modelling data (Bassett et al., 2017). Further studies, which take these additional concerns into account for inter-UCZ or inter-LCZ comparisons, will need to be undertaken.

Significant differences of both the $sUHII$ and $aUHII$ across UCZs under all different conditions (Figure 3.8) indicates that each UCZ apparently has its own regime of the land surface and screen-height temperatures. This is regardless of atmospheric stability/WS_{10m} and is supported by the statistical test from ANOVA with a confidence level of 0.05 (Table 3.4). It could be explained by the fact that the inter-urban thermal contrasts (i.e. UHII) are largely driven by land cover, building or street structure, and vehicle traffic or space heating/cooling strongly linked to the release of anthropogenic

heat, particularly during clam, cloudiness nights (Stewart and Oke, 2012) As a result, many studies have been motivated to investigate the associations between the spatial variation of the UHII and properties of urban sites that mainly include the urban structure (e.g. sky view factor (Unger, 2009)), urban cover (e.g. urban fraction (Song and Park, 2019) and vegetation cover (Ferreira and Duarte, 2019)), urban fabric (e.g. reflectance of the building/pavement materials (Taleghani and Berardi, 2018)) and urban metabolism (e.g. anthropogenic heating (Bohnenstengel et al., 2014)) (Oke et al., 2006).

Figure 3.9 provides evidence for the potential controls of the $\mathrm{WS_{10m}}$ exerted on the spatial pattern of the UHII, by presenting the mean UHII (i.e. $aUHII$ or $sUHII$) of each station under class D and G during summer period. Although the spatial pattern of the UHI generally follows the UCZ typology, which is dominantly driven by the land surface characteristics according to the results from Figure 3.8 (i.e., greatest in UCZ1), the comparisons among stations clearly show that the spatial patterns of both the $sUHII$ and $aUHII$ varies under different WS_{10m} conditions. Specifically, the thermal contrasts across stations are more consistent with the UCZ typology under low wind condition (class G), which generally decreases from UCZ1 to UCZ7. In particular to stations classified UCZ1, UHII tends to be reduced comparing to UCZ2 and UCZ4 under high wind condition according to Figure 3.9. It is therefore suggested that the horizontal spatial form of the nocturnal UHI patterns is likely to be affected by the $\mathrm{WS_{10m}}$.

The differentiated inter-urban variances from class D to G, reflected by the standard deviations of the UHII (σ_{aUHII} for $aUHII$; σ_{sUHII} for $sUHII$) across the UCZs shown in Figure 3.10, further suggest that the spatial variations of both the $aUHII$ and $sUHII$ could be potentially modified by the background atmospheric condition indicated by the $\mathrm{WS_{10m}}$. During nights with 'ideal' conditions when wind speed becomes extremely low,

the inherently generic factor (i.e. land surface characteristics) largely accounts for the inter-urban differences of the UHII. Results herein discover the negligible influence of the $\mathrm{WS}_{10\mathrm{m}}$ on the spatial variations of UHII, particularly during summer when both the σ_{aUHII} and σ_{sUHII} increases from class D ($\sigma_{aUHII} \approx 0.28℃$; $\sigma_{sUHII} \approx 0.65$) to class E ($\sigma_{aUHII} \approx 0.72℃$; $\sigma_{sUHII} \approx 1.04$). The varying spatial variance of the UHII across different wind conditions implicates the local disparity of the wind speed conditions across UCZs. Indeed, the local wind speed (screen-height level) and cloud condition will differ from site to site. In particular, local wind speed is highly influenced by each individual urban element (e.g. roughness length, aspect ratio and orientation etc.) within a radius of only a few hundred meters within the UCL (Oke et al., 2017). Therefore, the stronger wind speed ($< 7m/s$ herein) from rural background potentially contributes to greater contrasts of the local wind speed across UCZs and modifies the spatial pattern of the surface or air temperature and ultimately the $sUHII$ and $aUHII$. Meanwhile, it could also reduce the spatial differences of the UHII by strong wind advection, supported by the consistent decrease of both the σ_{aUHII} and σ_{sUHII} from low (class G) to high wind speed condition (class D), except for the class E during transition season that is likely to be affected by the background temperature discussed in Section 3.2.4.

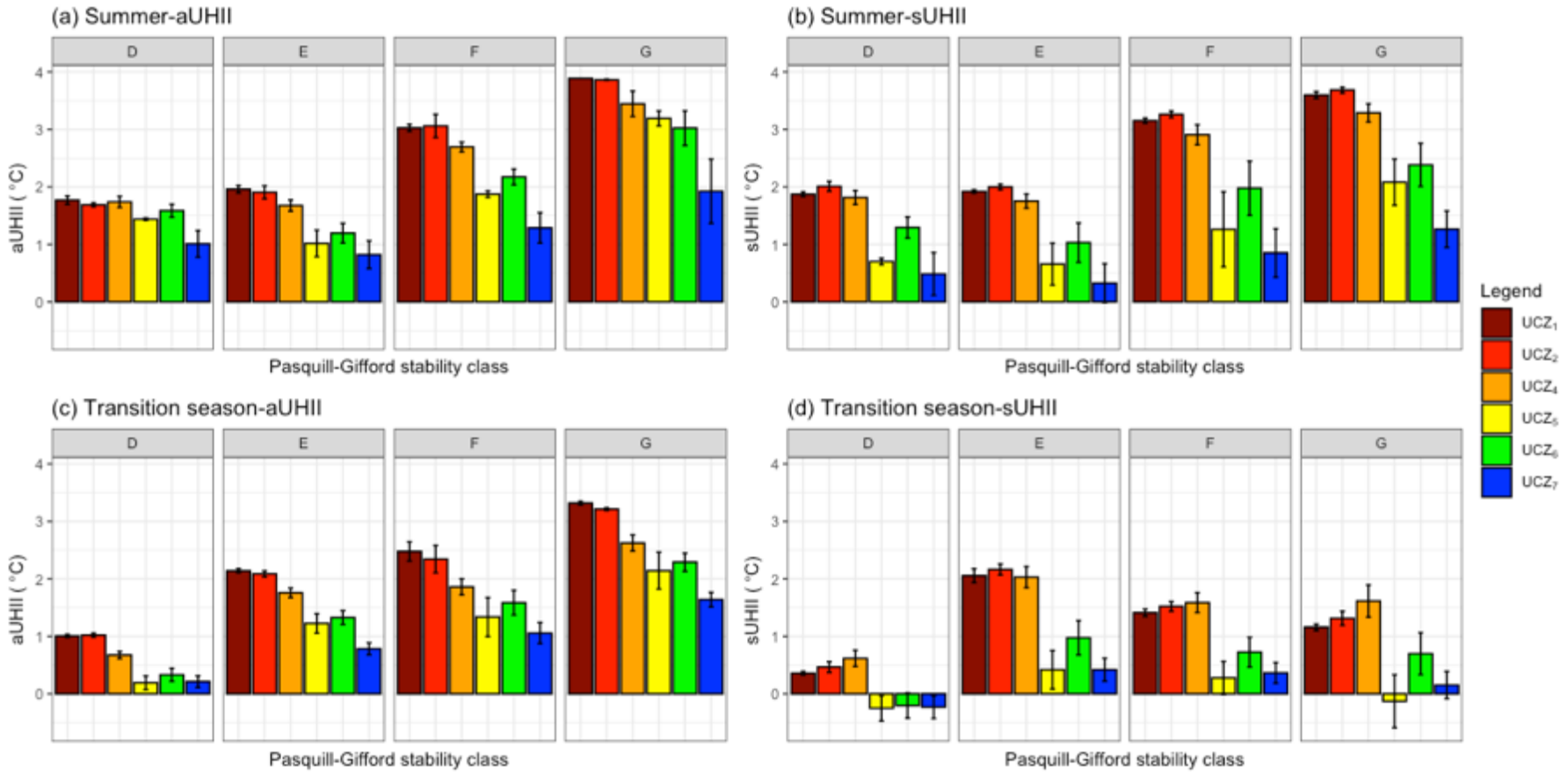

Figure 3. 8 Bar plot with standard error bars of the (a) mean sUHII and (b) mean aUHII for each Pasquill-Gifford stability class distributed by the UCZ classification

Table 3.4 ANOVA test for $aUHII$ and $sUHII$ across UCZs under the four atmospheric stability classes during summer and transition seasons.

Summer				
UHII Type	Pasquill-Gifford stability classes			
	D	E	F	G
$aUHII$	$F = 5.649, p = 0.002$	$F = 8.398, p < 0.001$	$F = 20.95, p < 0.001$	$F = 3.215, p = 0.030$
$sUHII$	$F = 7.662, p < 0.001$	$F = 7.407, p < 0.001$	$F = 8.249, p < 0.001$	$F = 11.770, p < 0.001$
Transition seasons				
UHII Type	Pasquill-Gifford stability classes			
	D	E	F	G
$aUHII$	$F = 7.752, p < 0.001$	$F = 14.880, p < 0.001$	$F = 10.990, p < 0.001$	$F = 15.450, p < 0.001$
$sUHII$	$F = 3.976, p = 0.011$	$F = 6.408, p < 0.001$	$F = 4.074, p < 0.001$	$F = 5.009, p = 0.004$

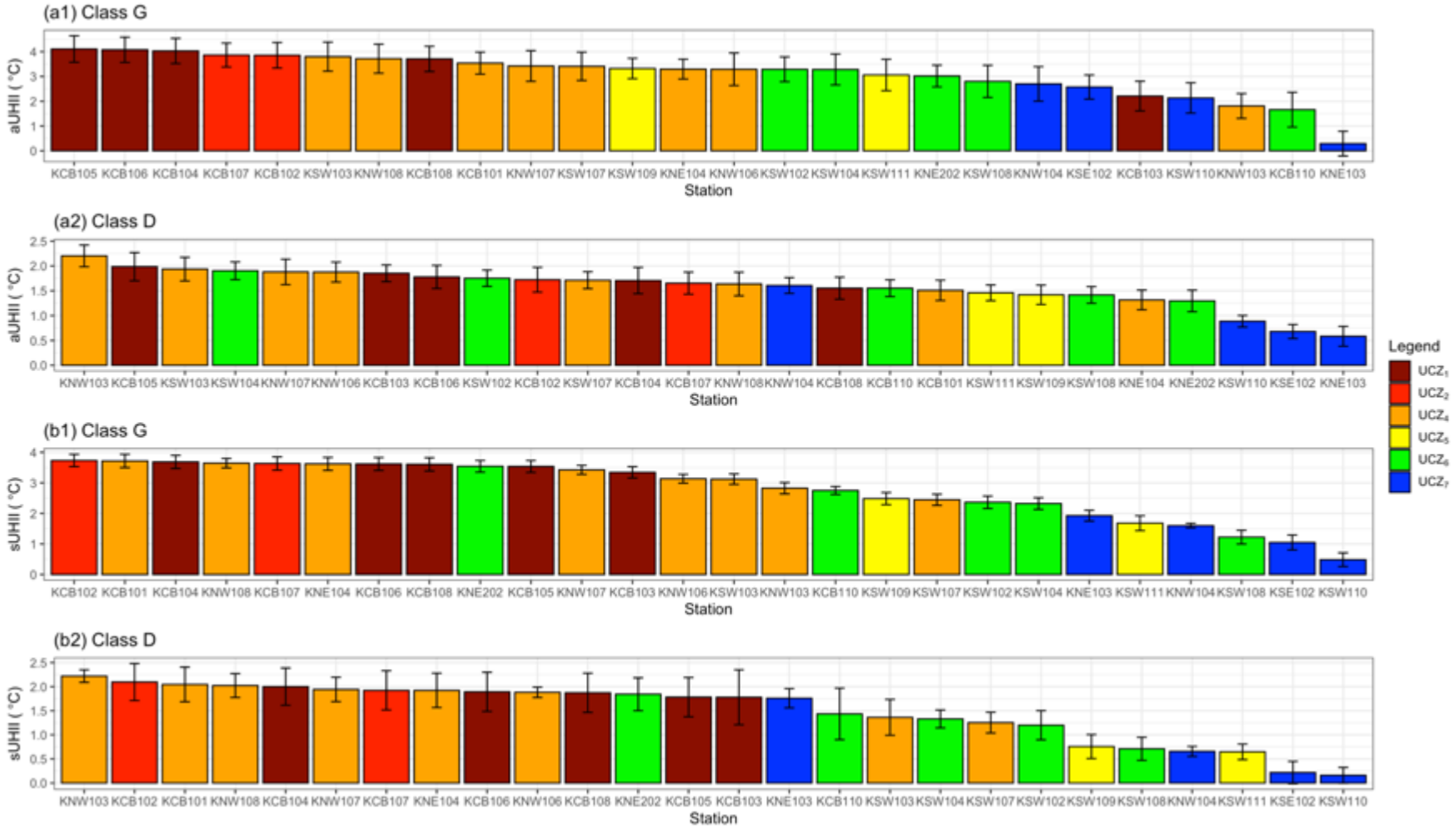

Figure 3. 9 Examples of Bar plots of averaged $aUHII$ (a1 and a2) and $sUHII$ (b1 and b2) from each station during summer under G (a1 and b1) and D (a2 and b2) stability classes

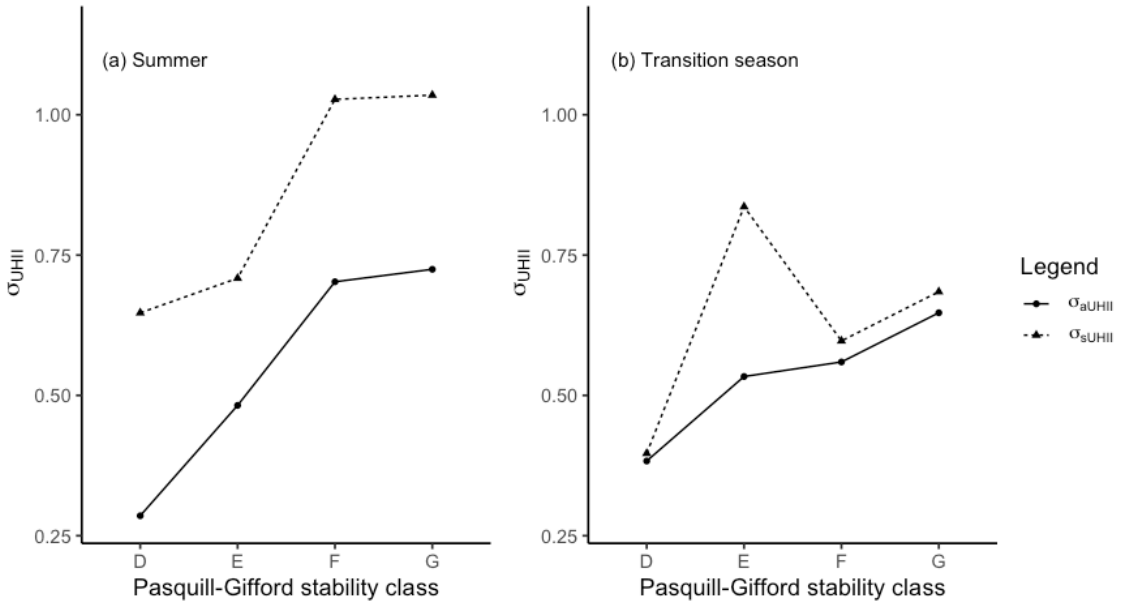

Figure 3. 10 Variation of the standard deviation of both the $aUHII$ and $sUHII$ across UCZs during (a) summer and (b) transition seasons

3.6 Conclusions

The configuration of OKCNET with multiple level temperature and wind measurements provides a unique opportunity to examine the effectiveness of the P-G classification scheme (i.e. comparisons with Ri) on characterising the seasonal and spatial patterns of the $aUHII$ and $sUHII$ durng night-time. The key findings for this analysis are summarised as follows:

(i) Although it was postulated that the P-G scheme could be improved by using additional measures such as Ri, it appears that the PG classification scheme (in its simplest form) is applicable for characterising the UHII. This was supported by the strongest correlation between UHII and WS_{10m} comparing to the other parameters studied. However, the sensitive nature of Ri to input data (at two levels) is highlighted as a caveat.

(ii) Without taking seasonal effects into consideration, the P-G classification indicated by WS_{10m} yields significant differences of $sUHII$ and $aUHII$ across different classes (from high to extremely low wind conditions) and the averagely increase of both of them under more calm conditions. This result highlights the important role of $\mathrm{WS_{10m}}$ on characterising the UHI.

(iii) The seasonal analysis provides evidence that the role of $\mathrm{WS_{10m}}$ is less well defined in Autumn and Spring. This is considered to be because the background temperature is more variable than during the summer months.

(iv) The analysis of the spatial variation of the UHII across UCZs implies the potential impacts of the atmospheric condition represented by $\mathrm{WS_{10m}}$ in determining the spatial pattern of both $aUHII$ and $sUHII$.

Although limited samples used in this study can increase some uncertainties in the results and the findings summarised above will doubtless be much scrutinised, there is an immediately dependable conclusion that it is imperative to consider the effects of $\mathrm{WS_{10m}}$ on investigating the relationship and difference between $sUHII$ and $aUHII$. Further research should be undertaken to repeat this analysis in other cities or during a longer time period to explicitly determine the response of both UHII to the atmospheric condition.

In addition, the contrasting magnitude of UHII from the two UCZs (UCZ5 and UCZ6) outlines the importance of (i) the local advection effect largely determined by surface wind conditions or synoptic weather system and (ii) the exact locations of the stations (i.e. distance to the CBD), which is worthy of consideration when further refining future typologies (e.g. UCZ, LCZ) for UHI studies.

3.7 Summary

This chapter has outlined the influence of the atmospheric condition indicated by the background wind speed condition on the behavior of nocturnal surface and urban canopy heat islands, using land surface temperature data from satellite and ground observations from UMN in OKC as a case study. By accounting for seasonal and intra-urban (UCZ) variations of UHII, results clearly show that the P-G classification scheme is workable for classifying the atmospheric conditions that have significant impacts on the temporal and spatial patterns of the UHI. This chapter provides scientific evidence for choosing WS_{10m} *as a key factor representing the atmospheric conditions to study the UHII, which is the fundamental basis for the analysis conducted in Chapter 4 and 5.*

Chapter 4 Impact of Atmospheric Conditions and Levels of Urbanisation on the Relationship between Nocturnal Surface and Urban Canopy Heat Islands

This chapter aims to investigate into the relationship between sUHII and aUHII under specific atmospheric conditions and land surface characteristics. This is an important step for trying to compare it in difference cities for the generalisation purpose in Chapter 5.

This Chapter has been published as:

***Feng, J.L.**, Cai, X.M. and Chapman, L., 2019. Impact of atmospheric conditions and levels of urbanization on the relationship between nocturnal surface and urban canopy heat islands. Quarterly Journal of the Royal Meteorological Society, 145(724), pp.3284-3299. https://doi.org/10.1002/qj.3619*

4.1 Introduction

The Urban Heat Island (UHI) - the phenomenon that the temperature in urban areas is warmer than the surrounding rural areas, has been investigated for several decades due to its potential impacts on human life in urban areas (Voogt and Oke, 2003), which has been fully introduced in Chapter 2. UHI has been well studied and quantified in many different cities (Kolokotroni and Giridharan, 2008, Shao et al., 2006, Streutker, 2002, Morris et al., 2001). However, it remains a compelling focus in urban climatology because the land-atmosphere interaction is far more complicated than originally hypothesised. The land-atmosphere interactions at city scale are based on various energy and moisture exchanges within a complicated urban ecosystem with feedback systems between the land-atmosphere interactions and the whole urban ecosystem that are still ambiguous, therefore there are more uncertainties in UHI studies (Jain et al., 2017).

The intensity of the canopy air UHI ($aUHII$) is generally quantified from a comparison of air temperatures (T_a) derived from weather stations within the urban canopy layer (UCL) with reference sites in rural areas (Oke, 1982). In this way, the energy exchange processes controlling the characteristics of $aUHII$ are dominantly controlled by site-specific characteristics and the microscale turbulence processes. However, in the frequent absence of urban weather stations, surface heat island intensity ($sUHII$) can instead be derived using the land surface temperature (T_s) from satellite instruments (Tomlinson et al., 2011a). $sUHII$ data provide opportunities to study the UHI in a spatially continuous way with higher spatial resolution and lower cost compared to the approach of urban meteorological networks (UMN: (Muller et al., 2013a)). However, there exist significant compromises of low temporal resolution (i.e. a daily snapshot, and

the measurement of T_s as opposed to T_a). Therefore, it is both advantageous and practical to investigate the relationship between $sUHII$ and $aUHII$ (the $sUHII$-$aUHII$ relationship) in order to work backwards and estimate air temperatures from surface temperatures. However, this is a complex task with T_s having a different physical meaning compared to T_a, which has been mentioned in Chapter 2. In brief, satellites have a view of ground surface from a sensor that receives the average radiative information from the surface for each pixel which depends on the satellite viewing angle. Explicitly, only radiative source areas and surfaces within the line of sight of the sensor can be detected. In this case, the different physical representations between T_s and T_a in the complicated city-atmosphere system induce more uncertainties between $sUHII$ and $aUHII$.

There are numerous factors influencing the $sUHII$-$aUHII$ relationship which can be simply divided into three classifications: meteorological/climatological conditions (e.g. solar radiation, wind conditions and season etc.), land surface properties (e.g. land and cover types, albedo, and building structures etc.), instruments' issues, e.g. satellite (e.g. overpassing time, viewing angle etc.) and weather stations (e.g. accuracy, exposure etc.) characteristics, as discussed in Chapter 2. However, it is difficult to simultaneously consider all due to interdependencies and difficulties in quantification. As discussed in Chapter 2, a direct investigation of the $sUHII$-$aUHII$ relationship can minimise the impact of background temperature variability submerged in the T_s and T_a, therefore, this study will focus on the impact of season, wind speed (WS) and basic land-use categories modified from local climate zones (LCZ) (urban / suburban) (Stewart, 2011) on the $sUHII$-$aUHII$ relationship during night-time. All three impacts are of great importance to the $sUHII$-$aUHII$ relationship as discussed in Chapter 2. In brief, seasonal patterns of

the $sUHII$-$aUHII$ relationship need to be considered because of the noticeable differences of the seasonal climate conditions whereas WS condition and different LCZs (i.e. land-use) can represent the evaporation or condensation tendency, atmospheric stability conditions and the amount of the reflected or emitted radiation fluxes in the urban environment. Specifically, WS in the atmospheric boundary layer can influence the transport of moisture, heat, momentum and pollutants horizontally and vertically by advection and turbulent mixing. The LCZ system is defined to classify the urban and rural sites based on "climatopes" (Wilmers, 1990) which are closely linked to surface structures and land-use types (Stewart and Oke, 2012).

In order to investigate the nocturnal $sUHII$-$aUHII$ relationship, a unique statistical analysis combining linear regression models with two-dimensional (2-D) distribution tests is applied in this study. The high resolution T_a data from a dense UMN (Birmingham Urban Climate Laboratory, BUCL) (Chapman et al., 2015) in Birmingham, UK, along with T_s datasets from the Moderate Resolution Imaging Spectroradiometer (MODIS) are used.

4.2 Methods and data

4.2.1 Study area and meteorological station data

4.2.1.1 BUCL Network

Birmingham ($52.4862° N, 1.8904° W$) is the second largest city in the UK (approximate 278 km^2) located at the centre of the England with an estimated population of 1.1 million (Birmingham City Council, 2013). Further descriptions have been provided in Chapter 2.

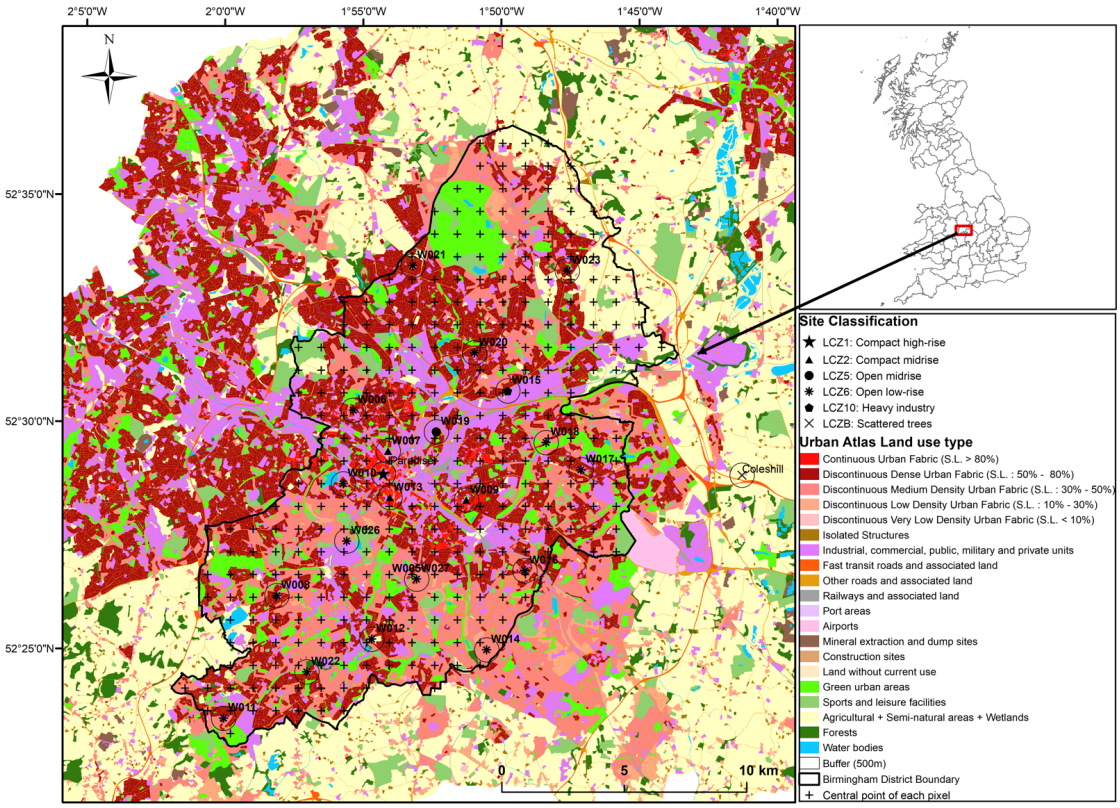

Figure 4. 1 Locations and LCZ classification of weather stations from BUCL and Met office in this study in Birmingham. Note: The Urban Atlas land use type is classified by the European Environment Agency based on SPOT 5 images (2010) and city map (2008)

4.2.1.2 Site Classification

LCZ is an indicator for urban studies which considers the surface properties and the surrounding environment of a weather station, such as the sky view factor, aspect ratio and roughness etc.(Stewart and Oke, 2012). In particular, the structures of buildings and other roughness elements are of great importance to the modification of the longwave radiation emission and reflection from the urban surface that affects both the air temperature and surface temperature. For instance, the building height and sky-view factor are key parameters for the estimation of multi-reflected radiation inside a street canyon. The different density and orientation of roughness elements can enhance anisotropy effects which produces more uncertainties in sending or receiving the radiation information from the urban surface caused by different satellite viewing angles (Voogt and Oke, 1998). Moreover, the different materials (and age) of the roughness elements have diverse heat capacities, leading to the variant storage heat fluxes and the upward longwave radiation fluxes. The magnitude of the impact on airflow varies considerably across different roughness elements, which makes the surface-air temperature relationship substantially more complicated in urban areas. In addition, LCZ can also indirectly reflect the humidity condition for each station.

The LCZ classification of the weather stations (Figure 4.1) used in this study are documented in (Bassett et al., 2016). There are five LCZs assigned to the weather stations in Birmingham (LCZ1: Compact high rise, LCZ2: Compact mid-rise, LCZ5: Open mid-rise, LCZ10: Heavy industry, LCZ6: Open low rise). Only one station classified as LCZ1, LCZ10 or LCZ5; three stations are classified as LCZ2 and the remaining 15 stations belong to LCZ6. The details of surface and geometric properties of different LCZs were shown by Stewart and Oke (2012).

4.2.2 MODIS Land surface temperature data

MODIS daily T_s products (MOD11A1 and MYD11A1) are used in this study (further details can be found in Chapter 2). In summary, there are 63 and 88 images available for Aqua and Terra satellites respectively during the study period. The temporal and spatial consistence between T_s and T_a follows the method introduced in Chapter 2.

4.2.3 Estimation of UHII

Both $sUHII$ and $aUHII$ are calculated according to the method introduced in Chapter 2.

4.2.4 Statistical methodology

Data from all stations are grouped by (i) seasons, (ii) WS and (iii) levels of urbanisation (urban / suburban) respectively (Table 4.1 provides the summary of the sample size in terms of these three variables). The influences of season, WS and levels of urbanisation on the $sUHII$-$aUHII$ relationship are initially investigated, based on linear regression models (LRM) (Montgomery et al., 2012). LRM is chosen because of its simplicity compared to other non-linear regression models and it is easier to interpret the relationship between the two variables. Significance tests for the LRM and regression coefficients (slope and intercept) are conducted subsequently based on 0.01 level of significance.

Table 4. 1 Summary of the available satellite imageries and sample size according to different moderate variables

Moderate variable	Group	Available imagery for Aqua satellite	Available imagery for Terra satellite	Total sample size from all stations (combined two satellites)
WS	WG1: 0-2 m/s	33	39	1073
	WG2: 2-4 m/s	27	45	1127
	WG3: 4-6 m/s	3	4	116
Season	Spring	14	21	660
	Summer	29	46	1048
	Autumn	10	13	351
	Winter	10	8	257
Site classification	Urban group	63	88	432
	Suburban group	63	88	1884

NB: total sample size from all stations is based on the availability of T_s and T_a for each station

An interaction effect can exist in LRM when the impact of an independent variable on a dependent variable is affected by a third moderator variable (Jaccard et al., 2003). In this study, the influence of the three moderator variables and the overall interaction effect is then examined by the analysis of covariance (ANCOVA) that can be used to compare two regression lines corresponding to two values of moderator variable and to show if the two regression lines (represented by their respective slope and intercept) are significantly different. For instance, LRMs are derived for four seasons, and the slopes/intercepts assessed via ANCOVA. The differences between LRMs in four seasons will be reflected by the assessment of slopes/intercepts in ANCOVA. The overall interaction effect indicates the seasonal impacts on the linear $sUHII$-$aUHII$ relationship.

Uniquely, 2-D distribution analysis using confidence ellipses is implemented in this study. These are generated at the 90% confidence level (Monette, 1990) and used to visualise the 2-D distributions connected with linear models. This step adds a useful summary of the relationship between two variables such as the means and standard deviations etc. (Friendly et al., 2013). Specifically, the x-y coordinates of the centre of the confidence ellipse are the means of the two variables, i.e. $sUHII$ and $aUHII$. The magnitude and the orientation of the ellipse are the eigenvalues and eigenvectors, respectively, of the covariance matrix for the two variables, with consideration of a given confidence level (e.g. 90% in this study). In other words, the major and minor axes of the ellipse represent the direction and magnitude of the largest and second largest spread of the data. The samples (i.e. $sUHII$ and $aUHII$) can be decorrelated by rotating each data point such that the eigenvectors become the new reference axes – the major axis as y-axis and the minor axis as the x-axis. The principal component analysis (PCA) simply assumes that the most interesting feature is the one with the largest variance or spread. If all the

points are projected onto the largest eigenvector (major axis), the dimension of these data is reduced. In other words, the calculation of the confidence ellipse is equivalent to a two-dimensional PCA. The confidence level is chosen based on the Chi-Square distribution (Wilson and Hilferty, 1931) with specific "degrees of freedom" (representing the number of unknowns) (Spruyt, 2014). The 2-D Kolmogorov-Smirnov (K-S) test is then applied to further investigate the goodness-of-fit for the 2-D distributions of the $sUHII$-$aUHII$ relationship in terms of season, WS and LCZ. The 2-D K-S test developed by Peacock (1983) is the analogue of the one-dimensional K-S test. The statistical result of the 2-D K-S test is the maximum difference of the corresponding integrated probabilities (the fraction of the points for a quadrant) in four natural quadrants at a given point in the data, called statistic D, which is the maximum absolute difference between the two cumulative distributions. The key parameters calculated in the K-S test are demonstrated in the study of Peacock (1983).

4.3 Results

LRMs are generated based on different moderator variables, where a is slope and b is intercept coefficient, and the independent (x) and dependent (y) variables are $sUHII$ and $aUHII$ respectively:

$$y = a * x + b \qquad \text{Equation (4.1)}$$

The LRM for whole datasets was also calculated to compare with the LRMs with consideration of any moderator variable:

$$y = 0.57x + 0.26,\ (R^2 = 0.35) \qquad \text{Equation (4.2)}$$

This study is primarily focused on the regression output (R^2, slope and intercept) from the LRMs, the confidence ellipses and the results from ANCOVA and K-S tests based on the three moderator variables. The R^2 value herein is interpreted as the percentage of the variation of $aUHII$ explained by the regression equation using $sUHII$ as the only independent variable. The slope coefficient effectively represents an increment of the $aUHII$ for every one-degree increment of the $sUHII$, which can reflect the physical processes between surface and air. The intercept coefficient represents the value of $aUHII$ when the $sUHII$ becomes zero. A positive value of the intercept indicates that the $aUHII$ still exists despite the lack of a $sUHII$. Although there is limited available physical information from the interpretation of the intercept, the value of the intercept does appear to be statistically correlated with the slope.

4.3.1 The effect of wind speed

$sUHII$ and $aUHII$ data from all stations are grouped as low (WG1: WS<2m/s), median (WG2: WS=2-4m/s) and high (WG3: WS=4-6m/s) WS conditions. The linear regressions and 2-D distributions between $sUHII$ and $aUHII$ are visualised in Figure 4.2a and 4.2b. The mean values of the $sUHII$ and $aUHII$ decrease with increasing WS, illustrated by the moving tendency of the centre of the estimated ellipses to (0,0). The ratio of major axis to minor axis is largest in the WG2, indicating the more apparent linear relationship.

The slope coefficient of the regression models becomes smaller with increasing WS (Figure 4.2a), which suggests the reduced sensitivity of the $aUHII$ to WS compared to $sUHII$. In addition, the intercept coefficients tend to decrease with increasing WS as well, demonstrating the smaller $aUHII$ when $sUHII$ comes to zero under high WS condition.

It should be noticed that most values of intercept are positive due to the prevalent existence of the UHI phenomenon in cities.

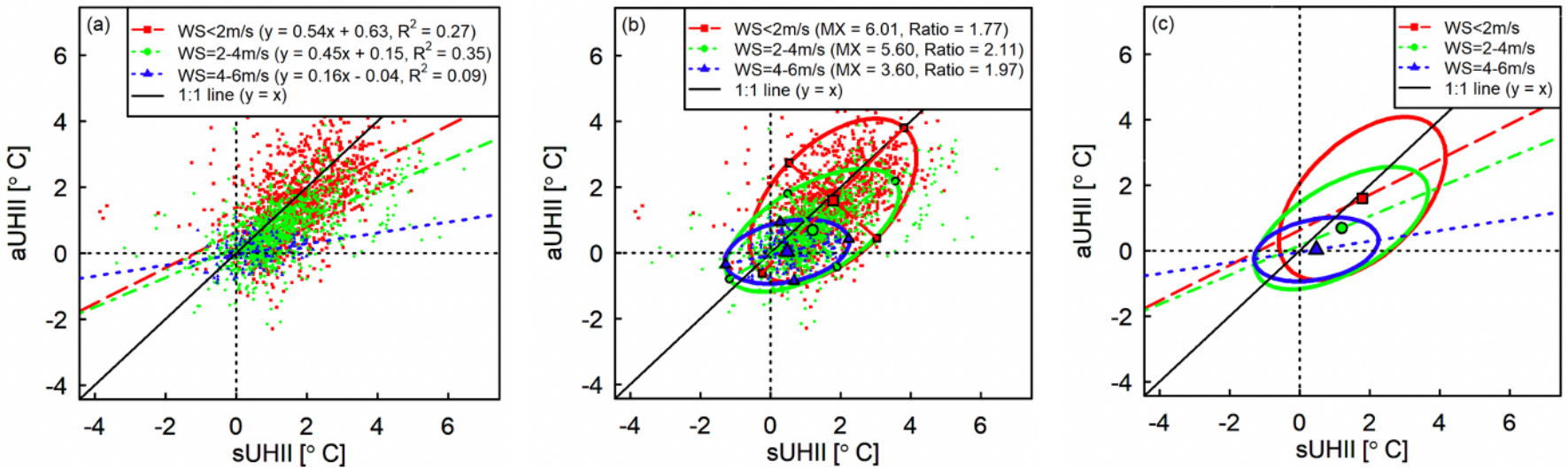

Figure 4. 2 Linear and elliptical trends of sUHII and aUHII based on three wind speed conditions in Birmingham: (a) LRM only; (b) confidence ellipse only and (c)LRM and confidence ellipse without data points, where the larger circles are the centre of corresponding ellipses, the smaller circles are the corresponding points of the major/minor axis, MX is major axis length and Ratio is the ratio of major to minor axis in (b)

The R^2 value of the regression model is highest in median WS group (WG2) ($R^2 = 0.35$) but is slightly lower in WG1 ($R^2 = 0.27$). In WG3, both $sUHII$ and $aUHII$ are small so that the influence from other processes become visible and these are viewed as noise in Figure 4.2 where the R^2 value is smallest (0.09). The decrease of R^2 values from WG2 to WG3 suggests a smaller sensitivity of $sUHII$ to $aUHII$. Moreover, the decrease of the slopes under high WS condition is also indicative to the decline of the R^2 values. For example, a slope value of zero implies that the value of $aUHII$ will be independent of $sUHII$. Thus, it is much less confident to estimate $aUHII$ based on $sUHII$ under high WS condition. In addition, the R^2 values decreased after classifying the data based on different WS because the data are subtracted to a more specific or smaller range.

The results from ANCOVA (Table 4.2) for the three wind groups (WGs) show that the overall WS effect on the linear $sUHII$-$aUHII$ relationship is significant at 99% confidence level (F=9.77). Moreover, the slopes and intercepts in the three WS groups are all significantly different at the 99% confidence level. The K-S test (Table 4.3) illustrates that the 2-D distributions are significantly different at 0.001 level in the three WGs. According to the D statistics, a 76% difference of the 2-D $sUHII$ - $aUHII$ distribution is found between WG1 and WG3, followed by 46% between WG2 and WG3 and 39% between WG1 and WG2.

Table 4. 2 ANCOVA results based on the updated wind speed groups

Base level	Slope	Intercept	Interaction effect
WG1 (WG2, WG3)	WG1≠WG2*** WG1≠WG3***	WG1≠WG2*** WG1≠WG3***	≠*** (F=9.77, p<0.001)
WG2 (WG3)	WG2≠ WG3**	WG2≠ WG3***	≠*** (F=12.81, p<0.001)

*NB: "≠" means "reject null hypothesis" — significant different (slope and intercept) or significant interaction effect exists (WS effect) (0.001***, 0.01**, 0.05*, 0.1)*

Table 4. 3 D statistics from K-S test results based on the three wind speed groups

Paired group	WG1	WG2	WG3
WG1	--		
WG2	0.39 (0.08)	--	
WG3	0.76 (0.19)	0.46 (0.19)	--

NB: the significant tests reached 0.001 confidence level for all paired groups and the numbers in brackets are the $D_{\alpha(\alpha=0.001)}$

4.3.2 Seasonal differences

The LRM and confidence ellipses for the $sUHII$-$aUHII$ relationship for four seasons are shown in Figure 4.3a and 4.3b. It is evident that the centre points of the ellipses, representing the mean values of $sUHII$ and $aUHII$, have a clear tendency to move towards the origin (0,0) in the order of summer, spring, autumn and winter, indicating a greater magnitude of the UHI in summer and spring. The longer major axis of the confidence ellipses and the larger ratio of major axis to minor axis are also indicative of the stronger linear trend in summer and spring. Although the available data in winter (n=257) is more limited than other seasons (Table 4.1), the lowest ratio of major axis to minor axis and the more rounded shape of the confidence ellipses indicate that the $sUHII$-$aUHII$ relationship is much less prominent in winter.

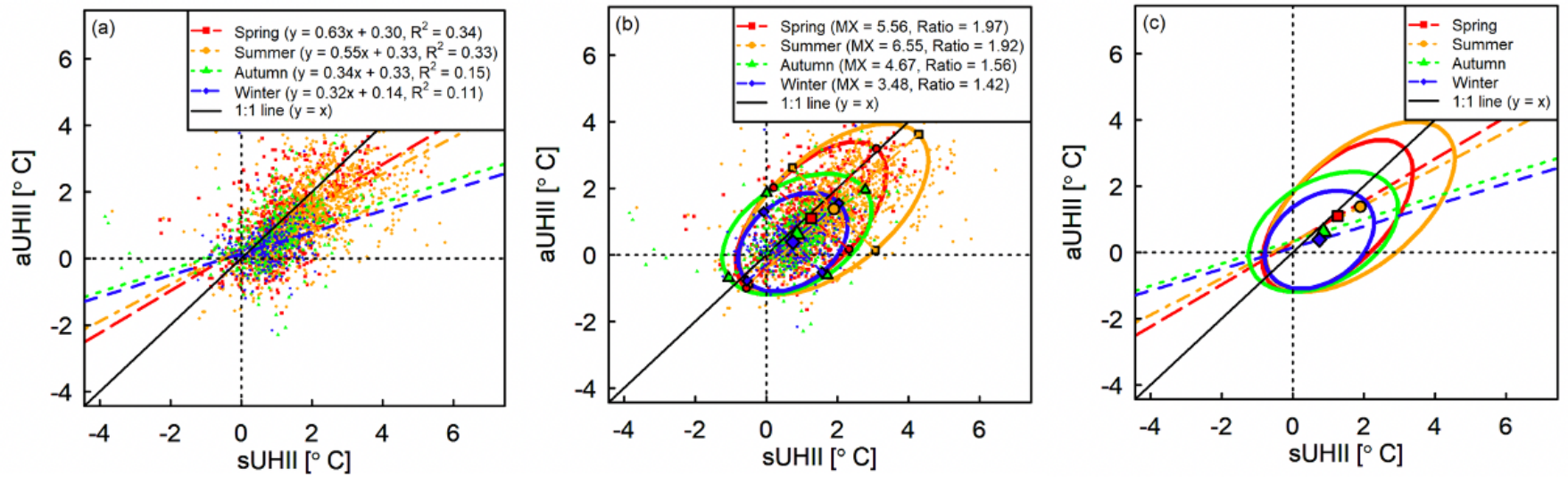

Figure 4. 3 Linear and elliptical trends of sUHII and aUHII based four seasons in Birmingham: (a) LRM only; (b) confidence ellipse only and (c) LRM and confidence ellipse without data points, where the larger circles are the centre of corresponding ellipses, the smaller circles are the corresponding points of the major/minor axis, MX is major axis length and Ratio is the ratio of major to minor axis in (b).

Figure 4.3a also shows the summary of the estimated LRM in four seasons. The rate of change of the linear models (slope) is small for autumn and winter. All LRMs were statistically significant at 99.9% confidence level except for the intercept in winter (not shown here), suggesting less reliability of the linear models in colder weather. In Figure 4.3a, the low R^2 values for autumn and winter suggest more uncertain influencing factors affecting the $sUHII$-$aUHII$ relationship. A more limited sample size (Table 4.1) in autumn and winter due to fewer clear-sky nights is also one of the potential factors causing the lower R^2 values. Moreover, the smaller magnitude of both $sUHII$ and $aUHII$ in colder seasons contributes to the reduced confidence of the estimated LRM. Furthermore, stronger anthropogenic heat (especially from space heating) may be responsible for the less correlated data between $sUHII$ and $aUHII$, leading to the decrease of R^2 values as well.

Table 4.4 and Table 4.5 demonstrate the results from the subsequent ANCOVA and K-S test that present interaction effects and differences of intercepts and slopes between different seasons and the significant test of 2-D distributions between $sUHII$ and $aUHII$, respectively. Overall, results from the two statistical tests provide the confidence to support the previous discussion of the regression models. The seasonal impacts (overall effect) are significant at 0.001 level in the group of four but less significant in these two groups – "spring and summer" and "autumn and winter". However, K-S test (Table 4.4) demonstrates that in all tests, $D > D_{\alpha(\alpha=0.001)}$ where $D_{\alpha(\alpha=0.001)}$ is the critical value of the statistics D at 99.9% confidence level; in other words, the 2-D distributions between $sUHII$ and $aUHII$ are all significantly different at 99.9% confidence level between any pair of two seasons from the K-S test result. Moreover, the D statistics represent the maximum 2-D distribution differences as well as the overlapping portions in a quadrant

of the data points in a paired group. In particular, the differences are greater in "summer, autumn (45%)" and "summer, winter (55%)" paired groups. In addition, the differences between D and D_a ($\Delta D = D - D_a$) are greatest in "summer, autumn" and "summer, winter" paired groups, which also indicated the bigger differences of the distribution comparing summer to autumn and winter.

Table 4. 4 ANCOVA results based on the four seasons

Paired group	Spring	Summer	Autumn	Winter	Four seasons
Spring	--	(≠*, =)	(≠***, =)	(≠***, =)	--
Summer	**≠* (F=3.44)**	--	(≠***, =)	(≠***, ≠**)	--
Autumn	**≠*** (F=27.45)**	**≠*** (F=14.61)**	--	(=, ≠**)	--
Winter	**≠*** (F=15.74)**	**≠** (F=7.35)**	**= (F=0.04)**	--	--
Four seasons	--	--	--	--	**≠*** (F=10.80)**

*Note: bold font – interaction effect, regular font – significant tests of slope and intercept; "=" means "cannot reject null hypothesis", "≠" means "reject null hypothesis" — significant interaction effect exists (seasonal effect) (0.001***, 0.01**, 0.05*, 0.1)*

Table 4. 5 D statistics from K-S test results based on the four seasons

Paired group	Spring	Summer	Autumn	Winter
Spring	--			
Summer	0.29 (0.10)	--		
Autumn	0.25 (0.13)	0.45 (0.12)	--	
Winter	0.43 (0.14)	0.55 (0.14)	0.22 (0.16)	--

Note: the significant tests reached 0.001 confidence level for all paired groups and the numbers in brackets are the $D_{\alpha(\alpha=0.001)}$

4.3.3 The role of site characteristics

The analysis is conducted to infer the role of LCZ. Due to the limited stations for some LCZs in the city, LCZ1 and LCZ2 are classified as urban group, whereas LCZ5, LCZ6 and LCZ10 are classified as suburban group. Figure 4.4 shows the confidence

ellipses and linear regression models based on the urban and suburban groups. As expected, the $UHII$ is stronger for urban group and weaker for suburban group whose ellipse's centre is closer to (0,0). The longer major axis and the larger ratio of the major to the minor axis indicate a more noticeable linear relationship for urban group.

Overall, differences in the regression coefficients between urban and suburban groups are evident, which increase from urban to suburban group for both slope and intercept. The pattern of the slopes of the LRMs indicates a lower sensitivity of the $aUHII$ than $sUHII$ for suburban group. In terms of intercepts, the positive values in both urban and suburban linear regression models indicate that $aUHII$ tends to exist even when the $sUHII$ becomes zero. Meanwhile, the higher value of the intercept suggests that the magnitude of the $aUHII$ tends to be higher in urban than suburban group. R^2 values are higher in urban group (0.46) than suburban group (0.28). Compared with the R^2 value of 0.35 for the whole dataset, a higher R^2 value of 0.46 is obtained for the subset, urban group. It is therefore concluded that among the three moderator variables (season, wind speed, and LCZ), LCZ can increase the R^2 value of the linear $sUHII$-$aUHII$ relationship for a subset of data. This is consistent with the finding in Figure 4B that for the subset of 'urban', both the major axis length and ratio of major to minor axis are the largest among all subsets for all three moderator variables (see Figures 4.2b & 3b).

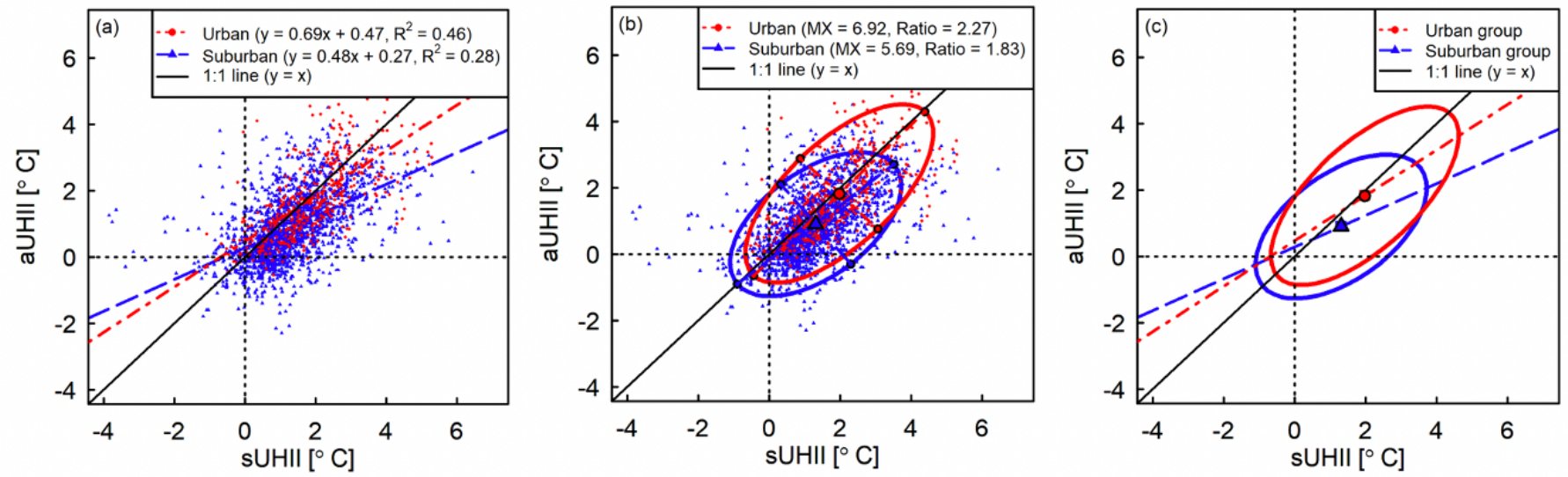

Figure 4. 4 Linear and elliptical trends of sUHII and aUHII based on urban and suburban groups: (a) LRM only; (b) confidence ellipse only; (c)LRM and confidence ellipse without data point, where the larger circles are the centre of corresponding ellipses, the smaller circles are the corresponding points of the major/minor axis, MX is major axis length and Ratio is the ratio of major to minor axis in (b).

The ANCOVA (Table 4.6) and K-S tests (Table 4.7) are conducted for each LCZ subset and for the urban and suburban subsets. With respect to different LCZs, the two statistical tests show more evidence for the comparison between different paired groups. The results from ANCOVA test (Table 4.6) illustrate that the differences between the regression models are mostly significant among many of the different paired groups for LCZs (green highlighted section). However, the differences of some paired groups: LCZ6 and LCZ1, LCZ6 and LCZ2 are not significant. Moreover, additional statistical tests for slope and intercept (blue highlight section) infer that the LRM differences between some paired groups of LCZs are not significant in this respect. From the K-S test (Table 4.7), the 2-D distributions are all significantly different between the five LCZs ($p < 0.001$). Moreover, it is evident that the differences between the values of D and D_a (ΔD) become larger when the compared group is less urbanised for each column. For example, the values of ΔD increase as the following order of the paired groups: "LCZ1, LCZ2", "LCZ1, LCZ5", "LCZ1, LCZ10", "LCZ1, LCZ6". In contrast, the ΔD values will decrease when the paired groups are more similar, such as "LCZ10, LCZ6".

For the urban and suburban groups, ANCOVA test (Table 4.6) provides sufficiently high confidence levels for the differences of the linear $sUHII$ - $aUHII$ relationship. Moreover, the highest F value (F=11.20) is found in the urban and suburban paired group, which indicates the reliability of this classification compared to analyse individual LCZ. The K-S test (Table 4.7) shows that the D statistics ($D = 0.32, D_a = 0.10$) are almost the largest among all other paired groups at 0.01 confidence level, which also indicates the urban and suburban classification is appropriate and can be implemented for further analysis.

Table 4. 6 ANCOVA results based on different LCZs and levels of urbanisation

Paired group	LCZ1	LCZ2	LCZ5	LCZ6	LCZ10	Urban group	Suburban group	All LCZ
LCZ1	--	(=, ≠***)	(≠***, =)	(=, ≠**)	(≠***,≠***)	--	--	--
LCZ2	**= (F=0.66)**	--	(≠***, =)	(=, =)	(≠***, =)	--	--	--
LCZ5	**≠** (F=9.99)**	**≠*** (F=10.87)**	--	(≠**, =)	(≠*,≠**)	--	--	--
LCZ6	**= (F<0.01)**	**= (F=0.14)**	**≠** (F=10.22)**	--	(≠, =)	--	--	--
LCZ10	**≠** (F=7.87)**	**≠*** (F=11.10)**	**≠* (F=3.24)**	**≠* (F=2.90)**	--	--	--	--
Urban group	--	--	--	--	--	--	(≠***,≠***)	--
Suburban group	--	--	--	--	--	**≠*** (F=11.20)**	--	--
All LCZ	--	--	--	--	--	--	--	**≠*** (F=8.979)**

*Note: bold font – interaction effect, regular font – significant tests of slope and intercept; "=" means "cannot reject null hypothesis", "≠" means "reject null hypothesis" — significant interaction effect exists (0.001***, 0.01**, 0.05*, 0.1)*

Table 4. 7 D statistics from K-S test results for different LCZs

Paired group		LCZ1	LCZ2	LCZ5	LCZ6	LCZ10
		Urban group		Suburban group		
LCZ1	Urban group	--		0.32 (0.10)		
LCZ2		0.24 (0.20)	--			
LCZ5	Suburban group	0.36 (0.26)	0.23 (0.23)	--		
LCZ6		0.44 (0.17)	0.32 (0.12)	0.33 (0.21)	--	
LCZ10		0.42 (0.27)	0.28 (0.24)	0.34 (0.29)	0.27 (0.21)	--

Note: the significant tests reached 0.001 confidence level for all paired groups and the numbers in brackets are the $D_{\alpha(\alpha=0.001)}$

4.4 Discussion

The statistical significance of the two regression coefficients (slope and intercept) of the LRMs analysed in Sections 4.3.1 - 4.3.3 can indicate some useful information about the relationship between $sUHII$ and $aUHII$. In fact, the slope can be related to the covariance between $sUHII$ and $aUHII$ (denoted by $Cov(sUHII, aUHII)$) and the standard deviation of these two variables (denoted by SD_{sUHII} and SD_{aUHII}) (Fisher, 1934):

$$slope = \frac{Cov(sUHII,aUHII)}{Var(sUHII)} = r \cdot \frac{SD(aUHII)}{SD(sUHII)} \quad \text{Equation (4.3a)}$$

$$r = \frac{Cov(sUHII,aUHII)}{SD(sUHII) \cdot SD(aUHII)} \quad \text{Equation (4.3b)}$$

where r is the correlation coefficient ($r = \sqrt{R^2}$) and $Var(sUHII)$ is the variance of $sUHII$. Table 4.8 lists the results of the statistical parameters for $sUHII$ and $aUHII$. The following discussion will be based on these statistical quantities.

Table 4. 8 Statistical quantities related to sUHII and aUHII for different wind speed groups, season groups and urban/suburban groups

Moderate variable		$Cov(sUHII, aUHII)$	SD_{sUHII}	SD_{aUHII}	SD Ratio ($= \frac{SD_{aUHII}}{SD_{sUHII}}$)	Slope from LRM
WS	WG1	0.66	1.11	1.16	1.05	0.54
	WG2	0.59	1.15	0.87	0.76	0.45
	WG3	0.11	0.81	0.45	0.56	0.16
Season	Spring	0.61	0.99	1.07	1.08	0.63
	Summer	0.85	1.24	1.19	0.96	0.55
	Autumn	0.32	0.96	0.84	0.88	0.34
	Winter	0.16	0.71	0.69	0.97	0.32
Site characteristic	Urban group	1.04	1.23	1.25	1.02	0.69
	Suburban group	0.60	1.12	1.01	0.90	0.48

4.4.1 Difference of the $sUHII$-$aUHII$ relationship under three WGs

According to the derived LRMs and confidence ellipses in Section 4.3.1, an increase of WS reduces the slope and intercept values. This is consistent with the rotation of the confidence ellipses with WS. From Table 4.8, the decrease of both SD_{aUHII} and SD_{sUHII} with increasing WS indicates that WS can reduce the variabilities of both $aUHII$ and $sUHII$ by turbulent mixing, but is more effective for $aUHII$, which is reduced to 0.45℃ for WG3, compared with 0.81℃ for $sUHII$. These imply that T_a is more affected by WS than T_s due to different processes influencing these two variables by wind flow. In addition, $Cov(sUHII, aUHII)$ decreases significantly with WS, indicating a much weaker joint variability of $sUHII$ and $aUHII$ for WG3. This suggests that there are more similarities between $sUHII$ and $aUHII$ for low WS scenarios, but more dissimilarities for high WS scenarios. The implication is that use of satellite data to infer $aUHII$ has a higher confidence for low WS conditions than for high WS conditions.

The slope is likely to be related to wind advection. The spatial pattern of $aUHII$ is shifted by advection due to the wind transport of air temperature directly (Bassett et al., 2016, Heaviside et al., 2015). In contrast, the spatial pattern of $sUHII$ should be more influenced by the local-scale radiation processes and less affected by advection (the surface heat needs to be transferred to air first before the advection and heat transfer back to the surface in a downwind location). The shift of spatial pattern between $sUHII$ and $aUHII$ can be reflected by the statistical value of $Cov(sUHII, aUHII)$ which decreases with WS. In other words, the covariance between $sUHII$ and $aUHII$ is increasingly smaller under higher WS conditions. From Equation 4.3a, the value of the slope of LRM equates to the ratio of $Cov(sUHII, aUHII)$ to $Var(sUHII)$, and it can also be interpreted

as a normalised covariance. As seen in Table 4.8, although $Var(sUHII)$ decreases with WS (by about 50% from WG1 to WG3, estimated from the values of SD_{sUHII}), the decrease of $Cov(sUHII, aUHII)$ with WS is much faster (~83% from WG1 to WG3). Therefore, the decrease of slope with increasing WS is due to the change of the $Cov(sUHII, aUHII)$ from statistical aspect. Moreover, a higher WS tends to destroy the nocturnal stable layer over the rural surface and to entrain the warmer air aloft downwards to warm the T_a there, thus reducing the magnitude of $aUHII$. Although this process may also warm the T_s at the rural site, the magnitude of reduced $sUHII$ could be smaller. Such reductions of UHII can be reflected from the magnitudes of SD_{sUHII} and SD_{aUHII} in Table 4.8. Consequently, the slope of the LRM will be reduced because the slope is linearly proportional to the SD ratio (Equation 4.3a).

In Figure 4.2b or 4.2c, the centres of the ellipses represent the mean values of $UHII$: $(\overline{sUHII}, \overline{aUHII})$. The results show that all three centres are below the 1:1 long-dashed line. This is interpreted as a higher $\overline{sUHII}$ than $\overline{aUHII}$ for all wind groups, consistent with the dominating processes of storage-heat release and radiative trapping in urban areas. For the low WS group, WG1, the circle is very close to the 1:1 long-dashed line, indicating that $\overline{sUHII} \approx \overline{aUHII}$. From the perspective of processes, under calm conditions, surface temperature drops rapidly by emitting longwave radiation, cooling the air near the ground, and the surface layer may become extremely stable and shallow (T_s is lower than T_a). Therefore, a thermal inversion may be formed near the surface with a limited amount of heat in the shallow surface layer being transferred to the ground, reducing $T_a^{(r)}$ more compared with windier conditions under which the surface layer is deeper. This leads to similar magnitudes of $T_a^{(r)}$ and $T_s^{(r)}$ within the shallow surface layer

and therefore, the characteristics of $aUHII$ and $sUHII$ are similar because the magnitude of UHII is sensitive to the extent of rural radiative cooling. For a high WS group, WG3, Figure 4.2c shows that $\overline{aUHII}$ is close to zero, whereas $\overline{sUHII}$ still has a finite value. As discussed above, surface loses radiative energy irrespective of high WS but the nocturnal stable layer (or temperature inversion) above the surface layer over the rural site could be destroyed under high wind speed conditions, leading to an entrainment of warmer air in the residual layer aloft into the surface layer (Stull, 1988) and a subsequent less cooling effect of air temperature in rural areas. Therefore, $\overline{aUHII}$ may reach zero while $\overline{sUHII}$ still exists.

4.4.2 Effect of climatology (seasonal effect)

Figure 4.3 indicates that both $sUHII$ and $aUHII$ are stronger in summer and spring, and weaker in winter and autumn at night-time. These were also reported by many previous studies (Fenner et al., 2014, Van Hove et al., 2015, Peng et al., 2011, Meng and Liu, 2013). Studies carried out in central Europe argued that the development of the UHI is favourable during summer at night-time because of the greater likelihood of clear skies and lighter winds for mid-latitudes climate (Fortuniak et al., 2006, Kłysik and Fortuniak, 1999). Furthermore, the seasonal variation of rural thermal admittance related to soil moisture is considered as another significant contributor to seasonal differences of UHI (Arnfield, 1990, Runnalls and Oke, 2000). The seasonality of soil moisture has been found to be related to the heat island intensity in London (Zhou et al., 2016). Likewise, the drier seasonal climate during summer in Birmingham may reduce soil moisture, and therefore thermal admittance differences between urban and rural areas become greater (Oke et al., 1991, Imamura, 1991). The increased thermal admittance differences cause larger differences of the cooling rates between urban and rural areas, which could

contribute to faster decrease of temperature at rural site and increase of UHI consequently during the summer period (Runnalls and Oke, 2000). Moreover, the increase of solar insolation during summer time induces a greater amount of energy to be stored and released during daytime and night time respectively. Fenner et al. (2014) stated that the decoupling of the urban sites from the rural site is largely strengthened due to the stronger radiative forcing during summer compared to winter, leading to the strongest UHI developed on summer nights. In addition, the timing of sunset is between 21:00Z and 22:00Z during the summer period, which is close to the satellite passing time mentioned in Chapter 2. This means that cooling might start later compared to other seasons, which could induce a larger UHII, especially $sUHII$ (e.g., larger mean differences of $sUHII$ compared to $aUHII$ (represented by the horizontal and vertical distance of the centre points of ellipses respectively) between summer and spring). However, causative factors governing the seasonal differences of the magnitude of both $sUHII$ and $aUHII$ are still needed to be further explored, e.g., seasonal variations of rural moisture and heat storage or temperature cooling rates differences between urban and rural areas etc.

Table 4.8 shows very high values of $Cov(sUHII, aUHII)$ for summer (0.85) and spring (0.61) and a very low value for winter (0.16), whereas the magnitudes of SD_{sUHII} and SD_{aUHII} show much less contrast across the seasons. This is consistent with the slope values in Figure 4.3a, larger slopes for spring and summer, and smaller for autumn and winter. The values of $Cov(sUHII, aUHII)$ and the slopes suggest some similarities between $sUHII$ and $aUHII$ for summer, but dissimilarities for winter. The implication is that use of satellite data to infer $aUHII$ has a higher confidence for summer and spring than for autumn and winter. The result is also in line the R^2 values shown in Figure 4.3a.

To link the results here to mechanisms in the WS categorisation, we have calculated the mean wind speed for the four seasons: Spring: 1.98 m/s, Summer: 1.95 m/s, Autumn: 2.21 m/s, Winter: 3.18 m/s. Use of the results in 4.3.1 and discussions in 4.4.1 suggests that low wind speed for spring and summer is one of the reasons why the magnitudes of both $sUHII$ and $aUHII$ and the slopes of the LRMs are greatest among four seasons. The values of $(\overline{sUHII}, \overline{aUHII})$ represented by the centres of the ellipses in Figure 4.3c can be partially explained by the WS mechanism discussed earlier, i.e. the faster WS is, the smaller the values of $\overline{sUHII}$ and $\overline{aUHII}$. As the values of mean wind speed are similar for summer and spring, the larger $\overline{sUHII}$ and $\overline{aUHII}$ for summer is explained by stronger solar insolation. Although the mean wind speed for winter is much larger than that for autumn, the values of $\overline{sUHII}$ and $\overline{aUHII}$ for winter are as large as those for autumn. This could be attributed to the release of anthropogenic heat due to more energy consumption during the winter season. In addition, the reduced surface albedo because of the removal of crops in rural areas and the loss of canopy cover in urban areas could increase the absorption of solar radiation during winter, which could be one of the reasons for similar magnitude of $\overline{sUHII}$ and $\overline{aUHII}$ between autumn and winter seasons.

4.4.3 Difference of the $sUHII$-$aUHII$ relationship from urban to suburban group

The results for two land-use groups are shown in Figure 4.4. It is worth mentioning that except for data missing scenarios, both groups of data cover similar wind conditions and seasonal distributions. Therefore, the differences shown in Figure 4.4 should be mainly attributed to the disparity of the land-cover characteristics between the two groups. It is evident in Figure 4.4c that larger $\overline{sUHII}$ and $\overline{aUHII}$ are found for the Urban group

than for the Suburban group. In addition, a larger slope is also evident for the urban group, which is caused by the larger joint variability between $sUHII$ and $aUHII$, i.e. $Cov(sUHII, aUHII)$, for the urban group, as shown in Table 4.8. In order to gain more insight into the relationships, a quadrant analysis is conducted and the results are shown in Figure 4.5, in which the values of $(\overline{sUHII}, \overline{aUHII})$ represented by the circle of the ellipse are used to separate the parameter space into four quadrants, Z1-Z4. A higher percentage of data points in Z1 (in which $sUHII > \overline{sUHII}$ AND $aUHII > \overline{aUHII}$) and Z3 (in which $sUHII < \overline{sUHII}$ AND $aUHII < \overline{aUHII}$) will enhance the value of $Cov(sUHII, aUHII)$, and increase the slope of the LRM. Likewise, a higher percentage of data points in Z2 (in which $sUHII < \overline{sUHII}$ AND $aUHII > \overline{aUHII}$) and Z4 (in which $sUHII > \overline{sUHII}$ AND $aUHII < \overline{aUHII}$) will reduce the value of $Cov(sUHII, aUHII)$, decreasing the slope of the LRM. One imperative factor that may have an impact on the distribution of data points is wind advection. Warm advection can raise T_a promptly with T_s unchanged or warmed later; this could induce a greater chance of the Z2 scenario. Similarly, cold advection could induce a greater chance of the Z4 scenario. It should be noticed that an urban site near the city centre has a small chance of experiencing warm advection but is more subject to cold advection; this is supported by the data in Figure 4.5a, showing 7% of Z2 and 12% of Z4. The stations in the suburban group in Birmingham, however, are scattered around the city centre, some near rural area and some close to parks (Figure 4.1). Therefore, they are collectively subject to both warm advection (from upwind urban patches) and cold advection (from upwind rural area or nearby parks), consequently yielding a higher percentage for Z2 (14%) and for Z4 (13%) as shown in Figure 4.5b. Accordingly, these explain that the value of

$Cov(sUHII, aUHII)$ is higher for the urban group (1.04 in Table 4.8) and lower for the suburban group (0.60 in Table 9).

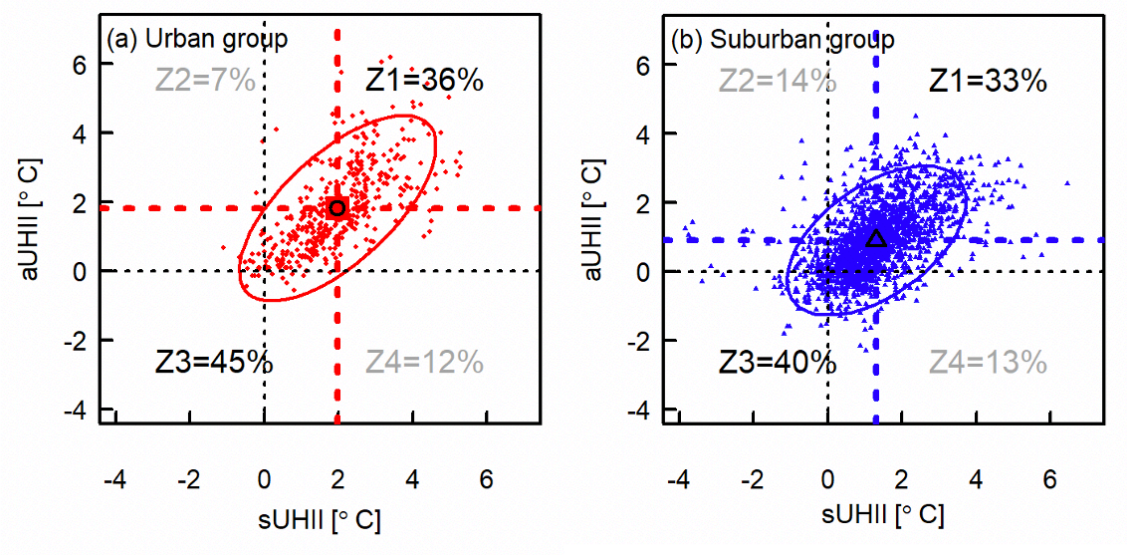

Figure 4. 5 Percentage of the data points in four quadrants (Z1, Z2, Z3 and Z4) dividing by the centre of ellipse, shown by red and blue dotted lines for (a) urban group and (b) suburban group.

Considering that SD_{sUHII} is similar for the two groups (1.23 and 1.12 in Table 4.8), according to Equation (4.3a), the slope of LRM is higher for the urban group than the suburban group; the result is also shown in Figure 4.4a. Based on the discussions, we may conclude that the data of $sUHII$ for the urban sites are better correlated with $aUHII$ compared with those of the suburban sites. The implication is that wind advection (together with other factors not discussed here) may obscure the interpretation of satellite-sensed land surface temperature for the purpose of representing $aUHII$ by $sUHII$, and caution should be taken particularly for suburban locations.

In addition, the positive intercept values in the regression models might provide an implication of the "lagged development" of $aUHII$ compared to $sUHII$ which is also

indicated by Oke et al. (2017). This implication is based on the assumption that the temporal variation of $sUHII$ and $aUHII$ is similar in pattern but with a time lag during night time due to the processes of heat storage in the surface during the daytime and heat transfer from the surface to the air during the night. According to Oke (2002b), the typical temporal variation of $aUHII$ is that $aUHII$ will increase after sunset and reach the maximum a few hours after sunset and it tends to decrease afterwards. The "lagged development" of $aUHII$ means that the increase and decrease of $sUHII$ take place earlier compared to $aUHII$ during night-time. Therefore, the point where $sUHII$ approaches 0 but $aUHII > sUHII \sim 0$ (intercept value) will appear at some time during the development of UHI. For a stronger UHI event, this point may occur later at night, whereas for a weak UHI event, this point may occur earlier (e.g. at the hours of this analysis). The positive intercept values are consistent based on different seasons and WS classification. In addition, the intercept value tends to be 0 when the wind speed increases (Figure 4.2a), indicating that the lag effect diminishes with increasing WS. However, most of the data points are away from the (0,0) point and we don't have strong supporting evidence from our data.

4.5 Conclusion

An investigation of the $sUHII$-$aUHII$ relationship has been challenged by the complicated interactions between varying meteorological processes and the multi-scale, heterogeneous urban environment. However, using the methodology outlined in this paper, the linear $sUHII$-$aUHII$ relationship is shown to be statistically reliable, and clearer characteristics of this relationship are revealed for the categorised data groups based on three moderator variables: wind speed (WS), season and level of urbanisation.

The following results are highlighted: (i) The linear $sUHII$-$aUHII$ relationship significantly varies with respect to the three moderator variables; results indicate that satellite data can be used to infer $aUHII$ with a higher confidence for low wind speed conditions. Results also demonstrate better confidence in the approach for summer and spring seasons and for more urbanised sites. (ii) For the WS category, the decrease of the slope of LRM with increasing WS is explained by the same decreasing trend of the value of covariance between $sUHII$ and $aUHII$, $Cov(sUHII, aUHII)$; subsequently, the decreasing $Cov(sUHII, aUHII)$ with WS is partially attributed to wind advection which causes different shifts of the spatial pattern of $sUHII$ and $aUHII$. (iii) The larger slopes in summer and spring are partly explained by the lower WS conditions during these two seasons; however, further investigations of other causative factors are needed. (iv) The quadrant analysis applied to two land-use groups (urban vs. suburban) yields the evidence to support the argument that wind advection may be responsible for the lower correlation between $sUHII$ and $aUHII$ for the suburban group. Therefore, different impacts of wind advection on T_a and T_s may affect the representation of $aUHII$ by $sUHII$, and cautions should be taken particularly for suburban locations.

In summary, investigation into the $sUHII$-$aUHII$ relationship based on LRMs has previously been found difficult by a few studies. Compared with previous studies, the unique combination of analyses adopted in this study to investigate the $sUHII$-$aUHII$ relationship is able to provide more statistical evidence to estimate the magnitude and the range of the $aUHII$ from $sUHII$ under different conditions. In addition, the exploration of the $sUHII$-$aUHII$ relationship in this study provides more evidence and knowledge for the modelling of the T_s - T_a relationship, which may also be useful to further understand the applicability of MOST in the urban environment.

Several limitations should be highlighted in this study. Firstly, it is unfortunate that the study did not determine the same or similar sample size for each group of the data based on different stratification levels. The different sample size of the data might produce some uncertainties in the estimation of LRMs, although the statistical tests for LRMs and regression coefficients have been conducted based on the 0.01 significance level. Secondly, the generalisability of these models is subject to certain limitations. For instance, the values of regression coefficients are valid only based on these specific datasets in Birmingham, under the specific regional climate conditions during the study period. Another weakness of this study is the lack of consideration of how these three moderator variables affect the $sUHII$ and $aUHII$ jointly due to the limited data size.

Despite the above limitations, the study adds to the understanding of the $sUHII$-$aUHII$ relationship. Further research based on this method needs to be conducted in other cities. Moreover, when sufficient data are available, multiple factors can be considered at the same time to study the $sUHII$-$aUHII$ relationship and it is expected that such refined studies may yield improved outcome. In addition, $sUHII$ mainly depends on the quality of the satellite datasets. It is necessary to use other or higher-resolution remote sensing data to check or to validate the results of this study in the future.

4.6 Summary

This chapter has added a deeper understanding of the sUHII-aUHII relationship by using UMN data under different wind speed condition, seasons and levels of urbanisations. The decision to base the analysis on these three parameters is results from Chapter 2 that finds significant role of them in modulating both sUHII and aUHII. In addition to wind, specific characteristics of the sUHII-aUHII relationship have been

found for two further influencing factors of season and urbanisation. Further investigation is now required into the applicability of these characteristics in a different environment. This will be explored in Chapter 5.

Chapter 5 A tale of two cities: The influence of urban meteorological network design on the nocturnal surface versus canopy heat island relationship in Oklahoma City, US and Birmingham, UK

This chapter aims to further confirm the characteristics of the sUHII-aUHII relationship discovered in Chapter 4. This is achieved by extending the analysis to Oklahoma City (OKC), US, which then enables a comparative study between the cities of OKC and Birmingham. The work has also provided an opportunity to explore the implications of distinct climatic differences as well as the role of the design / configuration of Urban Meteorological Networks (UMNs). Finally, an attempt is also made to explore the possibility of generalising the sUHII-aUHII relationship across different cities.

This chapter was published as:

***Feng, J.L.**, Cai, X.M. and Chapman, L., 2020. A tale of two cities: The influence of urban meteorological network design on the nocturnal surface versus canopy heat island relationship in Oklahoma City, US and Birmingham, UK. International Journal of Climatology. https://doi.org/10.1002/joc.6697 (In press).*

5.1 Introduction

Detailed introductions related to the surface ($sUHII$) and canopy air heat islands ($aUHII$) have been provided in Chapters 1 - 2. Overall, an exploration of the relationship between $sUHII$ and $aUHII$ (the $sUHII$- $aUHII$ relationship) in different cities is needed to provide stronger confidence of the patterns of this relationship, which are of fundamental importance to seek the generalisation of this relationship because possible generalisations would be more useful in urban climate research rather than unique forms of the UHI across different cities (Oke, 1973). In previous chapter, a unique analysis combining linear regression with confidence ellipse, together with two statistical tests provides a starting point to generalise patterns of the $sUHII$- $aUHII$ relationship across cities. This chapter uses this approach to provide a comparative study of the nocturnal $sUHII$- $aUHII$ relationship in Oklahoma City (OKC), US and Birmingham (BHAM), UK, by using MODIS satellite data and ground observations from two Urban Meteorological Networks (UMNs). In doing so, the impacts of different climatic background conditions (e.g. wind speed, daily accumulated solar radiation) can be investigated. More significantly, the use of two different UMNs that have been set up based on different standards and protocols, allows for an exploration of how different configurations of urban climate networks can impact upon the broader results.

5.2 Study areas

5.2.1 Geography and climate background

Table 5.1 provides the background with respect to the geography and climate characteristics across the OKC and Birmingham. Both cities are located inland with a roughly flat terrain where the range of the topography height (difference between the

highest and lowest values) is 60 m and 97 m within the city boundaries of OKC and Birmingham respectively. It should be noted that OKC is not a consolidated city-county, where the total area is approximately 1610 km^2 including 630 km^2 urbanised areas embedded by a central business district (CBD) with around 20 km^2. In contrast, the city of Birmingham (268 km^2) forms a conurbation where the total areas are around 901 km^2, e.g. the city of Wolverhampton to the north west of Birmingham and Coventry city to the east of Birmingham. Figure 5.1 provides a clearer visualisation of the size of the city and the land-cover types over the two cities, based on the MODIS yearly land cover type product (MCD12Q1) that is retrieved in the year of 2009 and 2013 for OKC and Birmingham respectively with an approximate 500-m (463.32 m) spatial resolution over the two cities.

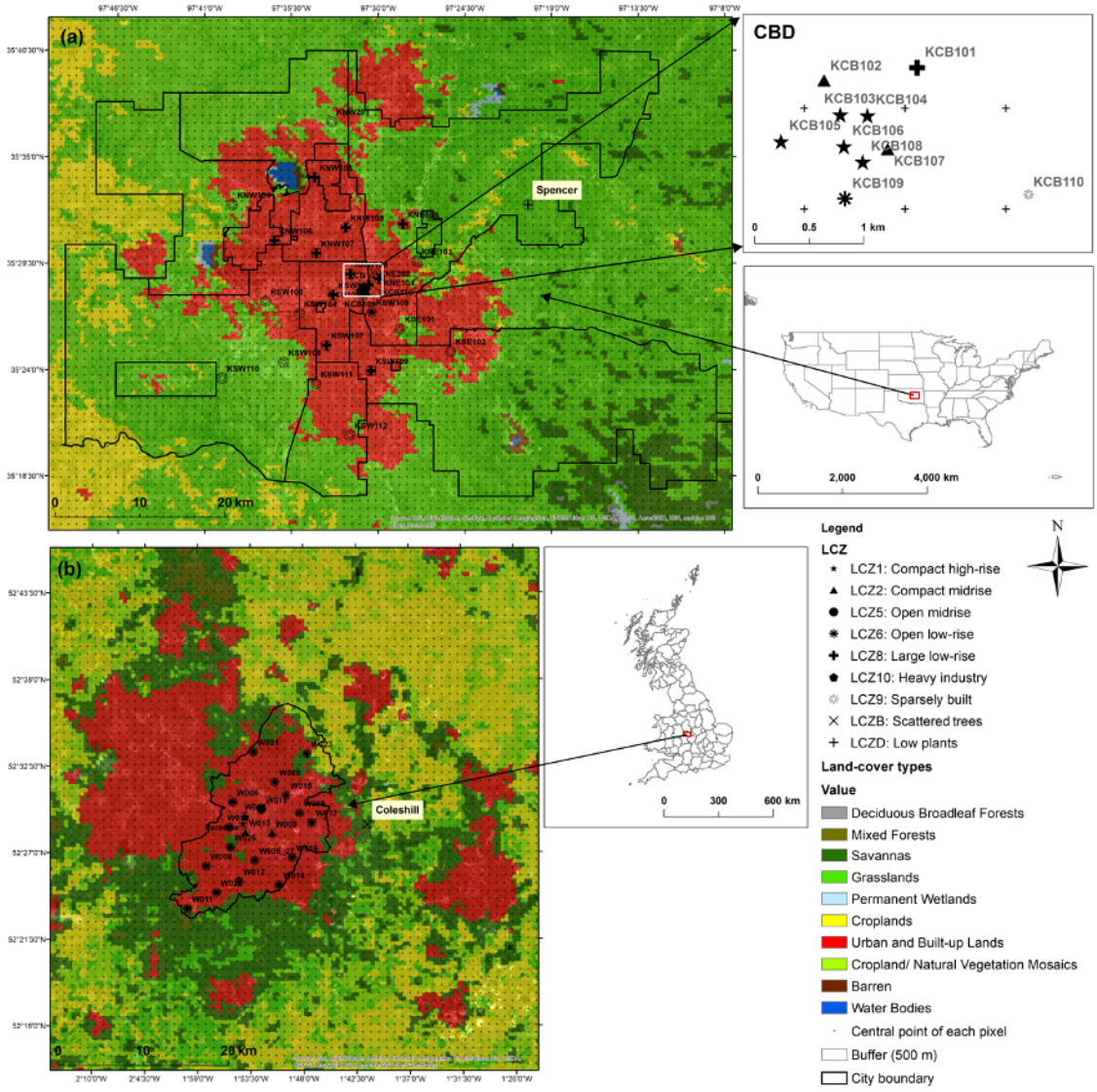

Figure 5. 1 MODIS Land cover map for (a) Oklahoma City and (b) Birmingham with LCZ classification of each station

Table 5. 1 General geography and climate background across two cities

Geographical information					
City	Location of city centre	Total areas (km^2)	Population	Topography height (above sea level) across the weather stations used in this study (m)	Average building height (m)
OKC	$35.4676° N, 97.5164° W$	1610 (urbanised areas: 630; CBD: 20)	562,343 (2009)	Max: 419 Min: 359 Average: 382	50-70 (max: 152) in CBD (Hu et al., 2016b)
Birmingham	$52.4862° N, 1.8904° W$	268 (901 for the whole conurbations)	1,073,045 (2011)	Max: 190 Min: 93 Average: 136	8 (max: 99) within the boundary of Birmingham (Ordnance Survey, 2014)
Climatic/meteorological characteristics					
City	Climate type with annual mean relative humidity within the bracket	Annual mean temperature (℃)	Annual total precipitation (mm)	Mean daily accumulated solar radiation (MJ/m^2)	Mean wind speed and wind direction
OKC	Humid subtropical climate (64%)	16*	847*	22.64	2.52 m/s (South - southeast)
Birmingham	Marine west coast climate (86%)	9*	660*	15.18	2.13 m/s (South - southwest)

*Note: statistics superscripted with * are derived from World Climate & Temperature (Climatemps.Com); Statistics including mean relative humidity, mean daily accumulated solar radiation, mean wind speed and wind direction are derived from rural stations (Spencer station in OKC and Coleshill station in Birmingham) during the study period.*

5.2.2 OKCNET and BUCL urban meteorological networks

OKC and Birmingham both have high-resolution UMNs which provide a dense dataset for T_a used to calculate $aUHII$ in this study. Unlike the consistency achieved with T_s products measured by the same satellite instrument (more details could be found in Section 5.3.2), large uncertainties of T_a measurement may arise due to the differences of UMNs' configurations. This is a consequence of no standard accepted protocol existing for the establishment of urban networks (e.g. Muller et al. (2013a)) and means that UMNs have often been designed for different purposes. All will have significant consequences on the nature of the data collected (and subsequent analysis), but no deployment solution is perfect and underpins the notion that there is no such thing as a representative urban temperature measurement (Muller et al., 2013a). Therefore, it is necessary to have a comprehensive background knowledge of the deployment strategy and configuration of the UMNs before investigating the characteristics of the $aUHII$ and $sUHII$ over OKC and Birmingham.

5.2.2.1 General deployment rationale

OKCNET (OKC Micronet) and BUCL (Birmingham Urban Climate Lab) are both UMNs that operate at the urban city scale based on the semi-random approach (Muller et al., 2013a).

Specifically, the stations considered in this study from OKCNET include 33 stations mounted on traffic signals at a height of 9 m with an average spacing of approximately 3 km over the OKC metropolitan area (Figure 5.1a). T_a from OKCNET is measured at the minute scale using Vaisala WXT510 weather stations (full technical details of the OKCNET stations are provided by Basara et al. (2011) and as such will not be covered

here). For the BUCL network in Birmingham, 21 stations located in a course array with a similar average spacing of around 3 km are considered in this study (Figure 5.1b). In contrast to OKCNET, T_a is sampled at a height of 3 m with a temporal interval of 15 minutes via Vaisala WXT520 weather stations. Immediately, the difference in measurement height highlights a challenge. A previous study found that the air temperature gradient between 2 m and 9 m within the urban core tends to be neutral (within ± 0.5℃) over OKC (Basara et al., 2008), but the different height of temperature sensor between the two UMNs might still induce some uncertainties of the measured T_a, e.g. turbulent source areas (Oke, 2007).

Another key difference in configuration between the networks, is the general exposure of the weather stations, with BUCL sites being generally more exposed than OKCNET sites. The deployment strategy for BUCL was to provide a site that was as representative as possible of the local environment (source areas/footprints with size generally extending within a few hundred metres of a station in urban areas (Stewart et al., 2014)). Therefore, the majority of the stations from BUCL are located on grass playing fields in schools or similar areas with fence protection (Chapman et al., 2015). In contrast, OKCNET sites are located directly in urban canyons where they will be affected by the urban fabric. For example, Figure 2 of Basara et al. (2011) and Figure 5 of Chapman et al. (2015) provide photographs of a weather station classified in urban group from OKCNET (KCB103) and BUCL (W026) respectively. It is evident that T_a measured from the stations classified in urban group in OKC will be substantially more influenced by the traffic and heat transfer from building surface (e.g. walls) than those in Birmingham. Furthermore, wind (speed) is more likely to be less evident over stations in OKC (especially for the sites over CBD areas shown in Figure 5.1a) where the local WS

tends to be smaller. Therefore, the turbulent source areas of T_a and the heat mitigation might be different across the two cities in spite of under the same background WS condition (measured from rural sites).

5.2.2.2 Site classification

Classification of the weather stations with regard to Urban Climate Zone (UCZ) (Oke et al., 2006) and Local Climate Zone (LCZ) (Stewart and Oke, 2012) are already documented in (Basara et al., 2011) for OKCNET and in (Bassett et al., 2016) for BUCL. To compare the two UMNs more consistently, stations in OKC have been reclassified from UCZ to LCZ based on the specific range of parameters such as building density and sky view factor etc. As shown in Figure 5.1, fewer stations are located in areas classified as LCZ1 (5 stations in OKC and 1 station in Birmingham) and LCZ2 (2 stations in OKC and 3 stations in Birmingham), which are classified as urban based on the higher level of urbanisation in later analysis. The rest of the stations are categorised as suburban. According to the suburban group, the LCZ type is more diverse and different between the two cities. For example, most of the stations are classified to LCZ6 in Birmingham whereas LCZ8 and LCZ9 are the most dominant LCZ types in OKC.

5.3 Data and methods

5.3.1 Ground observations

Air temperature observations derived from each UMN and one rural station (highlighted in Figure 5.1a: Spencer station and Figure 5.1b: Coleshill station) are used to calculate the $aUHII$ across the metropolitan areas over OKC and Birmingham. Only the data of T_a during the satellite passing time are used for the analysis (around 01:30 and 22:30 local solar time for Aqua and Terra satellites respectively). Thus T_a from each

station is calculated based on the average T_a from 01:00 to 02:00 and from 22:00 to 23:00 local time during the nights from 01/01/2009 to 31/12/2010 in OKC and from 01/06/2013 to 31/08/2014 in Birmingham when the satellite imagery are collected across the two cities in this chapter, as mentioned in Chapter 2. In contrast to the measurement height (T_a at 9 m and 3 m are collected in OKC and Birmingham respectively), T_a at 1.5 m and 1.25 m are used to indicate the background temperature in OKC (Spencer station) and Birmingham (Coleshill station) respectively. Although T_a in the OKC rural site is measured at both 1.5 and 9 m above ground level (AGL), the one at 1.5 m is used to minimise the height differences between the two cities.

Hourly averaged wind speed (WS), relative humidity (RH) and daily accumulated solar radiation from previous day (DASR) data are collected from the rural stations (Spencer station) to reflect the background climate condition, as introduced in Chapter 2.

5.3.2 Satellite observations

To generate $sUHII$ and characterise the surface properties over the two cities, two categories of MODIS products are used in this study (available from Earthdata Search: https://search.earthdata.nasa.gov/search): (i) night-time land surface temperature (T_s) daily data (MYD11A1 from Aqua satellite and MOD11A1 from Terra satellite) in version 5 (V005) and (ii) normalised difference vegetation index (NDVI) from the vegetation index products (MYD13A2 from Aqua satellite and MYD13A2 from Terra satellite). This study follows the method introduced in Chapter 2 to achieve the spatial consistency between satellite data and ground observation.

5.3.3 Regression-based analysis

$sUHII$ ($aUHII$) is defined as the T_s (T_a) differences between urban sites and rural site across the two cities respectively:

$$sUHII^{(c,i)} = T_s{}^{(c,i)} - T_s{}^{(c,r)} \quad \text{Equation (5.1a)}$$

$$aUHII^{(c,i)} = T_a{}^{(c,i)} - T_a{}^{(c,r)} \quad \text{Equation (5.1b)}$$

Where c represents the cities – OKC or Birmingham, i is for each station in urban areas and r is for the rural site (Spencer station in OKC and Coleshill station in Birmingham).

To compare the $sUHII$-$aUHII$ relationship between OKC and Birmingham, two possible influencing factors are considered: (i) climatic conditions and (ii) configurations of the two UMNs. The climate backgrounds introduced in Section 5.2.1 differ substantially between the two cities. Cloud cover, WS, and surface wetness have been recognised as the three important climatic factors notably affecting UHI magnitude during night time (Runnalls and Oke, 2000). Given that satellite data are derived under cloudless condition, two climatic parameters, including WS and DASR are used as a surrogate to represent the climate conditions (Note: RH is not considered because the correlation between RH and urban heat island intensity (UHII) is found to be too weak in this study which is consistent with the study conducted by Kim and Baik (2002). WS is used to imply the turbulence intensity and atmospheric stability. DASR is used to represent the solar radiative energy input to the local system.

The comparison analysis is firstly conducted with considerations of different climatic conditions. An indirect statistical method is then applied to remove or minimise the

impact of climate and the grouping analysis is further conducted in terms of urban and suburban groups. By doing this, the land surface properties of urban or suburban groups are less dissimilar between OKC and Birmingham, compared to using individual station, and its effects to the differences of the $sUHII$-$aUHII$ relationship are presumed to be less dominant while the impact of UMNs' configuration might be highlighted in the result.

Regarding the comparison of the $sUHII$- $aUHII$ relationship under different climatic conditions across the two cities, data from all stations are grouped based on four different conditions of WS and DASR, and LRMs of $sUHII$ on $aUHII$ (Equation 5.2) with confidence ellipse at 90% confidence level are built correspondingly. Meanwhile, the analysis of covariance (ANCOVA) (Rutherford, 2001) and 2-D Kolmogorov-Smirnov (K-S) test (Peacock, 1983) are implemented to test the difference between LRMs and between the 2-D distribution of the data across two cities.

$$sUHII^{(c)} = m^{(c)} \cdot aUHII^{(c)} + b^{(c)} \qquad \text{Equation (5.2)}$$

Where m and b are the slope and intercept coefficients respectively.

An approach called analysis of regression residuals (ANORES) (Maxwell et al., 1985) is adopted to remove the climate impact (WS and DASR) in $sUHII$ and $aUHII$. The overall variance of a dependent variable (e.g. $sUHII$ or $aUHII$) will always be induced by multiple factors (e.g. climatic factor, UMN's configuration etc.). However, only a portion of the variance will be explained by a factor (e.g. UMN's configuration). This variance can be dissected in parts that are uniquely induced by a factor (e.g. UMN's configuration) and other parts confounded with other factors (e.g. climatic factor). The underlying rationale of ANORES is to remove the confounded part of variance (climatic factor) and analyse the variance that are solely due to other factors (e.g. UMN's

configuration) (Pfister, 2011). The basic procedure of ANORES follows two steps: (i) (linear) regression models are generated to identify the impact of the confounding variables on the dependent variable; (ii) residuals can then be computed by subtracting the prediction of the regression models from observations and the impacts of other factors can be further analysed. In this study, climatic conditions of WS and DASR are considered as the confounding factors. Multiple linear regression model (MLRM) is generated to estimate the climatic contribution (WS and DASR) in $sUHII$ and in $aUHII$ based on the data from all stations for the two cities respectively:

$$sUHII^{(c)} = A_1{}^{(c)} \cdot WS + B_1{}^{(c)} \cdot DASR + k_1{}^{(c)} \quad \text{Equation (5.3a)}$$

$$aUHII^{(c)} = A_2{}^{(c)} \cdot WS + B_2{}^{(c)} \cdot DASR + k_2{}^{(c)} \quad \text{Equation (5.3b)}$$

where A_1, A_2, B_1, B_2, k_1 and k_2 are the corresponding regression coefficients in the MLRM. As discussed above, residual of a regression model is the difference between observed and predicted dependent variable (e.g. $sUHII$ in Equation 5.3a and $aUHII$ in Equation 5.3b), which can be taken as the variable excluding the impacts of climatic factors (WS and DASR). The LRMs below (Equation 5.4) built from the residuals from Equation 5.3a ($sUHII_{RES}{}^{(c)}$) and 5.3b ($aUHII_{RES}{}^{(c)}$) are subsequently compared with Equation 5.2, and therefore, the contribution of climatic impact could be estimated based on the difference of the R^2 values between Equation 5.2 and Equation 5.4. Meanwhile, as the residuals could be taken as the UHI after removing or minimising the climatic influences (WS and DASR), the impact of the different UMN's configurations on the difference of the $sUHII$ - $aUHII$ relationship can be further explored by building the regression model of $sUHII_{RES}{}^{(c)}$ on $aUHII_{RES}{}^{(c)}$ according to the classification of urban stations (urban and suburban groups).

$$aUHII_{RES}{}^{(c)} = m_{RES}{}^{(c)} \cdot sUHII_{RES}{}^{(c)} + b_{RES}{}^{(c)}$$ Equation (5.4)

5.4 Results

5.4.1 Comparison of the $sUHII$-$aUHII$ relationship under different climate conditions

To explore the impact of different climate conditions on the differences of the $sUHII$- $aUHII$ relationship across two cities, $sUHII$ and $aUHII$ data are classified into four groups with respect to different climate conditions (WS and DASR):

$C1$: $WS < 3\ m/s$ & $DASR < 20\ MJ\ m^{-2}$;

$C2$: $WS < 3\ m/s$ & $DASR > 20\ MJ\ m^{-2}$;

$C3$: $WS > 3\ m/s$ & $DASR < 20\ MJ\ m^{-2}$;

$C4$: $WS > 3\ m/s$ & $DASR > 20\ MJ\ m^{-2}$.

However, C4 is not considered in the result or discussion due to the limited data samples in Birmingham. In general, C2 would be the ideal condition for the development of UHI, which is under cloudless skies and light winds at night (the atmospheric surface layer is statically stable above the rural ground and possibly forms an inversion layer) as well as larger input of solar radiation during daytime. C1 and C3 could be used to compare the impacts of WS and DASR on the $sUHII$- $aUHII$ relationship, where the atmosphere is also statically stable at night in C1 but with lower input of solar radiation during daytime, comparing to C3, in which the atmospheric surface layer tends to be dynamically neutral due to large WS. The mean WS ($\overline{WS}$, $\overline{WS_{OKC}}$ for OKC and $\overline{WS_{BHAM}}$ for Birmingham) and mean DASR ($\overline{DASR}$, $\overline{DASR_{OKC}}$ for OKC and $\overline{DASR_{BHAM}}$ for

Birmingham) of the samples under each group have been demonstrated in Figure 5.2. The difference of the $\overline{WS}$ between two cities within each group is approximately smaller than 1 m/s and the influence of it on the comparison of the $sUHII$- $aUHII$ relationship could be neglected. The $\overline{DASR}$ is greater over OKC and differences of about 4.41, 1.61 and 7.9 MJ m^{-2} between OKC and Birmingham are found in C1, C2 and C3, respectively. The larger $\overline{DASR}$ in OKC might affect the results for the comparison of the $sUHII$- $aUHII$ relationship, however, it is extremely difficult to balance the sample size and the distribution of DASR across these two cities. Nevertheless, the difference of the $\overline{DASR}$ in C2 is relatively smaller and results under C2 could be used as a reference to compare the $sUHII$- $aUHII$ relationship under same WS and DASR conditions.

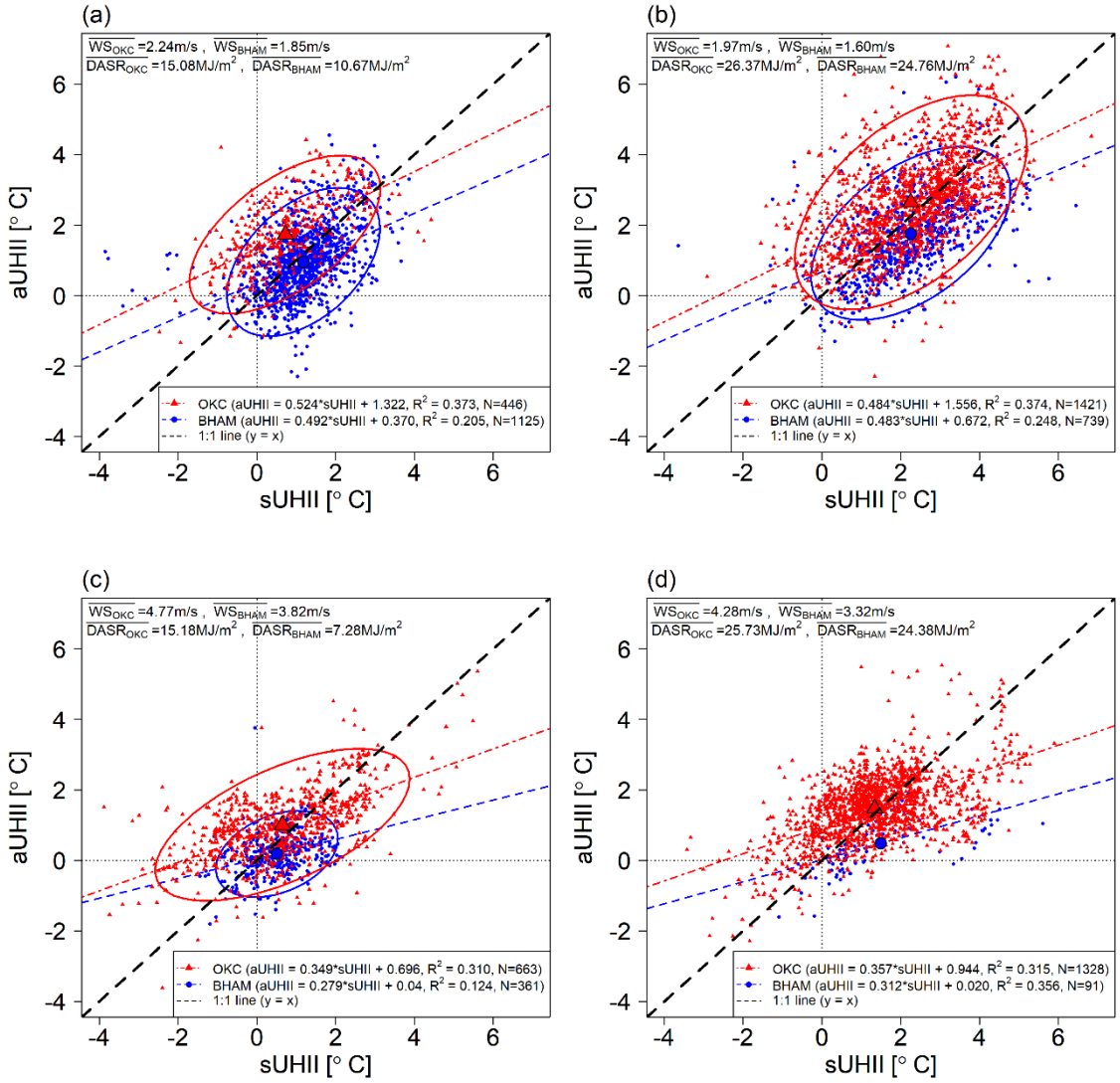

Figure 5. 2 Linear and elliptical trends of sUHII and aUHII based on four climatic conditions: (a) C1: WS < 3 m/s and DASR < 20 MJ/m^2; (b) C2: WS < 3 m/s and DASR > 20 MJ/m^2, (c) C3: WS > 3 m/s and DASR < 20 MJ/m^2 and (d) C4: WS > 3 m/s and DRAD > 20 MJ/m^2 in OKC (triangle) and Birmingham (circle), where the regression models are all significant at 0.01 confidence level and the larger triangle and circle are the corresponding mean values

Surprisingly, larger differences of the mean $aUHII$ ($\Delta\overline{aUHII}$, vertical distance between the two center points of ellipses) compared to mean $sUHII$ ($\Delta\overline{sUHII}$, horizontal distance between the two center points of ellipses) between the two cities are shown in Figure 5.2. Specifically, mean $aUHII$ is larger in OKC than Birmingham ($\overline{aUHII}^{OKC} > \overline{aUHII}^{BHAM}$) while mean $sUHII$ is nearly the same between the two cities ($\overline{sUHII}^{OKC} \approx \overline{sUHII}^{BHAM}$). The correlation analysis and regression analysis (Table 5.2 and Figure 5.3) provide statistical evidence to these results. It demonstrates that $\overline{sUHII}^{OKC}$ tends to be weaker than $\overline{sUHII}^{BHAM}$ under the same DASR condition (Figure 5.3a) but stronger than $\overline{sUHII}^{BHAM}$ under the same WS condition (Figure 5.3c). The result of $\overline{sUHII}^{OKC} \approx \overline{sUHII}^{BHAM}$ under C1, C2 and C3 conditions indicate that impacts of DASR and WS on $sUHII$ at city-scale between the two cities are counteracted. Regarding the $\Delta\overline{aUHII}$, $aUHII$ in OKC ($aUHII^{OKC}$) is found to be slightly larger than Birmingham ($aUHII^{BHAM}$) under same DASR condition (Figure 5.3b) and $aUHII^{OKC}$ is higher than $aUHII^{BHAM}$ more significantly under same WS condition (Figure 5.3d), hence, $\overline{aUHII}^{OKC} > \overline{aUHII}^{BHAM}$ and $\Delta\overline{aUHII} > \Delta\overline{sUHII}$ is expected.

Table 5. 2 Results of the Pearson correlation test across two urban contexts, where OKC is highlighted in the table

OKC / BHAM	$aUHII$	$sUHII$	WS	DASR
$aUHII$	--	**0.62**	**-0.53**	**0.34**
$sUHII$	0.59	--	**-0.41**	**0.40**
WS	-0.50	-0.36	--	--
DASR	0.38	0.51	--	--

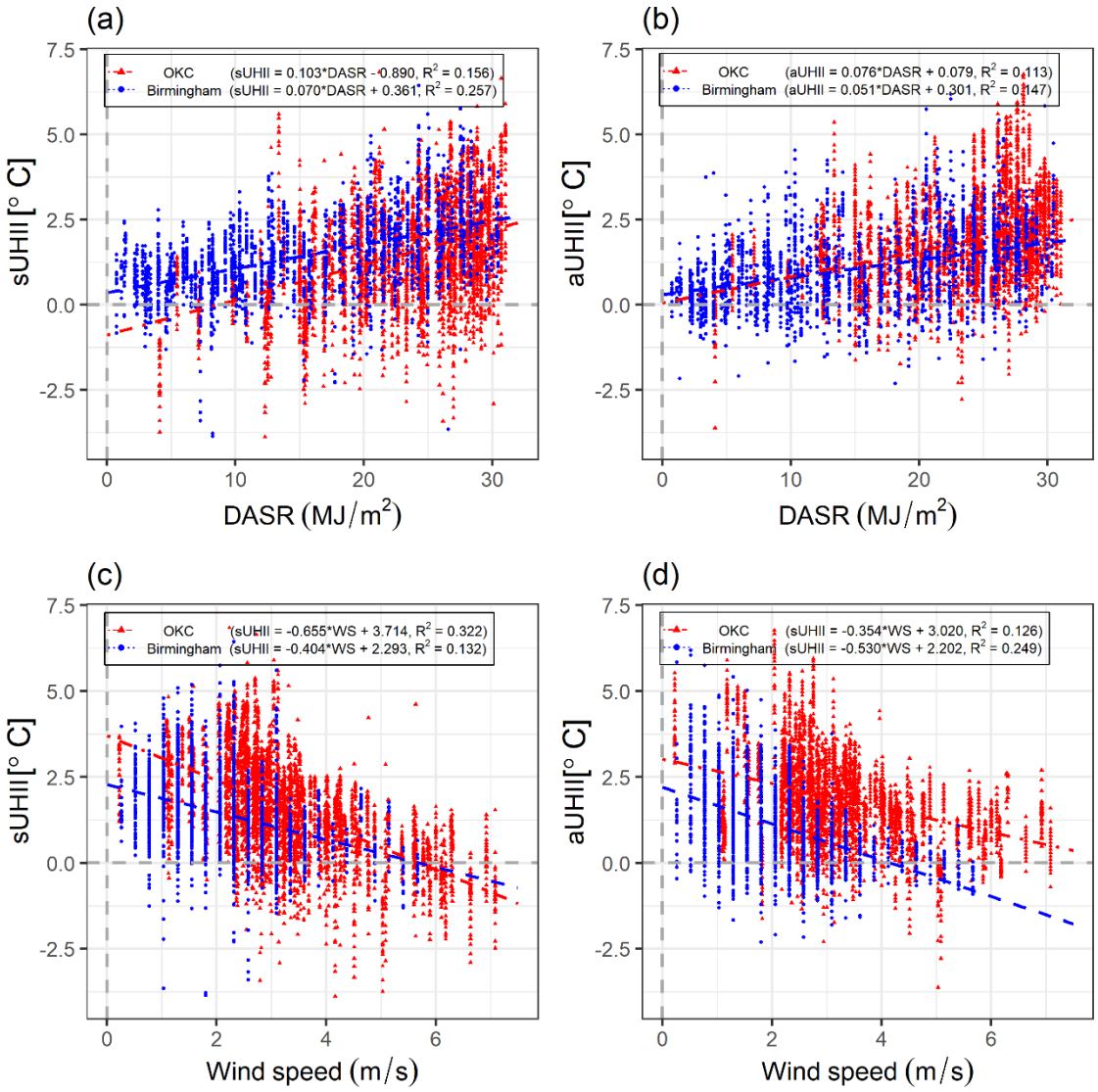

Figure 5. 3 Comparison of sUHII and aUHII according to the change of DASR (5.3a and 5.3b) and WS (5.3c and 5.3d) respectively between OKC (triangle) and Birmingham (circle)

Under all the three climatic conditions (C1, C2 and C3), stronger $sUHII$- $aUHII$ relationship with higher R^2 value and slope coefficient are found in OKC compared with Birmingham. From the perspective of statistics, slope and R^2 value are closely related to covariance between $sUHII$ and $aUHII$ ($cov(sUHII, aUHII)$). Stronger joint variability between $sUHII$ and $aUHII$ could cause the increase of covariance, which indicates the weaker advection effect on the UHII *(Feng et al., 2019)*. Therefore, the larger $cov(sUHII, aUHII)$ shown in Table 5.3 is statistically responsible for the higher R^2 value (defined as the standardised covariance) and slope in OKC. Weaker effect of advection on UHII is then suggested by the larger $cov(sUHII, aUHII)$ in OKC.

The differences of the linear $sUHII$- $aUHII$ relationship across the two cities vary under the three climatic conditions (C1, C2 and C3). Considering that the slope coefficient (m) is the key component in LRM that represents the rate of change of the $aUHII$ with respect to $sUHII$, even though the differences of slope between the two cities are not statistically significant at 0.1 confidence level according to the results from the ANCOVA test (Table 5.4), the discussion related to the differences of the $sUHII$- $aUHII$ relationship will be still mainly based on the variation of the differences of the slope ($\Delta m, \Delta m = m^{OKC} - m^{BHAM}$) between the two cities under the three climatic conditions. Results (Figure 2) demonstrate that Δm tend to be smaller in the order of C2, C1 and C3 ($\Delta m_{C2}[0.001] < \Delta m_{C1}[0.032] < \Delta m_{C3}[0.070]$). Meanwhile, the data distribution differences in 2-D K-S test between the two cities are also smallest under C2 followed by C1 and C3, indicated from the ΔD ($= D - D_a$) values, where D statistics represents the 2-D distribution differences between the two groups of data and ΔD is the relative D statistics that equals to the differences between D statistics and critical D statistics (critical D statistics is estimated based on the sample size) (Peacock, 1983)

(Table 5.4). The differences of the linear $sUHII$- $aUHII$ relationships between the two cities are more likely to be smallest under C2 that is considered as the extreme 'ideal' condition for the development of heat island.

Table 5. 3 Statistical quantities related to $sUHII$ and $aUHII$ according to the three climatic groups (C1, C2 and C3) and urban/suburban groups over two cities

Group	City	$Cov(sUHII, aUHII)$	SD_{sUHII}	SD_{aUHII}	SD Ratio ($=\frac{SD_{aUHII}}{SD_{sUHII}}$)	Slope from LRM
C1	OKC	0.752	1.198	1.027	0.857	0.524
	Birmingham	0.402	0.904	0.981	1.085	0.492
C2	OKC	0.913	1.372	1.488	1.085	0.483
	Birmingham	0.670	1.178	1.43	1.214	0.483
C3	OKC	0.775	1.489	0.936	0.629	0.349
	Birmingham	0.145	0.720	0.569	0.790	0.279
Urban	OKC	0.274	1.090	0.814	0.747	0.231
	Birmingham	0.362	0.891	0.913	1.025	0.456
Suburban	OKC	0.663	1.315	1.087	0.826	0.383

Birmingham	0.322	0.959	0.849	0.885	0.350

*Table 5. 4 ANCOVA and 2D K-S test between two cities according to the three climatic groups (C1, C2 and C3) (significance level: 0.001***, 0.01**, 0.05*, 0.1)*

Climatic group	ANCOVA test			2D K-S test	
	Slope	Intercept	Interaction effect	D	ΔD
$C1: WS < 3\ m/s\ \&\ DASR < 20\ MJ/m^2$	$=$	$\neq^{***}$	$= (F = 0.536, p = 0.464)$	0.514^{***}	0.405
$C2: WS < 3\ m/s\ \&\ DASR > 20\ MJ/m^2$	$=$	$\neq^{***}$	$= (F = 0.003, p = 0.960)$	0.341^{***}	0.254
$C3: WS > 3\ m/s\ \&\ DASR < 20\ MJ/m^2$	$=$	$\neq^{***}$	$= (F = 1.693, p = 0.194)$	0.570^{***}	0.442

*Table 5. 5 ANCOVA and 2D K-S test between two cities according to the following four paired data groups including (i) OKC_{OBS} and $Birmingham_{OBS}$; (ii) OKC_{RES} and $BHAM_{RES}$; (iii) ${OKC_{RES}}^{Urban}$ and ${BHAM_{RES}}^{Urban}$ and (iv) ${OKC_{RES}}^{Suburban}$ and ${BHAM_{RES}}^{Suburban}$ (significance level: 0.001***, 0.01**, 0.05*, 0.1)*

Paired group	ANCOVA test			2D K-S test	
	Slope	Intercept	Interaction effect	D	ΔD
$OKC_{OBS}, BHAM_{OBS}$	$=$	$\neq^{***}$	$= (F = 2.459, p = 0.117)$	0.338^{***}	0.287
$OKC_{RES}, BHAM_{RES}$	$\neq$	$=$	$\neq \ (F = 3.273, p = 0.070)$	0.124^{***}	0.073
${OKC_{RES}}^{Urban}, {BHAM_{RES}}^{Urban}$	$\neq^{***}$	$\neq^{***}$	$\neq^{***} (F = 20.791, p < 0.001)$	0.156^{***}	0.041
${OKC_{RES}}^{Suburban}, {BHAM_{RES}}^{Suburban}$	$=$	$\neq^{***}$	$= (F = 1.766, p = 0.184)$	0.148^{***}	0.091

5.4.2 Generalising the climatic effect

The differences of the linear $sUHII$- $aUHII$ relationship before and after subtracting the climatic impact in the two cities are demonstrated in Figure 5.4a ($sUHII$ and $aUHII$) and 5.4b ($sUHII_{RES}$ and $aUHII_{RES}$) correspondingly. The decreased R^2 values, from 0.380 to 0.227 in OKC and from 0.351 to 0.207 in Birmingham, indirectly point out the contributions of climate in the linear $sUHII$- $aUHII$ relationship are non-negligible in both cities.

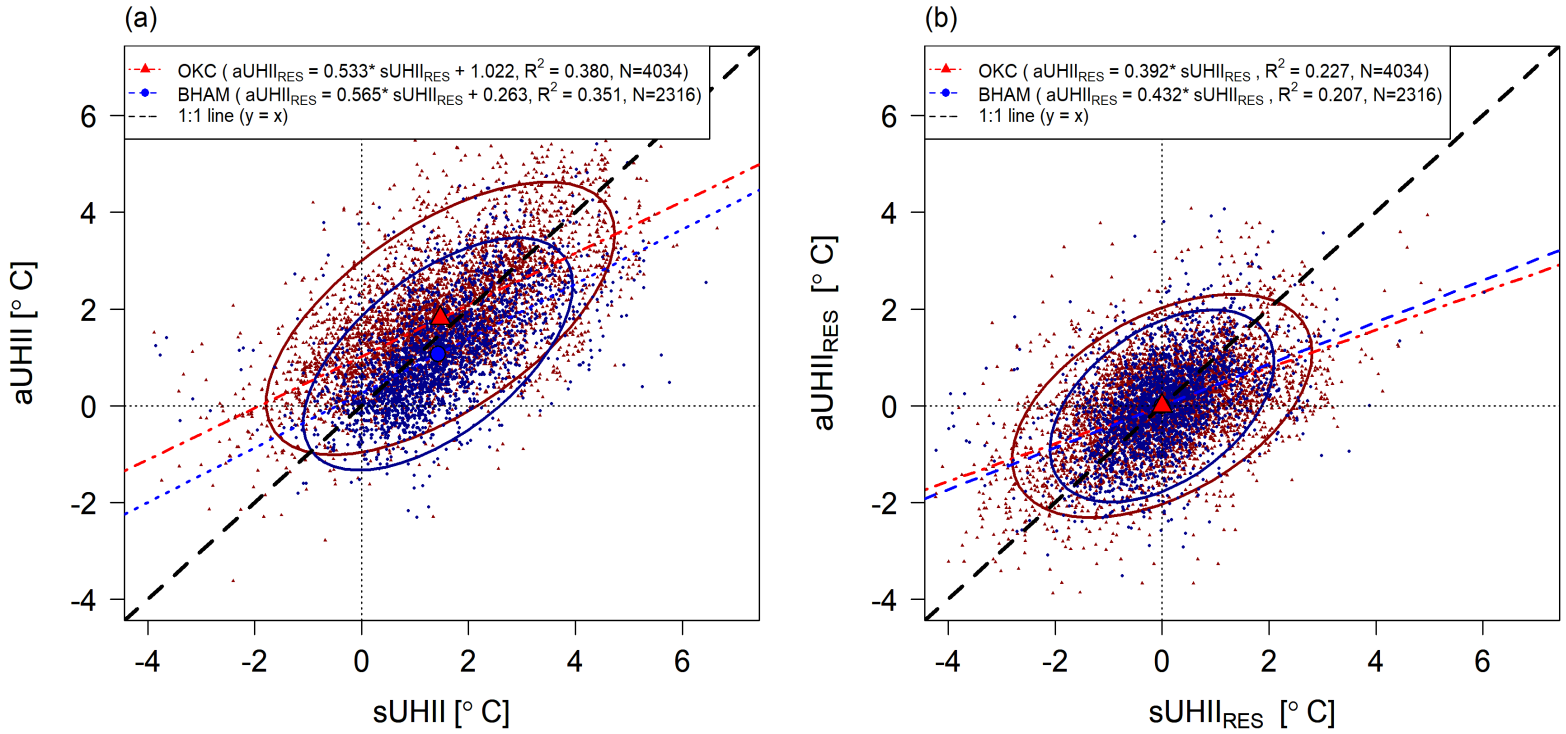

Figure 5.4 Linear and elliptical trends of sUHII and aUHII based on (a) observations and (b) residuals from MLRMs over OKC (triangle) and Birmingham (circle), where the regression models are all significant at 0.01 confidence level and the larger triangle and circle are the corresponding mean values

It is therefore, somewhat surprising that the linear $sUHII$- $aUHII$ relationships are more significantly different after removing the climatic impact between the two cities, given by the interaction effect that is significant at a higher confidence level with a larger F value in the OKC_{RES} and $BHAM_{RES}$ paired group ($F \approx 3.273, p \approx 0.070$) (Note: F value is the statistics used to test the significance of the interaction effect (Tabachnick et al., 2007)) comparing to the result from the OKC_{OBS} and $BHAM_{OBS}$ paired group ($F \approx 2.459, p \approx 0.117$) (Table 5.5). Specifically, the more noticeable interaction effect is reflected by the greater slope difference between OKC and Birmingham *after removing the climatic effect* which increases from ≈ 0.03 to ≈ 0.04 shown in Figure 5.4a and 5.4b respectively. The linear $sUHII$- $aUHII$ relationships at city scale contains the temporal and spatial information, while the MLRM used to remove the climatic impact does not account for the spatial information that will stand out in the $sUHII_{RES}$ - $aUHII_{RES}$ relationship (relationship between $sUHII_{RES}$ and $aUHII_{RES}$) illustrated in Figure 5.4b. The prominent spatial information that are reflected by the differences of a combinations of multiple factors (i.e. UMNs' configuration) are likely to be the primary reasons for the larger interaction effect (differences) in the linear $sUHII_{RES}$-$aUHII_{RES}$ relationship.

5.4.3 Comparison of the $sUHII_{RES}$-$aUHII_{RES}$ relationship under urban and suburban group

The LRMs of $aUHII_{RES}$ on $sUHII_{RES}$ and data distribution for urban (Figure 5.5a) and suburban (Figure 5.5b) groups btween the two cities are visulised in Figure 5.5. The differences of the $sUHII_{RES}$ - $aUHII_{RES}$ relationship between the two cities are more significantly in urban group, supported by the slope differences in LRMs (Figure 5.5) and statistical tests (Table 5.5). Specifically, ANCOVA test (Table 5.5) illustrates that the

differences of the interaction effect between the two cities is significant at 0.001 confidence level ($F = 20.791, p < 0.001$), indicating that the linear $sUHII_{RES}$ - $aUHII_{RES}$ relationships differ significantly claimed by this test for urban group over the two cities. In contrast, the differences of the linear $sUHII_{RES}$-$aUHII_{RES}$ relationships are not significant at 0.001 confidence level ($F = 1.766, p = 0.184$) for suburban group. However, the 2-D K-S test (Table 5.5) demonstrates larger differences of the data distribution in suburban group ($\Delta D \approx 0.091$) compared to urban group ($\Delta D \approx 0.041$) between OKC and Birmingham. Statistical parameters of the regression model shown in Table 5.3 provide the key output of the tests for the $sUHII_{RES}$-$aUHII_{RES}$ relationships. It it evident that the ratio of the standard deviation (SD) of $aUHII_{RES}$ to $sUHII_{RES}$ between the two cities are larger in urban group, e.g. ≈ 0.278 ($= |0.747 - 1.025|$) and ≈ 0.007 ($= |0.826 - 0.833|$) in urban and suburban group respectively. The difference of the variability of $aUHII_{RES}$ and $sUHII_{RES}$ between the two cities is therefore suggested to be larger in urban group. In addition, quadrant analysis demonstrated in Figure 5.6 also indicates the greater difference of the $sUHII_{RES}$-$aUHII_{RES}$ relationship in urban group between OKC and Birmingham. It should be noted that data points in Z2 and Z4 are the "biases" weakening the joint variability between the $sUHII_{RES}$ and $aUHII_{RES}$ (if the joint variability between $sUHII_{RES}$ and $aUHII_{RES}$ is extermely high , e.g. a perfect linear regression with $R^2 = 1$, the percentage of data points in Z2 and Z4 would be 0%). Therefore, if the total percentage of Z2 and Z4 (or Z1 and Z3) is more similar, the regression models and the 2-D distribution of a paried group of data would be more analogous. Result shows that the differences of the total percentage of data points in Z2 and Z4 between the two cities are smaller in urban group (10%: 39% for OKC vs. 29% for Birmingham) compared to suburban group (2%: 32% for OKC vs. 34% for

Birmingham), which provides further statistical evidence for the larger difference of the $sUHII_{RES}$-$aUHII_{RES}$ relationship in urban group between the two cities.

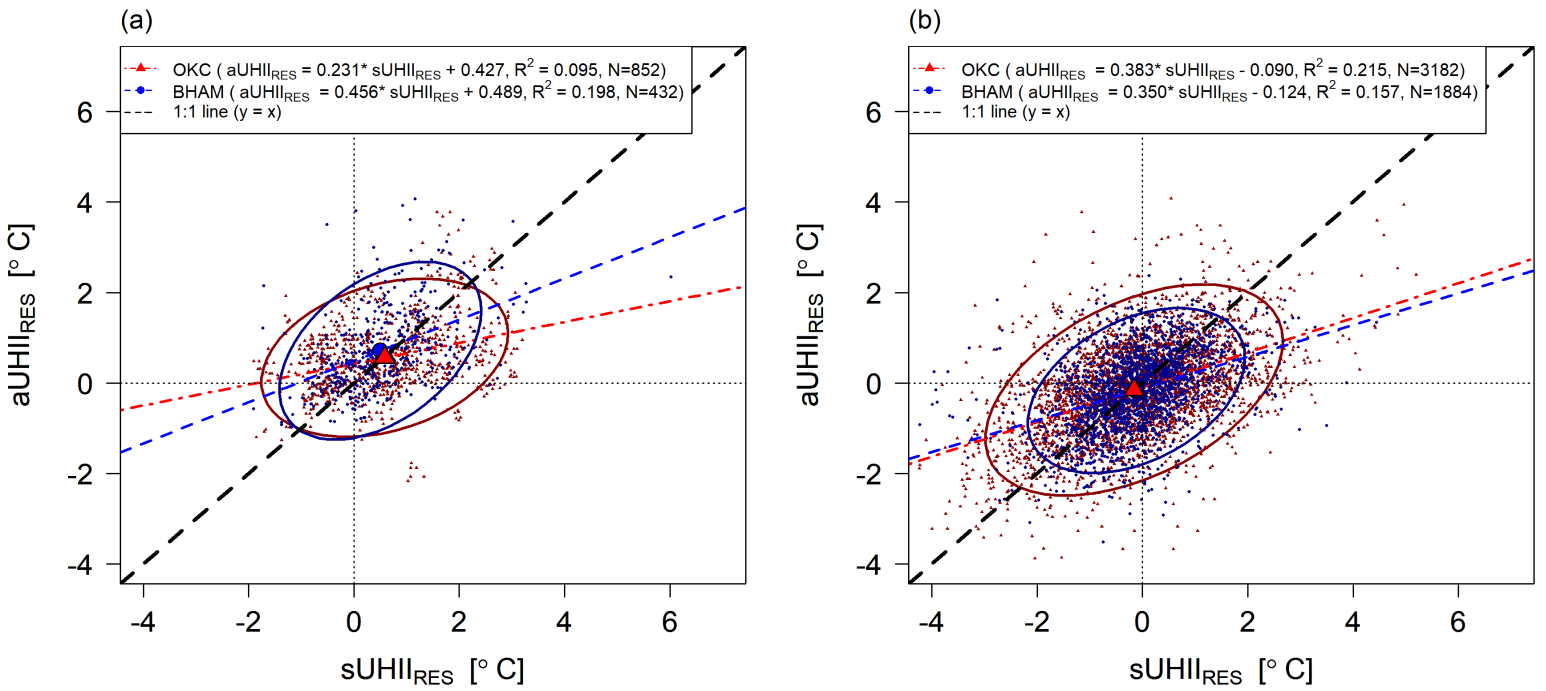

Figure 5. 5 Linear and elliptical trends of $sUHII_{RES}$ and $aUHII_{RES}$ based on (a) urban group and (b) suburban group in OKC (triangle) and Birmingham (circle), where the regression models are all significant at 0.01 confidence level and the larger triangle and circle are the corresponding mean values

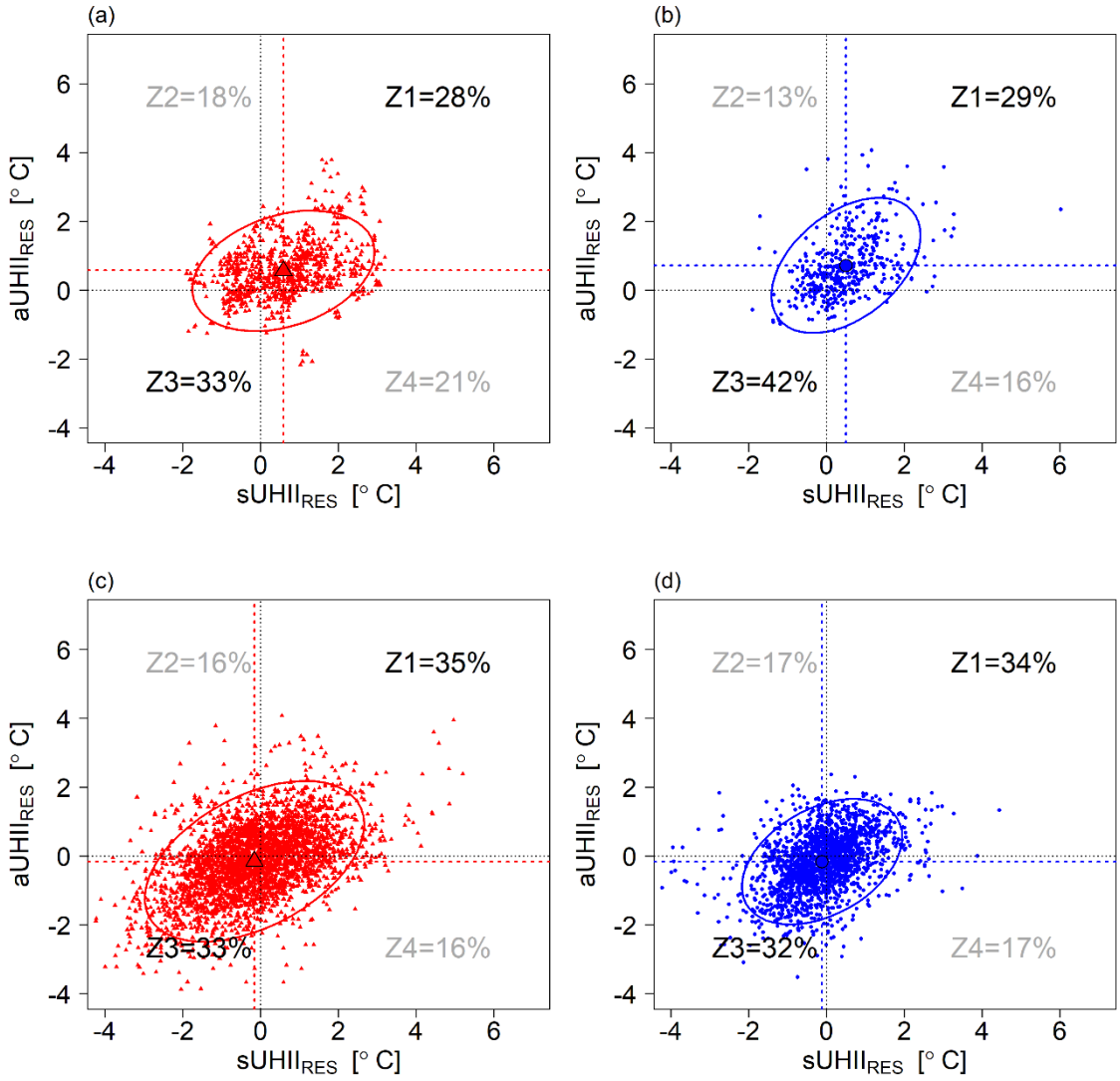

Figure 5. 6 Percentage of the data points in four quadrants (Z1, Z2, Z3 and Z4) dividing by the centre of ellipse for Urban group (a and b) and Suburban group (c and d) over OKC (triangle) and Birmingham (circle) respectively.

5.5 Discussion

5.5.1 The influence of climate

The differences of the linear $sUHII$-$aUHII$ relationship (i.e slope coefficient), with considerations of the 2-D spatial distributions of the data points, tend to be smaller under the 'ideal' condition (low WS and large DASR) for the UHI development (C2, C2<C1<C3) between OKC and Birmingham. Lee (1975) stated that UHII is strongly associated with atmospheric stability when the surface receipt of radiation is large during daytime and stronger radiation cooling of surface happens at night with calm wind, because the solar radiation receipt is normally larger than other heat supplied from human activities, which in turn becomes more importantly in determining the UHII. In other words, the more similar linear $sUHII$- $aUHII$ relationship between the two cities under C2 is because of the more stable atmospheric condition (low WS) during night-time with larger input of the radiation (DASR) into the urban system during daytime. The disparity of the linear $sUHII$- $aUHII$ relationship increases under C1 due to the released heat that is less dominantly controlled by DASR, and therefore, other heat sources (e.g. traffic, heating and cooling systems etc.) accounted for the release of heat fluxes across the two cities become more important for the UHI development (compared to C2). Likewise, the increased WS under C3 may intensify the impact of heat advection that plays an increasingly important role compared to C1 and C2 in controlling the UHII, leading to larger differences of the $sUHII$- $aUHII$ relationship between OKC and Birmingham. In addition, the prevalent low-level jets (LLJs) over the Great Plains in US may impact upon the $sUHII$- $aUHII$ relationship in OKC, which could increase the differences between the two cities particularly under high WS conditions (i.e. C3). It is suggested that strong

shear in response to LLJs caused more intense turbulent mixing and reduced the atmospheric stability in the nocturnal boundary layer (Hu et al., 2013). More specifically, strong LLJs could enhance the downward transport of warmer air from the residual layer, resulted in the weaker radiation cooling over ground surface (Fast et al., 2005). Meanwhile, the LLJs are found to be higher and weaker over urban areas (Kallistratova and Kouznetsov, 2012, Hu et al., 2013) and the reduced temperature inversion could be found in particular over rural areas. The reduced rural inversion intensity could weaken the $aUHII$ within the shallower and more stable atmospheric boundary layer ultimately (Hu et al., 2016b). Although it is expected that the classification of the data based on different wind speed conditions could indirectly cover the impacts of the LLJs on our results, further research is still needed to examine or quantify the influences of the LLJs on the differences of the $sUHII$-$aUHII$ relationship across these two cities.

5.5.2 The role of UMN configuration

Although it is difficult to explicitly quantify the impact of different network designs on the differences of the linear $sUHII$ - $aUHII$ relationship between OKC and Birmingham, the results from the LRMs based on grouping analysis indicate the significant role of the UMNs' configurations. To better illustrate the differences between the two UMNs, local environment and source areas of the stations are considered in the following discussions.

5.5.2.1 Local environment

The differences of the local environments between the two networks could be summarised in terms of the following three aspects: (i) larger mean building height around stations with most stations located within a street canyon in OKC, particularly in

the CBD; (ii) greenness (or amount of vegetation) around stations are lower in OKC with a site-average NDVI value of 0.35 compared to 0.46 in Birmingham; (iii) stations classified into the urban group are more distinguished with respect to site location and mean building height compared to the suburban group between the two cities. Several results can reflect the impacts of these aspects on the different linear $sUHII$- $aUHII$ relationships between the two cities.

(i) Contrasting magnitude of the mean sUHII and aUHII across the two cities

The grouping analysis in Section 5.4.1 shows an interesting result of the mean UHII magnitude where $\overline{sUHII}^{OKC} \approx \overline{sUHII}^{BHAM}$ and $\overline{aUHII}^{OKC} > \overline{aUHII}^{BHAM}$ (or $\overline{sUHII}^{OKC} < \overline{aUHII}^{OKC}$ and $\overline{sUHII}^{BHAM} > \overline{aUHII}^{BHAM}$). Importantly, these results appear consistent under all the three climate conditions (C1, C2 and C3), indicating that climate is not likely to be the prime reason for these results. Instead, the larger mean building height together with lower vegetation amount around stations in OKC might be the driving forces for $\overline{sUHII}^{OKC} < \overline{aUHII}^{OKC}$. Before providing more details of the explanations, differences between $sUHII$ and $aUHII$ ($sUHII$ minus $aUHII$, $\delta UHII$) could be also be computed by subtracting the difference between surface and air temperatures (T_s minus T_a, ΔT_{s-a}) at urban sites ($\Delta T_{s-a}{}^{(i)}$) by the one at rural site ($\Delta T_{s-a}{}^{(r)}$). By focusing on the mean value of these variables, $\delta UHII$ could be written as:

$$\overline{\delta UHII} = \overline{sUHII} - \overline{aUHII}$$

$$= \left(\overline{T_s{}^{(i)}} - \overline{T_s{}^{(r)}}\right) - \left(\overline{T_a{}^{(i)}} - \overline{T_a{}^{(r)}}\right)$$

$$= \left(\overline{T_s{}^{(i)}} - \overline{T_a{}^{(i)}}\right) - \left(\overline{T_s{}^{(r)}} - \overline{T_a{}^{(r)}}\right)$$

$$= \overline{\Delta T_{s-a}{}^{(i)}} - \overline{\Delta T_{s-a}{}^{(r)}} \qquad \text{Equation (5.5)}$$

Hence, $\overline{sUHII}^{OKC} < \overline{aUHII}^{OKC}$ also means the larger magnitude of the differences between surface and air temperature (note: $\overline{\Delta T_{s-a}}^{(\iota)}$ and $\overline{\Delta T_{s-a}}^{(r)}$ are normally negative during night and the density plots of them are presented Figure 5.6) over urban areas compared to rural areas in OKC. This result ($\overline{sUHII}^{OKC} < \overline{aUHII}^{OKC}$) was also found by previous studies (Song and Park, 2019, Marzban et al., 2018, Sheng et al., 2017). These could be possible because the roof and ground surfaces that usually induce lower T_s compared to building wall surface (Oke et al., 2017) take a greater proportion in a grid cell (i.e. pixel) over urban areas from the satellite product. T_a is usually measured at screen-level and it is hard to represent the local temperature (e.g. a radius of 500 m that is the about same as the spatial resolution of T_s herein) or temperature at roof-level, resulting in larger differences between surface and air temperatures ($\overline{\Delta T_{s-a}}^{\iota} < \overline{\Delta T_{s-a}}^{r}$ or $\overline{sUHII} < \overline{aUHII}$), particularly over urban areas with higher buildings and building density. The contrasting results found in Birmingham ($\overline{sUHII}^{BHAM} > \overline{aUHII}^{BHAM}$) are likely linked to the greater vegetation amount and lower mean building height. The percentage of roof/ground surfaces would decrease in a grid cell while the proportion of vegetation surfaces that commonly have higher T_s due to the lower emissivity compared to the roof/ground surfaces would increase, leading to the smaller differences between the surface and air temperatures at urban sites in Birmingham.

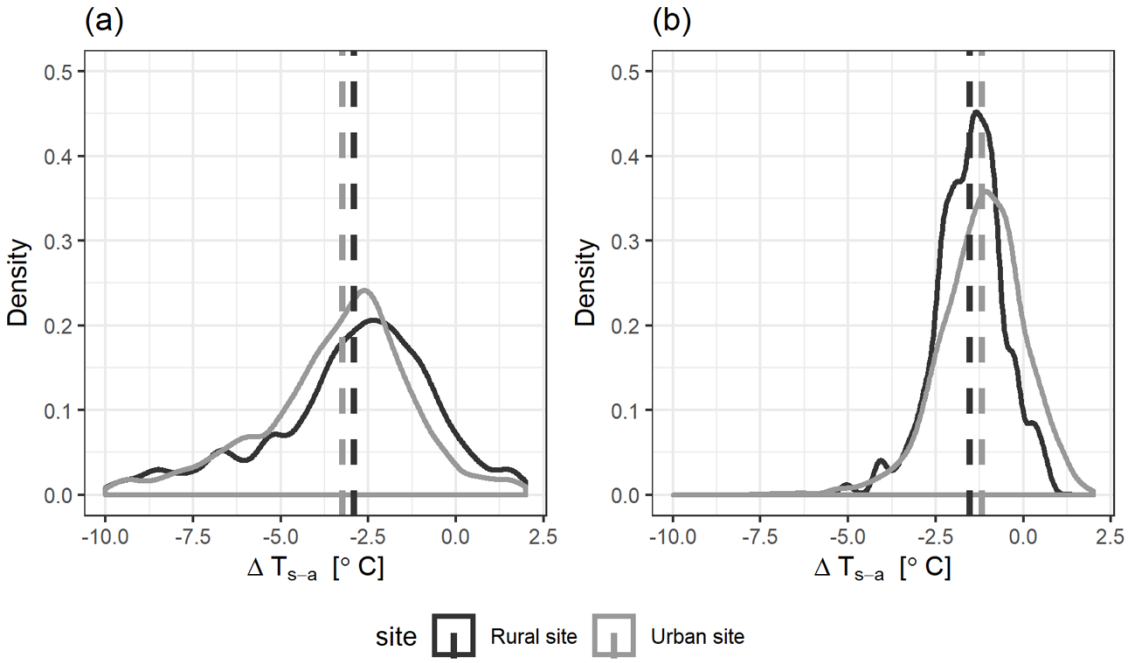

Figure 5. 7 Density plots of the ΔT_{s-a} of rural and urban sites across two cities: (a) OKC and (b) Birmingham, where the two dash lines are the mean values correspondingly.

(ii) Greater rate of change of aUHII with respect to sUHII in OKC before removing the climate effect

The grouping analysis in Section 5.4.1 shows greater slope values of the regression lines in OKC under the three climate conditions (C1, C2 and C3). The larger rate of change of $aUHII$ with respect to $sUHII$ in OKC is potentially attributed by the weaken advection effect on the $sUHII$- $aUHII$ relationship. Advection effect could increase the disparity between $sUHII$ and $aUIII$ as discussed in Chapter 4, which is represented by the lower $cov(sUHII, aUHII)$ in Birmingham (Table 5.3), leading to the smaller slope and reduced R^2 in the regression model. The underlying mechanism for these results could be the traffic light siting of the stations in OKC within the street canyon. This provides a shelter effect and more resistance to winds. WS is supposed to be smaller over the urban stations in OKC compared to Birmingham under same background WS, which in turns

weakens the lagged effect of wind on surface temperatures and increases the joint variability between $sUHII$ and $aUHII$. Thus, stronger $sUHII$- $aUHII$ relationship is expected with greater slope coefficient in OKC.

5.5.2.2 Source areas

Source areas (or footprints) are determined as the portion of the surrounding environments that can be 'seen' by a sensor/station. The temperature (T_a) measured by sensors is intended to come into equilibrium with its turbulent source areas (turbulent footprint) (Oke et al., 2017). It is suggested that the turbulent source areas are associated with (i) height of measurement (larger at greater heights), (ii) surface roughness and (iii) atmospheric stability (increase from unstable to stable) (Oke et al., 2006). The turbulent source areas are literally larger for OKCNET stations compared to BUCL because of greater height of the sensors if the comparison is under similar atmospheric conditions and for the same LCZ, which could be responsible for some of differences of the $sUHII$-$aUHII$ relationship between the two cities found in Section 5.4.3.

(i) Reduced rate of change of aUHII with respect to sUHII in OKC in urban group

The differences of the linear $sUHII_{RES}$-$aUHII_{RES}$ relationships between the two cities are represented by the reduced rate of change of $aUHII$ respect to $sUHII$ in OKC in the urban group. This result conflicts with the findings of "*Greater rate of change of aUHII with respect to sUHII in OKC before removing the climate effect*" discussed above and therefore provides further evidence of the impact of the different local environment and source areas between these two networks. Before removing the climate effect, the rate of change of $aUHII$ with regard to $sUHII$ is found to be larger in OKC,

resulted from the smaller WS around each site in OKC due to the siting within a street canyon where is more resistant from wind. After removing the climate effect, the wind effect has been minimised. In this way, OKCNET stations with larger turbulent source areas because of the greater sensor's height (9 m compared to 3 m for BUCL) tend to have more sufficient interaction with the upper layer compared to BUCL, causing the larger impacts of the wind advection on the $sUHII_{RES}$-$aUHII_{RES}$ relationships. Quadrant analysis that divides the data points into four quadrants based on the mean $sUHII$ and $aUHII$ is conducted over OKC and Birmingham (Figure 5.6), in order to further explore the characteristics of the $sUHII$ and $aUHII$. Figure 5.6 provides statistical support for the discussions above, where percentage of data points in Z2 and Z4 are higher in Figure 5.6a than Figure 5.6b, indicating the larger impact of warm/cold advection on temperature variation in OKC.

(ii) Greater rate of change of $aUHII$ with respect to $sUHII$ in OKC in suburban group

A greater slope coefficient is found in the linear $sUHII_{RES}$-$aUHII_{RES}$ relationships under the suburban group in OKC compared to Birmingham (Figure 5.5b), which is contradictory to the one in the urban group (Figure 5.5a). It has been discussed that larger impacts of advection on the $sUHII_{RES}$-$aUHII_{RES}$ relationships are suggested due to larger turbulent source areas of OKCNET stations. However, this is only true for urban groups in OKC. Given the lower NDVI and the fact that the city is generally drier (lower mean RH in OKC illustrated in Table 5.1), the horizontal and vertical heat transfers of an air layer are supposed to be more efficient under drier conditions due to the increased thermal conductivity of air. Therefore, the cold/warm air from advection could be more readily homogenised with the surroundings, inducing the shorter distance of the advection affecting the suburban areas at downwind side. In addition, total areas distributed with

stations are more extended in OKC regardless of the similar average spacing of 3 km in both cities. Therefore, the advection effect on the suburban group is less significant in OKC compared to Birmingham. Lower percentage of data points in Z2 (warm advection) and Z4 (cold advection) for OKC (Figure 5.6c) provides the statistical evidence for these.

5.6 Conclusions

If more standardisation can be achieved with respect to UMNs, the results in this paper indicate that the method of confidence ellipse with LRM to explore the linear $sUHII$- $aUHII$ relationship with quadrant analysis appears to be transferable to other cities (e.g. OKC). Indeed, several patterns of the linear $sUHII$- $aUHII$ relationship could be generalised based on the results in this study, which are consistent with the study presented in Chapter 4. For example, the slope pattern is found to decrease with increasing WS for both cities, indicating the non-negligible effect of heat advection on the linear $sUHII$- $aUHII$ relationship. The $sUHII$- $aUHII$ relationship from a city with UMN could be used as a reference to estimate the city-specific $sUHII$- $aUHII$ relationship under specific conditions for cities without UMNs.

It is clear that some elements of the linear $sUHII$- $aUHII$ relationship will be unique for each city. The results in this study highlight the differences of the UHI magnitude and the linear $sUHII$ - $aUHII$ relationship between OKC and Birmingham. These are attributed mainly to the climate differences and the network designs. Fortunately, the differences of the linear $sUHII$- $aUHII$ relationship and the data distributions between the two cities are found to be smallest under the 'ideal' conditions for the development of UHI according to the results from the grouping analysis, which provides a starting point for generalising the linear $sUHII$- $aUHII$ relationship. Furthermore, the grouping

analysis based on different climatic conditions (i.e. WS and DASR) highlights the following two differences across the two cities: (i) the greater rate of change of $aUHII$ with respect to $sUHII$ and higher R^2 values over OKC under all three climatic conditions; (ii) site-averaged $sUHII$ are similar but the site-averaged $aUHII$ are greater over OKC under the three climatic conditions (i.e. $\overline{sUHII}^{OKC} \approx \overline{sUHII}^{BHAM}$ and $\overline{aUHII}^{OKC} > \overline{aUHII}^{BHAM}$).

This study has attempted to remove the climate effect via a statistical method but the differences between the two cities are still significant. As such, the role of different network designs is more likely to be influential to the linear $sUHII$- $aUHII$ relationship. Specifically, larger differences were found over the urban group compared to the suburban group (i.e. linear regression models and 2-D data distributions) as a result of the more distinct differences of the local environment and source areas between the UMNs over OKC and Birmingham. In reality, the network designs such as the deployment of each station are definitely distinctive for different cities. These would induce disparity of stations' local environment and source areas between different UMNs, leading to network-derived differences of air temperature or $aUHII$ and particular linear $sUHII$- $aUHII$ relationship ultimately. This finding underlines the requirement of following a standardised protocol for UMN design such as the one introduced by (Muller et al., 2013b). In such a way, the generalisation of the $sUHII$- $aUHII$ relationship could be more possible and workable across cities, by considering different background climate and their land morphologies.

There are some limitations in this study, which are summarised as follows: (i) Wind direction is one of the determining factors on the impacts of heat advection on the $sUHII$-

$aUHII$ relationship. However, it is not considered in this study due to the limited sample; (ii) Although the local environments surrounding the rural stations across OKC and Birmingham have been investigated, it is still worth considering the impacts of the selections of rural station on the differences of the $sUHII - aUHII$ relationship across these two cities in future analysis; (iii) Temporal variation (i.e. daily) of the $sUHII - aUHII$ relationship is not considered in this study because of the coarse temporal resolution of the MODIS satellite. The thermal bands data from the GOES-16 satellite with approximately 15-min temporal resolution (Minamide and Zhang, 2017) could be useful to further characterise the temporal variation of the $sUHII - aUHII$ relationship across cities in the future.

Moving forward, further comparisons of the linear $sUHII$- $aUHII$ relationship in other cities is needed. In addition, numerical modeling could be possibly used to remove the impact of different climate backgrounds between cities by running different simulations. However, there are promising signs that a universal $sUHII$ - $aUHII$ relationship is increasingly achievable.

5.7 Summary

In this chapter, a comparison has been made for the $sUHII$-$aUHII$ relationship between OKC and Birmingham with consideration of different atmospheric conditions and levels of urbanisations. Regarding the differences arising due to the local climate, a grouping analysis was successfully applied to facilitate the comparisons. Furthermore, a statistical method is used to minimise the local climate effect in order to explore the role of UMN configuration on the different $sUHII$-$aUHII$ relationships between the two cities. More importantly, the results from this chapter provide increased confidence in the

generalisation of the sUHII-aUHII relationship for different cities. Particularly, the differences of the sUHII-aUHII relationships between the two cities are minimised during the 'ideal' condition for UHI development.

Chapter 6 Conclusions

This thesis aims to explore the characteristics of the sUHII-aUHII relationship for individual cities and seek the possibility of the generalisation of the relationship across different cities (i.e. Birmingham and OKC) under certain climatic conditions and land surface characteristics. The generalisation process mainly focused on comparing the outcome of the sUHI-aUHI relationship from two different cities and identifying the conditions under which the relationship can be equally applied to the two cities. This chapter reviews the findings in terms of the four objectives in order to fulfil the aim of this thesis from all the analysis in previous chapters, and to present a critique of the analysis with respect to future work.

6.1 Fulfilment of aims of the thesis

Interest in the investigation of the relationship between surface urban heat island intensity ($sUHII$) and canopy urban heat island intensity ($aUHII$) (the $sUHII$- $aUHII$ relationship) is growing mainly because of the global availability of satellite-sensed land surface temperature (T_s). It is hoped that if such a universal relationship can be found, it could compensate for the spatial discontinuity of air temperature (T_a) measurements that currently exist due to a paucity of weather stations in urban areas. As discussed in Section 1.3, the "generalisation" mainly focused on comparing the outcome of the $sUHII$- $aUHII$ relationship from the two cities and identifying the conditions under which the relationship can be equally applied to the two cities. It is achieved by firstly examining if there are some specific characteristics of the $sUHII$- $aUHII$ relationship under certain conditions (Chapters 4-5). Certain conditions were identified that the $sUHII$- $aUHII$ relationships have similar characteristics across the two cities, e.g. the variations of the linear $sUHII$- $aUHII$ relationship follows the change of wind speed (e.g. the reduction of the rate of change of $sUHII$ with respect to $aUHII$ with increasing WS) and the role of the site characteristics (i.e. non-negligible impacts of advection on the magnitude of UHII in urban and suburban groups). The $sUHII$- $aUHII$ relationships were then compared between the two cities under these certain conditions to seek the possibility of the generalisation. This seems to be hard to achieve at the moment, however, results from this thesis provides further understandings of the role of the UMNs and local climate on the differences of the $sUHII$- $aUHII$ relationships across cities. It concludes that a standard protocol of the UMN is the prerequisite in order to derive a universal $sUHII$- $aUHII$ relationship globally in the future.

Regarding the four objectives in this thesis, each of it is evaluated below with a summary and conclusion of the outcomes in relation to each chapter.

(i) Response of $aUHII$ and $sUHII$ to different atmospheric conditions

The magnitude of the Urban Heat Island (UHI) effect is well documented to be most significant during periods of high atmospheric stability and it is during these periods that its impacts are most acutely felt. Atmospheric condition is most commonly considered in UHI studies by using the Pasquill-Gifford (P-G) classification scheme to assign a class to each day or few hours of investigation. One advantage of this approach is its broad applicability, only requiring simple routine meteorological measurements to perform the classification.

The availability of the Urban Meteorological Network (UMN) implemented in Oklahoma City (OKC), US, with meteorological observations available at two heights, provided a unique opportunity to evaluate the effectiveness of the P-G classification scheme by conducting the correlation analysis between the intensity of UHI (UHII, including $aUHII$ and $sUHII$) and the other four parameters related to atmospheric conditions (e.g. Richardson number, vertical gradient of temperature, vertical gradient of wind speed and wind speed at a different height level [2 m a.g.l]).

Despite the added sophistication of multi-level data, the main findings of Chapter 3 surprisingly confirmed the superiority of the P-G scheme for characterising the UHII, comparing to the other four parameters, indicating that background wind speed (10 m a.g.l) showcases strong controls in the variations of both $sUHII$ and $aUHII$. The P-G scheme is also found to be workable in differentiating both the daily $aUHII$ and $sUHII$ under different stability classes.

The analysis in Chapter 3 also provided more details regarding the inherent characteristic of the satellite-sensed land surface temperature. It was shown that the reliability of the P-G scheme was reduced for characterising $sUHII$ during the transition seasons (Spring and Autumn). Furthermore, results show that the spatial variance (standard deviation) of both the $sUHII$ and $aUHII$ across different Urban Climate Zones (UCZs) generally increases from neutral to extremely stable conditions, particularly during summer seasons. It is therefore suggested that the atmospheric condition also potentially influences the spatial pattern of both $sUHII$ and $aUHII$.

In summary, Chapter 3 demonstrates the significance of atmospheric condition (approximated by wind speed as cloud cover reduces the utility of satellite imagery) for spatial and temporal (or seasonal) variations of $sUHII$ and $aUHII$. Results from this chapter are of great importance to explore the $sUHII$- $aUHII$ relationship in the later chapters.

(ii) Explore the effects of atmospheric conditions and levels of urbanisations on the nocturnal sUHI-aUHI relationship by developing a repeatable methodology

Previous investigations of UHI are primarily focused either on the canopy air heat island intensity ($aUHII$) and the surface urban heat island intensity ($sUHII$). $aUHII$ and $sUHII$ are calculated as the air (from ground observations) and land surface temperature (from satellite instruments) differences between urban and rural sites, respectively. Research of the relationship between $sUHII$ and $aUHII$ (the $sUHII$-$aUHII$ relationship) is limited and this study attempted to further progress this possibility by examining the night-time $sUHII$-$aUHII$ relationship for three factors: season, wind speed, and basic landuse categories modified from local climate zones (urban / suburban), in Birmingham,

UK. Overall, Chapter 4 provided evidence of the potential generalising the $sUHII$-$aUHII$ relationship, with considerations of the three factors mentioned above.

Other than the use of UMN data, the main contribution of Chapter 4 was the development of a new methodological approach consisting of regression analysis, confidence ellipse analysis of covariance (ANCOVA), and 2-D Kolmogorov-Smirnov (K-S) tests, and statistical evidence to present the varying patterns and magnitudes between $sUHII$ and $aUHII$. This approach has been shown to provide the means to visually explore new insights into the relationship, backed up be robust statistical analysis.

Using the method, the specific characteristics of the linear $sUHII$ - $aUHII$ relationship were found with regards to different seasons, wind speed conditions and levels of urbanisation in Birmingham. Specifically, the results indicate that satellite data can be used to infer $aUHII$ with a higher confidence for low wind speed conditions. Results also demonstrate better confidence in the approach for summer and spring seasons, and for more urbanised sites. Indeed, the analysis potentially indicates that wind advection is a key factor for the investigation of the $sUHII$-$aUHII$ relationship. More importantly, this chapter provided a transferable methodology and convincing results regarding the generalisation of the $sUHII$-$aUHII$ relationship.

(iii) Determine the specific characteristics of the $sUHII$ - $aUHII$ relationship found in (ii) in OKC

Chapter 5 attempted to accomplish confirms the specific characteristics of the $sUHII$- $aUHII$ found in Chapter 4 by using the earlier developed statistical methods in Oklahoma City (OKC), US and comparing with Birmingham, UK. Particularly, some similarities are found across the two cities, such as the reduced rate of change of $aUHII$

with respect to $sUHII$ with increasing WS and the non-negligible advection effect regarding the urban and suburban groups of stations in this relationship, which was also found in Chapter 4. Results from Chapter 5 provided evidence regarding the methodology developed in Chapter 4 that can be applied in other cities to study the $sUHII$- $aUHII$ relationship confidently.

(iv) Investigate the possibility of generalisation of the sUHII-aUHII relationship by considering the role of local climate background and configurations of the UMNs in two cities

This objective was accomplished in Chapter 5 by comparing the $sUHII$- $aUHII$ relationship between OKC and Birmingham.

The differences of the linear $sUHII$- $aUHII$ relationship across two cities were found to reduce under ideal conditions (clear skies, calm and large input of solar radiation from previous day [DASR] into urban system). It was mainly explained by the larger controls of the local meteorological conditions (WS and DASR) on the $UHII$- $aUHII$ relationship, comparing to other influential factors. This implicated the higher chance of generalising the $sUHII$- $aUHII$ relationship across cities under ideal conditions for UHI development.

More importantly, the study emphasises the influence the configuration of UMNs on the $sUHII$- $aUHII$ relationship. By removing the climatic element in the relationship (i.e. WS and DASR), the impacts of the different local environments, source areas and general configurations of the UMN become evident, indicating that a standardised protocol for the designs of UMN is the prerequisite for the generalisation of the $sUHII$- $aUHII$ relationship across cities. Although there is ongoing work in this area (e.g. Muller et al. (2013b), World Meteorological Organization (2007)), this thesis has exposed the fact that

best practice in UMN design is urgently required to be established to ensure the full benefits of research efforts.

Overall, this thesis has validated the unique variations of the $sUHII$ - $aUHII$ relationship under specific conditions and importantly, the comparisons between these two cities provide more confidence in the generalisation process for future analysis. Particularly, climatic effects and the setting of UMN in each city are the most considerable concerns in this process.

6.2 Critique of thesis

There are a number of uncertainties according to the data and methodologies applied in this thesis. These are mainly included the accuracy of data and the effectiveness of the methods, potentially leading to other issues and uncertainties in the results (e.g. the $sUHII$- $aUHII$ relationship). These have been discussed thoroughly at the end of each analysis chapter (Chapters 3 - 5), but the following discussion will draw attentions to the major limitations in this thesis. The corresponding future work aiming to reduce these uncertainties and achieve the generalisation of the $sUHII$- $aUHII$ relationship globally is introduced in Section 6.4.

6.2.1 Data

Data used in this thesis have been introduced in Chapter 2, mainly incorporating the MODIS satellite products and the ground observations from the two UMNs in the two cities. The following discussions underline the limitation of the data and the corresponding potential effects on the results in this thesis.

(i) Satellite product (land surface temperature)

The accuracy of the land surface temperature estimated from satellite mainly depends upon the correction process of the atmospheric and emissivity effects which are highly variable under different atmospheric and surface conditions (Li et al., 2013). Although the freely access land surface temperature products from MODIS are used in this thesis, the corresponding constraints of the approximations and assumptions for estimating the land surface temperature are not considered due to the difficulties in light of the validation processes (e.g. availability of the ground measurements). Unfortunately, the validation of the land surface temperature products from MODIS has not been broadly conducted over urban areas. It is supposed that the highly heterogenous urban surface could inevitably induce some ambiguities of the estimation process (Wan, 2008). It is therefore likely to affect the estimation of $sUHII$. The ground observations are used to filter the images from satellite and prevent them from being affected by cloud, to a large extent, even though this would reduce the available images and sample size in this study which is another limitation in respect to the data processing.

In addition, the thermal anisotropy effects of the land surface temperature (T_s) induced by the variations of the satellite viewing angles, especially over urban areas, are considered to be negligible in this thesis because of (i) the lower level of the urbanisation over OKC and Birmingham, comparing to the study areas from previous studies that explored the anisotropy effect (Dyce and Voogt, 2018, Lagouarde et al., 2012) and (ii) the negligible effect of the thermal anisotropy at night-time (Hu et al., 2016a), as per discussed in Chapter 2. However, it may still increase the variation of the T_s over urban areas particularly during summer period when the daylight is longer. As the research related to the anisotropy effects is still limited, further analysis needs to be undertaken before considering it into the study of the $sUHII$- $aUHII$ relationship.

(ii) Ground observations from UMNs

Although the accuracy (a systematic errors: the closeness of the observations to a specific/real value) of the sensors for measuring temperature, wind speed or relative humidity from the two UMNs has been assessed and validated (Warren et al., 2016, Basara et al., 2011), different models of the sensors that usually have different levels of tolerance could potentially generate uncertainties during data retrieval, which is the acknowledged limitation in this thesis. Nonetheless, these two extensive networks ensure the sufficiency of the data used in this work and to a certain extent, it could reduce its corresponding effect in our results. This is not withstanding the earlier conclusion that a standard protocol for UMN design is urgently needed, because of the highly heterogenous temperature field in the urban canopy layer (UCL).

6.2.2 Methodology

Although there is a desire to produce a universal relationship, Birmingham and Oklahoma City are the only case study areas considered in this thesis. Even though the methods are designed to be transferable and findings are probable to be similar in other cities, much of the work is only relevant to these two cities and further comparison and validation are needed in other cities. The main limitation to the replicability is determined by the availability of the UMN and the protocol used to design and configure it. Furthermore, several constraints with reference to the methodology applied in the thesis are discussed as below.

UHI is the main focus of this study. The traditional method is used to calculate the UHI by subtracting the temperature at urban sites from rural sites. In doing so, the uncertainties induced by the measurements may increase. However, this is unavoidable

for observations. Therefore, a strict rule regarding the accuracy of the temperature sensors is necessary for configuring the weather station.

Simple methods are used to achieve the spatial and temporal consistency between surface and air temperature in this work. The spatial consistency between T_s and T_a is achieved based on IDW with 500-m radius buffer, as mentioned in Chapter 2. Therefore, the calculation of T_s corresponding to a weather station (T_a) has considered at least three pixels surrounding the weather station as the spatial resolution of the T_s product from MODIS is about 926.63 m. Although this is not the focus in this work, it is certainly not ideal and it could impact the results. Likewise, the temporal variations of the T_s from Aqua and Terra satellites are ignored, which is assumed to be derived at 01:30 AM and 22:30 PM, respectively. Accordingly, the average T_a during 01:00 – 02:00 AM and 22:00 – 23:00 PM are used. This approximation may trigger some uncertainties in the results, which is an important issue for future research.

Selections of different rural stations would contribute to variations of the $aUHII$ and $sUHII$. Local environments of the two rural reference stations -- Coleshill station is classified as scattered trees and Spencer station is classified as low plants, which are similar. The two rural stations are selected because they are the closest rural stations from the urban areas, which could reflect the rural conditions surrounding the urban areas more objectively. Moreover, southerly winds are prevalent during the study periods for the two cities while the two rural stations are located in the south of the cities, therefore, they could be less influenced by the heat advection from city centres. It is still worth considering the impacts of the selections of rural station on the differences of the $sUHII$-$aUHII$ relationship across these two cities in future studies.

The analysis of the work is mainly based on linear regression techniques. linear regression model (LRM) is chosen because of its simplicity compared to other non-linear regression models and it is easier to interpret the relationship two variables. More statistical techniques can be implemented to assess the reliability of the LRM, e.g. significant test for whole LRM and regression co-efficients. However, it is well known that the T_s-T_a relationship and $sUHII$-$aUHII$ relationship are extremely complicated and are expected to be non-linear. The specific characteristics found in terms of the LRMs are better for discovering the physical process between surface and air layers but the mathematical equations for building up the true relationships are more convincible by using non-linear models in future analysis.

6.3 Research impact

Overall, this thesis aims at moving closer to address the ambitious target of finding a universal $sUHII$-$aUHII$ relationship. Among many controlling quantities, a couple of 'universal' ones representing weather/climate processes, namely wind speed (WS) and daily accumulated solar radiation from previous day (DASR) were chosen to test. Using the linear regression method, we attempted to examine whether the slope of the regression lines or the mean UHII possess any universal information, independent of cities, or not. If not, e.g. contrasting magnitude of the mean $sUHII$ and $aUHII$ across the two cities discovered in Chapter 5, we tried to raise the issue to the research community for further studies to identify any attributable (either universal or city-specific) quantities, in order to enhance our understanding. One attributable city-specific factor is urban environmental conditions (i.e. building height and vegetation amount). According to the results from Chapter 5, the contrasting magnitude of the mean $sUHII$ and $aUHII$ across the two cities

are shown in both urban and suburban groups and all climatic conditions. Therefore, these differences could be attributed to the differing urban environments.

The impacts of the background atmospheric conditions and the configurations of the UMN are emphasized in generalisation process and the recommendation of a standardised protocol for configuration of UMNs. The standardised protocol is not trying to minimise the urban effect, but to highlight whether the differences of the UHI are induced by the UMN design, or by other factors such as urban structures and climate conditions. For example, for two identical hypothetical cities, but with UMNs of different configurations, the *sUHII-aUHII* relationship should be different, but this is not resulted from the urban structures but from different settings of their own UMNs. The latter is unavoidable and almost impossible to be quantified. The generalisation of the *sUHII-aUHII* relationship is also difficult to achieve due to the different climate background and urban structures across cities. However, the configuration of the UMNs across cities based on a standardised protocol is the first and important step to achieve this goal in the near future. Although it is hard to issue the standardised protocol that is workable for each city in the world, some specific guidelines can be proposed and followed. For example, for the configuration of the UMN aiming for UHI studies, stations are restricted to fixed height above ground level (i.e. 2 m) and there should be a threshold for the distance from the stations to the surrounding obstacles etc.

In conclusion, the findings from this thesis provide a deeper understanding of the *sUHII-aUHII* relationship and differences between nocturnal surface and canopy heat island. This is an important step for applying satellite products to studies referring to the UHI. The comparisons of the *sUHII-aUHII* relationship across cities used a transferable

methodology that can be readily to be applied in other cities, in order to achieve the generalisation of the $sUHII$-$aUHII$ relationship globally.

6.4 Future development and perspectives

Completing a set of perfect, systematic and rigorous tests of the $sUHII$-$aUHII$ relationship for different continents, with different morphologies and different background climates, and different UMN designs is an extremely challenging target. To achieve this ambitious target, multiple steps are required with regard to the data collection and data analysis. This work endeavours to take one step forward; this effort includes the development of a methodology to isolate the impact from one or two factors (e.g. background climate for different continents). Further research to compare the $sUHII$-$aUHII$ relationship in cities with different continents, with different urban settings and climate background is needed and it is subjective to the availability of the UMN. It would be great if the same network design could be replicated in several cities and hopefully, and this will become possible in due course as WMO (World Meteorological Organization) protocols evolve. Moreover, the comparisons of the $sUHII$ - $aUHII$ relationship between these two cities could be further investigated by running numerical models (i.e. weather forecasting and research model) that could provide physical parameters in light of the interaction between surface and air layers. The impacts of different climate background or urban structures could then be estimated by utilising an expanded case study approach.

List of References

Ackerman, B. 1985. Temporal march of the Chicago heat island. *Journal of Climate and Applied Meteorology,* 24**,** 547-554.

Alves, E. D. L. 2016. Seasonal and Spatial Variation of Surface Urban Heat Island Intensity in a Small Urban Agglomerate in Brazil. *Climate,* 4.

Anniballe, R., Bonafoni, S. & Pichierri, M. 2014. Spatial and temporal trends of the surface and air heat island over Milan using MODIS data. *Remote Sensing of Environment,* 150**,** 163-171.

Arnfield, A. J. 1990. Canyon geometry, the urban fabric and nocturnal cooling: a simulation approach. *Physical Geography,* 11**,** 220-239.

Arnfield, A. J. 2003. Two decades of urban climate research: a review of turbulence, exchanges of energy and water, and the urban heat island. *International Journal of Climatology: a Journal of the Royal Meteorological Society,* 23**,** 1-26.

Arya, P. S. 2001. *Introduction to micrometeorology*, Elsevier.

Auer Jr, A. H. 1978. Correlation of land use and cover with meteorological anomalies. *Journal of Applied Meteorology,* 17**,** 636-643.

Azevedo, J., Chapman, L. & Muller, C. 2016. Quantifying the daytime and night-time urban heat island in Birmingham, UK: A comparison of satellite derived land surface temperature and high resolution air temperature observations. *Remote Sensing,* 8**,** 153.

Bahi, H., Rhinane, H. & Bensalmia, A. 2016a. Contribution of MODIS satellite image to estimate the daily air temperature in the Casablanca City,

Morocco. *The International Archives of Photogrammetry, Remote Sensing and Spatial Information Sciences,* 42**,** 3.

Bahi, H., Rhinane, H., Bensalmia, A., Fehrenbach, U. & Scherer, D. 2016b. Effects of Urbanization and Seasonal Cycle on the Surface Urban Heat Island Patterns in the Coastal Growing Cities: A Case Study of Casablanca, Morocco. *Remote Sensing,* 8.

Banta, R. M., Pichugina, Y. L. & Newsom, R. K. 2003. Relationship between low-level jet properties and turbulence kinetic energy in the nocturnal stable boundary layer. *Journal of the atmospheric sciences,* 60**,** 2549-2555.

Bardal, L. M., Onstad, A. E., Sætran, L. R. & Lund, J. A. 2018. Evaluation of methods for estimating atmospheric stability at two coastal sites. *Wind Engineering,* 42**,** 561-575.

Basara, J. B., Hall Jr, P. K., Schroeder, A. J., Illston, B. G. & Nemunaitis, K. L. 2008. Diurnal cycle of the Oklahoma City urban heat island. *Journal of Geophysical Research: Atmospheres,* 113.

Basara, J. B., Illston, B. G., Fiebrich, C. A., Browder, P. D., Morgan, C. R., Mccombs, A., Bostic, J. P., Mcpherson, R. A., Schroeder, A. J. & Crawford, K. C. 2011. The Oklahoma city micronet. *Meteorological Applications,* 18**,** 252-261.

Bassett, R., Cai, X., Chapman, L., Heaviside, C., Thornes, J. E., Muller, C. L., Young, D. T. & Warren, E. L. 2016. Observations of urban heat island advection from a high-density monitoring network. *Quarterly Journal of the Royal Meteorological Society,* 142**,** 2434-2441.

Bassett, R., Cai, X. M., Chapman, L., Heaviside, C. & Thornes, J. E. 2017. Methodology to separate urban from regional heat advection by use of the Weather Research and Forecasting mesoscale model. *Quarterly Journal of the Royal Meteorological Society,* 143**,** 2016-2024.

Basu, S. & Lacser, A. 2017. A cautionary note on the use of Monin–Obukhov similarity theory in very high-resolution large-eddy simulations. *Boundary-Layer Meteorology,* 163**,** 351-355.

Bergeron, O. & Strachan, I. B. 2012. Wintertime radiation and energy budget along an urbanization gradient in Montreal, Canada. *International Journal of Climatology,* 32**,** 137-152.

Best, M., Grimmond, C. & Villani, M. G. 2006. Evaluation of the urban tile in MOSES using surface energy balance observations. *Boundary-Layer Meteorology,* 118**,** 503-525.

Birmingham City Council. 2013. *2011 Birmingham Population & Migration Topic report* [Online]. Available: https://www.birmingham.gov.uk/downloads/file/9742/2011_birmingham_population_and_migration_topic_report [Accessed].

Bohnenstengel, S., Hamilton, I., Davies, M. & Belcher, S. 2014. Impact of anthropogenic heat emissions on London's temperatures. *Quarterly Journal of the Royal Meteorological Society,* 140**,** 687-698.

Boybeyi, Z. 2000. *Mesoscale atmospheric dispersion*, Computational Mechanics.

Brazel, A., Selover, N., Vose, R. & Heisler, G. 2000. The tale of two climates Baltimore and Phoenix urban LTER sites. *Climate Research,* 15**,** 123-135.

Businger, J. A., Wyngaard, J. C., Izumi, Y. & Bradley, E. F. 1971. Flux-profile relationships in the atmospheric surface layer. *Journal of the atmospheric Sciences,* 28**,** 181-189.

Cao, W., Hu, J. & Yu, X. A study on temperature interpolation methods based on GIS. 2009 17th International Conference on Geoinformatics, 2009. IEEE, 1-5.

Cavan, G., Lindley, S., Jalayer, F., Yeshitela, K., Pauleit, S., Renner, F., Gill, S., Capuano, P., Nebebe, A. & Woldegerima, T. 2014. Urban morphological determinants of temperature regulating ecosystem services in two African cities. *Ecological indicators,* 42**,** 43-57.

Chandler, T. J. 1965. *The climate of London*, Hutchinson.

Chapman, L., Muller, C. L., Young, D. T., Warren, E. L., Grimmond, C. S. B., Cai, X.-M. & Ferranti, E. J. 2015. The Birmingham urban climate laboratory: An open meteorological test bed and challenges of the smart city. *Bulletin of the American Meteorological Society,* 96**,** 1545-1560.

Chapman, L., Thornes, J. E. & Bradley, A. V. 2001. Modelling of road surface temperature from a geographical parameter database. Part 2: Numerical. *Meteorological Applications,* 8**,** 421-436.

Chen, Y., Jiang, W. M., Zhang, N., He, X. F. & Zhou, R. W. 2009. Numerical simulation of the anthropogenic heat effect on urban boundary layer structure. *Theoretical and Applied Climatology,* 97**,** 123-134.

Chieppa, J., Bush, A. & Mitra, C. 2018. Using "Local Climate Zones" to Detect Urban Heat Island on Two Small Cities in Alabama. *Earth Interactions,* 22**,** 1-22.

Chow, S. D., Zheng, J. C. & Wu, L. 1994. SOLAR-RADIATION AND SURFACE-TEMPERATURE IN SHANGHAI CITY AND THEIR RELATION TO URBAN HEAT-ISLAND INTENSITY. *Atmospheric Environment,* 28**,** 2119-2127.

Chow, W. T. & Roth, M. 2006. Temporal dynamics of the urban heat island of Singapore. *International Journal of Climatology: A Journal of the Royal Meteorological Society,* 26**,** 2243-2260.

Chowienczyk, K., Mccarthy, M., Hollis, D., Dyson, E., Lee, M. & Coley, D. 2020. Estimating and mapping urban heat islands of the UK by interpolation from the UK Met Office observing network. *Building Services Engineering Research and Technology***,** 0143624419897254.

Climatemps.Com. *World Climate & Temperature* [Online]. Available: http://www.climatemps.com [Accessed].

Clinton, N. & Gong, P. 2013. MODIS detected surface urban heat islands and sinks: Global locations and controls. *Remote Sensing of Environment,* 134**,** 294-304.

Coll, C., Caselles, V., Galve, J. M., Valor, E., Niclos, R., Sánchez, J. M. & Rivas, R. 2005. Ground measurements for the validation of land surface temperatures derived from AATSR and MODIS data. *Remote sensing of Environment,* 97**,** 288-300.

Collier, C. G. 2006. The impact of urban areas on weather. *Quarterly Journal of the Royal Meteorological Society: A journal of the atmospheric sciences, applied meteorology and physical oceanography,* 132**,** 1-25.

Cork, R. C., Vaughan, R. W. & Humphrey, L. S. 1983. Precision and accuracy of intraoperative temperature monitoring. *Anesthesia and analgesia,* 62**,** 211-214.

Cui, Y. Y. & De Foy, B. 2012. Seasonal variations of the urban heat island at the surface and the near-surface and reductions due to urban vegetation in Mexico City. *Journal of Applied Meteorology and Climatology,* 51**,** 855-868.

Culbertson, D. P. 2001. Surface temperature sensor. Google Patents.

Darnell, W. L., Gupta, S. K. & Staylor, W. F. 1986. Downward longwave surface radiation from sun-synchronous satellite data: Validation of methodology. *Journal of climate and applied meteorology,* 25**,** 1012-1021.

Dash, P., Göttsche, F.-M., Olesen, F.-S. & Fischer, H. 2002. Land surface temperature and emissivity estimation from passive sensor data: Theory and practice-current trends. *International Journal of remote sensing,* 23**,** 2563-2594.

De Wilde, P. & Coley, D. 2012. The implications of a changing climate for buildings. Elsevier.

Deilami, K., Kamruzzaman, M. & Liu, Y. 2018. Urban heat island effect: A systematic review of spatio-temporal factors, data, methods, and mitigation measures. *International journal of applied earth observation and geoinformation,* 67**,** 30-42.

Dian, C., Pongracz, R., Dezso, Z. & Bartholy, J. 2020. Annual and monthly analysis of surface urban heat island intensity with respect to the local climate zones in Budapest. *Urban Climate,* 31.

Dong, L., Mitra, C., Greer, S. & Burt, E. 2018. The Dynamical Linkage of Atmospheric Blocking to Drought, Heatwave and Urban Heat Island in Southeastern US: A Multi-Scale Case Study. *Atmosphere,* 9**,** 33.

Dos Santos, I. G., De Lima, H. G. & De Assis, E. S. 2003. A comprehensive approach of the sky view factor and building mass in an urban area of the city of Belo Horizonte, Brazil. *The Federal University of Minas Gerais, Belo Horizonte, MG, Brazil*.

Drach, P., Krüger, E. L. & Emmanuel, R. 2018. Effects of atmospheric stability and urban morphology on daytime intra-urban temperature variability for Glasgow, UK. *Science of the Total Environment,* 627**,** 782-791.

Dyce, D. R. & Voogt, J. A. 2018. The influence of tree crowns on urban thermal effective anisotropy. *Urban Climate,* 23**,** 91-113.

Einarsson, E. & Lowe, A. 1955. *A Study of Horizontal Temperature Variations in the Winnipeg Area on Nights Favouring Radiational Cooling*, Department of Transport, Meteorological Division.

Ellefsen, R. 1991. Mapping and measuring buildings in the canopy boundary layer in ten US cities. *Energy and Buildings,* 16**,** 1025-1049.

Emeis, S. 2018. *Wind energy meteorology: atmospheric physics for wind power generation*, Springer.

Estoque, R. C., Murayama, Y. & Myint, S. W. 2017. Effects of landscape composition and pattern on land surface temperature: An urban heat island study in the megacities of Southeast Asia. *Science of the Total Environment,* 577**,** 349-359.

Estournel, C., Vehil, R., Guedalia, D., Fontan, J. & Druilhet, A. 1983. Observations and modeling of downward radiative fluxes (solar and infrared) in urban/rural areas. *Journal of Climate and Applied Meteorology,* 22**,** 134-142.

Fast, J. D., Torcolini, J. C. & Redman, R. 2005. Pseudovertical temperature profiles and the urban heat island measured by a temperature datalogger network in Phoenix, Arizona. *Journal of applied meteorology,* 44**,** 3-13.

Feng, J. L., Cai, X. M. & Chapman, L. 2019. Impact of atmospheric conditions and levels of urbanization on the relationship between nocturnal surface and urban canopy heat islands. *Quarterly Journal of the Royal Meteorological Society,* 145**,** 3284-3299.

Fenner, D., Meier, F., Scherer, D. & Polze, A. 2014. Spatial and temporal air temperature variability in Berlin, Germany, during the years 2001–2010. *Urban Climate,* 10**,** 308-331.

Ferreira, L. S. & Duarte, D. H. S. 2019. Exploring the relationship between urban form, land surface temperature and vegetation indices in a subtropical megacity. *Urban Climate,* 27**,** 105-123.

Fiebrich, C. A. & Crawford, K. C. 2001. The impact of unique meteorological phenomena detected by the Oklahoma Mesonet and ARS Micronet on automated quality control. *Bulletin of the American Meteorological Society,* 82**,** 2173-2188.

Figuerola, P. I. & Mazzeo, N. A. 1998. Urban-rural temperature differences in Buenos Aires. *International Journal of Climatology: A Journal of the Royal Meteorological Society,* 18**,** 1709-1723.

Fisher, R. A. 1934. Statistical methods for research workers. *Statistical methods for research workers*.

Flerchinger, G. N., Reba, M. L., Link, T. E. & Marks, D. 2015. Modeling temperature and humidity profiles within forest canopies. *Agricultural and Forest Meteorology,* 213**,** 251-262.

Foken, T. 2006. 50 years of the Monin–Obukhov similarity theory. *Boundary-Layer Meteorology,* 119**,** 431-447.

Fortuniak, K., Kłysik, K. & Wibig, J. 2006. Urban–rural contrasts of meteorological parameters in Łódź. *Theoretical and applied climatology,* 84**,** 91-101.

Friendly, M., Monette, G. & Fox, J. 2013. Elliptical insights: understanding statistical methods through elliptical geometry. *Statistical Science,* 28**,** 1-39.

Frouin, R., Gautier, C. & Morcrette, J. J. 1988. Downward longwave irradiance at the ocean surface from satellite data: Methodology and in situ validation. *Journal of Geophysical Research: Oceans,* 93**,** 597-619.

Gaffin, S., Rosenzweig, C., Khanbilvardi, R., Parshall, L., Mahani, S., Glickman, H., Goldberg, R., Blake, R., Slosberg, R. & Hillel, D. 2008. Variations in New York city's urban heat island strength over time and space. *Theoretical and applied climatology,* 94**,** 1-11.

Gallo, K. P., Tarpley, J. D., Mcnab, A. L. & Karl, T. R. 1995. Assessment of urban heat islands: a satellite perspective. *Atmospheric Research,* 37**,** 37-43.

Galperin, B., Sukoriansky, S. & Anderson, P. S. 2007. On the critical Richardson number in stably stratified turbulence. *Atmospheric Science Letters,* 8**,** 65-69.

Geletic, J., Lehnert, M., Savic, S. & Milosevic, D. 2019. Inter-/intra-zonal seasonal variability of the surface urban heat island based on local climate zones in three central European cities. *Building and Environment,* 156**,** 21-32.

Golder, D. 1972. Relations among stability parameters in the surface layer. *Boundary-Layer Meteorology,* 3**,** 47-58.

Gosling, S. N., Lowe, J. A., Mcgregor, G. R., Pelling, M. & Malamud, B. D. 2009. Associations between elevated atmospheric temperature and human mortality: a critical review of the literature. *Climatic change,* 92**,** 299-341.

Greenberg, J. A., Rueda, C., Hestir, E. L., Santos, M. J. & Ustin, S. L. 2011. Least cost distance analysis for spatial interpolation. *Computers & Geosciences,* 37**,** 272-276.

Grimmond, C. S. B., Blackett, M., Best, M., Barlow, J., Baik, J., Belcher, S., Bohnenstengel, S., Calmet, I., Chen, F. & Dandou, A. 2010. The

international urban energy balance models comparison project: first results from phase 1. *Journal of applied meteorology and climatology,* 49**,** 1268-1292.

Grover, A. & Singh, R. B. 2015. Analysis of urban heat island (UHI) in relation to normalized difference vegetation index (NDVI): A comparative study of Delhi and Mumbai. *Environments,* 2**,** 125-138.

Gu, Y. & Li, D. 2018. A modeling study of the sensitivity of urban heat islands to precipitation at climate scales. *Urban climate,* 24**,** 982-993.

Gupta, P. & Sastri, P. 1990. Stability determination over crop surfaces by different methods and their comparison. *Journal of Aerosol Science,* 21**,** S303-S305.

Hanes, J. M. & Schwartz, M. D. 2011. Modeling land surface phenology in a mixed temperate forest using MODIS measurements of leaf area index and land surface temperature. *Theoretical and applied climatology,* 105**,** 37-50.

Hari Prasad, K., Venkata Srinivas, C., Venkateswara Naidu, C., Baskaran, R. & Venkatraman, B. 2016. Assessment of surface layer parameterizations in ARW using micro-meteorological observations from a tropical station. *Meteorological Applications,* 23**,** 191-208.

Harman, I. & Belcher, S. 2006. The surface energy balance and boundary layer over urban street canyons. *Quarterly Journal of the Royal Meteorological Society: A journal of the atmospheric sciences, applied meteorology and physical oceanography,* 132**,** 2749-2768.

Hawkins, T. W., Brazel, A. J., Stefanov, W. L., Bigler, W. & Saffell, E. M. 2004. The role of rural variability in urban heat island determination for Phoenix, Arizona. *Journal of Applied Meteorology,* 43**,** 476-486.

Heaviside, C., Cai, X. M. & Vardoulakis, S. 2015. The effects of horizontal advection on the urban heat island in Birmingham and the West Midlands, United Kingdom during a heatwave. *Quarterly Journal of the Royal Meteorological Society,* 141**,** 1429-1441.

Heaviside, C., Vardoulakis, S. & Cai, X.-M. 2016. Attribution of mortality to the urban heat island during heatwaves in the West Midlands, UK. *Environmental health,* 15**,** 49-59.

Herbel, I., Croitoru, A. E., Rus, A. V., Rosca, C. F., Harpa, G. V., Ciupertea, A. F. & Rus, I. 2018. The impact of heat waves on surface urban heat island and local economy in Cluj-Napoca city, Romania. *Theoretical and Applied Climatology,* 133**,** 681-695.

Hou, P., Chen, Y., Qiao, W., Cao, G., Jiang, W. & Li, J. 2013. Near-surface air temperature retrieval from satellite images and influence by wetlands in urban region. *Theoretical and applied climatology,* 111**,** 109-118.

Hu, L., Monaghan, A., Voogt, J. A. & Barlage, M. 2016a. A first satellite-based observational assessment of urban thermal anisotropy. *Remote sensing of environment,* 181**,** 111-121.

Hu, X.-M., Klein, P. M., Xue, M., Lundquist, J. K., Zhang, F. & Qi, Y. 2013. Impact of low-level jets on the nocturnal urban heat island intensity in Oklahoma City. *Journal of applied meteorology and climatology,* 52**,** 1779-1802.

Hu, X.-M., Xue, M., Klein, P. M., Illston, B. G. & Chen, S. 2016b. Analysis of urban effects in Oklahoma City using a dense surface observing network. *Journal of Applied Meteorology and Climatology,* 55**,** 723-741.

Hu, Y., Hou, M., Jia, G., Zhao, C., Zhen, X. & Xu, Y. 2019. Comparison of surface and canopy urban heat islands within megacities of eastern China. *ISPRS Journal of Photogrammetry and Remote Sensing,* 156**,** 160-168.

Imamura, I. 1991. *Observational studies of urban heat island characteristics in different climate zones*. Ph. D. Thesis.

Izumi, Y. 1971. *Kansas 1968 field program data report*, Air Force Cambridge Research Laboratories, Air Force Systems Command, United ….

Jaccard, J., Turrisi, R. & Jaccard, J. 2003. *Interaction effects in multiple regression*, Sage.

Jain, M., Dimri, A. & Niyogi, D. 2017. Land-Air Interactions over Urban-Rural Transects Using Satellite Observations: Analysis over Delhi, India from 1991–2016. *Remote Sensing,* 9**,** 1283.

Janjic, Z. 1996. The Surface Layer Parameterization in the NCEP Eta Model, 444 pp. *World Meteorol. Organ. Publ., Geneva, Switzerland*.

Jauregui, E. 1973. The urban climate of Mexico City. *Erdkunde***,** 298-307.

Jauregui, E. 1997. Heat island development in Mexico City. *Atmospheric Environment,* 31**,** 3821-3831.

Jin, M. & Shepherd, J. M. 2005. Inclusion of urban landscape in a climate model: How can satellite data help? *Bulletin of the American Meteorological Society,* 86**,** 681-690.

Johnson, D. 1985. Urban modification of diurnal temperature cycles in Birmingham, UK. *Journal of climatology,* 5**,** 221-225.

Kahl, J. D. & Chapman, H. L. 2018. Atmospheric stability characterization using the Pasquill method: A critical evaluation. *Atmospheric Environment,* 187**,** 196-209.

Kallistratova, M. A. & Kouznetsov, R. D. 2012. Low-level jets in the Moscow region in summer and winter observed with a sodar network. *Boundary-layer meteorology,* 143**,** 159-175.

Kanda, M., Moriwaki, R. & Kasamatsu, F. 2006. Spatial variability of both turbulent fluxes and temperature profiles in an urban roughness layer. *Boundary-layer meteorology,* 121**,** 339-350.

Kanda, M., Moriwaki, R. & Kimoto, Y. 2005. Temperature profiles within and above an urban canopy. *Boundary-Layer Meteorology,* 115**,** 499-506.

Kassomenos, P. 2003. Anatomy of the synoptic conditions occurring over southern Greece during the second half of the 20 th century. Part I. Winter and summer. *Theoretical and applied climatology,* 75**,** 65-77.

Kato, S. & Yamaguchi, Y. 2005. Analysis of urban heat-island effect using ASTER and ETM+ Data: Separation of anthropogenic heat discharge and

natural heat radiation from sensible heat flux. *Remote Sensing of Environment,* 99**,** 44-54.

Kent, C. W., Grimmond, S., Barlow, J., Gatey, D., Kotthaus, S., Lindberg, F. & Halios, C. H. 2017. Evaluation of urban local-scale aerodynamic parameters: implications for the vertical profile of wind speed and for source areas. *Boundary-Layer Meteorology,* 164**,** 183-213.

Kim, Y.-H. & Baik, J.-J. 2002. Maximum urban heat island intensity in Seoul. *Journal of applied meteorology,* 41**,** 651-659.

Kim, Y.-H. & Baik, J.-J. 2005. Spatial and temporal structure of the urban heat island in Seoul. *Journal of Applied Meteorology,* 44**,** 591-605.

Kimura, F. 1989. Heat flux on mixtures of different land-use surface: Test of a new parameterization scheme. *Journal of the Meteorological Society of Japan. Ser. II,* 67**,** 401-409.

Kłysik, K. & Fortuniak, K. 1999. Temporal and spatial characteristics of the urban heat island of Łódź, Poland. *Atmospheric environment,* 33**,** 3885-3895.

Koken, P. J., Piver, W. T., Ye, F., Elixhauser, A., Olsen, L. M. & Portier, C. J. 2003. Temperature, air pollution, and hospitalization for cardiovascular diseases among elderly people in Denver. *Environmental health perspectives,* 111**,** 1312-1317.

Kolokotroni, M. & Giridharan, R. 2008. Urban heat island intensity in London: An investigation of the impact of physical characteristics on changes in outdoor air temperature during summer. *Solar energy,* 82**,** 986-998.

Kolokotsa, D., Psomas, A. & Karapidakis, E. 2009. Urban heat island in southern Europe: The case study of Hania, Crete. *Solar Energy,* 83**,** 1871-1883.

Kong, F., Yin, H., Wang, C., Cavan, G. & James, P. 2014. A satellite image-based analysis of factors contributing to the green-space cool island intensity on a city scale. *Urban forestry & urban greening,* 13**,** 846-853.

Kotharkar, R. & Bagade, A. 2018. Evaluating urban heat island in the critical local climate zones of an Indian city. *Landscape and Urban Planning,* 169**,** 92-104.

Krüger, E. & Emmanuel, R. 2013. Accounting for atmospheric stability conditions in urban heat island studies: The case of Glasgow, UK. *Landscape and Urban Planning,* 117**,** 112-121.

Kukla, G., Gavin, J. & Karl, T. 1986. Urban warming. *Journal of climate and applied meteorology,* 25**,** 1265-1270.

Kuzevicova, Z., Palkova, J., Kuzevic, S. & Gergel'ova, M. 2016. A Comparison of Interpolation Methods for Estimation of Air Temperature. *Inżynieria Mineralna,* 17**,** 163--170.

Lagouarde, J.-P., Hénon, A., Irvine, M., Voogt, J., Pigeon, G., Moreau, P., Masson, V. & Mestayer, P. 2012. Experimental characterization and modelling of the nighttime directional anisotropy of thermal infrared measurements over an urban area: Case study of Toulouse (France). *Remote Sensing of Environment,* 117**,** 19-33.

Lagouarde, J.-P., Moreau, P., Irvine, M., Bonnefond, J.-M., Voogt, J. A. & Solliec, F. 2004. Airborne experimental measurements of the angular variations in surface temperature over urban areas: case study of Marseille (France). *Remote Sensing of Environment,* 93**,** 443-462.

Lamb, H. H. & Hh, L. 1972. British Isles weather types and a register of the daily sequence of circulation patterns 1861-1971.

Larsen, S. E. & Gryning, S.-E. 1986. Dispersion climatology in a coastal zone. *Atmospheric Environment (1967),* 20**,** 1325-1332.

Laskin, D. N., Montaghi, A. & Mcdermid, G. J. 2017. An open-source method of constructing cloud-free composites of forest understory temperature using MODIS. *Remote Sensing Letters,* 8**,** 165-174.

Laskin, D. N., Montaghi, A., Nielsen, S. E. & Mcdermid, G. J. 2016. Estimating understory temperatures using MODIS LST in mixed cordilleran forests. *Remote Sensing,* 8**,** 658.

Lauwaet, D., De Ridder, K., Saeed, S., Brisson, E., Chatterjee, F., Van Lipzig, N. P., Maiheu, B. & Hooyberghs, H. 2016. Assessing the current and future urban heat island of Brussels. *Urban Climate,* 15**,** 1-15.

Lee, D. 1975. Rural atmospheric stability and the intensity of London's heat island. *Weather,* 30**,** 102-109.

Lee, D. 1979. The influence of atmospheric stability and the urban heat island on urban-rural wind speed differences. *Atmospheric Environment (1967),* 13**,** 1175-1180.

Lemonsu, A. & Masson, V. 2002. Simulation of a summer urban breeze over Paris. *Boundary-Layer Meteorology,* 104**,** 463-490.

Levermore, G., Parkinson, J., Lee, K., Laycock, P. & Lindley, S. 2018. The increasing trend of the urban heat island intensity. *Urban climate,* 24**,** 360-368.

Li, D., Malyshev, S. & Shevliakova, E. 2016. Exploring historical and future urban climate in the Earth System Modeling framework: 2. Impact of urban land use over the Continental United States. *Journal of Advances in Modeling Earth Systems,* 8**,** 936-953.

Li, H. & Liu, Q. Comparison of NDBI and NDVI as indicators of surface urban heat island effect in MODIS imagery. International conference on earth observation data processing and analysis (ICEODPA), 2008. International Society for Optics and Photonics, 728503.

Li, L. & Zha, Y. 2019. Satellite-Based Spatiotemporal Trends of Canopy Urban Heat Islands and Associated Drivers in China's 32 Major Cities. *Remote Sensing,* 11**,** 102.

Li, Z.-L., Tang, B.-H., Wu, H., Ren, H., Yan, G., Wan, Z., Trigo, I. F. & Sobrino, J. A. 2013. Satellite-derived land surface temperature: Current status and perspectives. *Remote sensing of environment,* 131**,** 14-37.

Lowry, W. P. 1977. Empirical estimation of urban effects on climate: a problem analysis. *Journal of applied meteorology,* 16**,** 129-135.

Lumley, J. L. & Panofsky, H. A. 1964. *The structure of atmospheric turbulence*, Interscience publishers New York.

Manoli, G., Fatichi, S., Schläpfer, M., Yu, K., Crowther, T. W., Meili, N., Burlando, P., Katul, G. G. & Bou-Zeid, E. 2019. Magnitude of urban heat islands largely explained by climate and population. *Nature,* 573**,** 55-60.

Martilli, A., Roth, M., Chow, W. T., Demuzere, M., Lipson, M., Krayenhoff, E. S., Sailor, D., Nazarian, N., Voogt, J. & Wouters, H. 2020. Summer average urban-rural surface temperature differences do not indicate the need for urban heat reduction.

Marzban, F., Sodoudi, S. & Preusker, R. 2018. The influence of land-cover type on the relationship between NDVI–LST and LST-T air. *International journal of remote sensing,* 39**,** 1377-1398.

Masiri, I., Janjai, S., Nunez, M. & Anusasananan, P. 2017. A technique for mapping downward longwave radiation using satellite and ground-based data in the tropics. *Renewable Energy,* 103**,** 171-179.

Masson, V. 2000. A physically-based scheme for the urban energy budget in atmospheric models. *Boundary-layer meteorology,* 94**,** 357-397.

Maxwell, S. E., Delaney, H. D. & Manheimer, J. M. 1985. ANOVA of residuals and ANCOVA: Correcting an illusion by using model comparisons and graphs. *Journal of Educational Statistics,* 10**,** 197-209.

Mcpherson, R. A., Fiebrich, C. A., Crawford, K. C., Kilby, J. R., Grimsley, D. L., Martinez, J. E., Basara, J. B., Illston, B. G., Morris, D. A. & Kloesel, K. A. 2007. Statewide monitoring of the mesoscale environment: A technical update on the Oklahoma Mesonet. *Journal of Atmospheric and Oceanic Technology,* 24**,** 301-321.

Meehl, G. A. & Tebaldi, C. 2004. More intense, more frequent, and longer lasting heat waves in the 21st century. *Science,* 305**,** 994-997.

Meerkoetter, R. & Grassl, H. 1984. Longwave net flux at the ground from radiances at the top. *IRS'84: Current Problems in Atmospheric Radiation***,** 220-223.

Meng, F. & Liu, M. 2013. Remote-sensing image-based analysis of the patterns of urban heat islands in rapidly urbanizing Jinan, China. *International journal of remote sensing,* 34**,** 8838-8853.

Minamide, M. & Zhang, F. 2017. Adaptive observation error inflation for assimilating all-sky satellite radiance. *Monthly Weather Review,* 145**,** 1063-1081.

Mirzaei, P. A. & Haghighat, F. 2010. Approaches to study Urban Heat Island - Abilities and limitations. *Building and Environment,* 45**,** 2192-2201.

Mohan, M. & Siddiqui, T. 1998. Analysis of various schemes for the estimation of atmospheric stability classification. *Atmospheric Environment,* 32**,** 3775-3781.

Monette, G. 1990. Geometry of multiple regression and interactive 3-D graphics. *Modern methods of data analysis***,** 209-256.

Monin, A. S. & Obukhov, A. M. 1954. Osnovnye zakonomernosti turbulentnogo peremesivanija v prizemnom sloe atmosfery. *Trudy geofiz. inst. AN SSSR,* 24**,** 163-187.

Monin, A. S. & Yaglom, A. 1999. Statistical fluid mechanics: The mechanics of turbulence. MASSACHUSETTS INST OF TECH CAMBRIDGE.

Montandon, L. & Small, E. 2008. The impact of soil reflectance on the quantification of the green vegetation fraction from NDVI. *Remote Sensing of Environment,* 112**,** 1835-1845.

Montávez, J. P., Rodríguez, A. & Jiménez, J. I. 2000. A study of the urban heat island of Granada. *International Journal of Climatology: A Journal of the Royal Meteorological Society,* 20**,** 899-911.

Montgomery, D. C., Peck, E. A. & Vining, G. G. 2012. *Introduction to linear regression analysis*, John Wiley & Sons.

Morris, C. & Simmonds, I. 2000. Associations between varying magnitudes of the urban heat island and the synoptic climatology in Melbourne, Australia. *International Journal of Climatology: A Journal of the Royal Meteorological Society,* 20**,** 1931-1954.

Morris, C., Simmonds, I. & Plummer, N. 2001. Quantification of the influences of wind and cloud on the nocturnal urban heat island of a large city. *Journal of Applied Meteorology,* 40**,** 169-182.

Muller, C. L., Chapman, L., Grimmond, C., Young, D. T. & Cai, X. 2013a. Sensors and the city: a review of urban meteorological networks. *International Journal of Climatology,* 33**,** 1585-1600.

Muller, C. L., Chapman, L., Grimmond, C., Young, D. T. & Cai, X.-M. 2013b. Toward a standardized metadata protocol for urban meteorological networks. *Bulletin of the American Meteorological Society,* 94**,** 1161-1185.

Mutiibwa, D., Strachan, S. & Albright, T. 2015. Land surface temperature and surface air temperature in complex terrain. *IEEE Journal of Selected Topics in Applied Earth Observations and Remote Sensing,* 8**,** 4762-4774.

Nguyen, X. T., Nguyen, B. T., Do, K. P., Bui, Q. H., Nguyen, T. N. T., Vuong, V. Q. & Le, T. H. 2015. Spatial Interpolation of Meteorologic Variables in Vietnam using the Kriging Method. *JIPS,* 11**,** 134-147.

Nichol, J. & Wong, M. 2008. Spatial variability of air temperature and appropriate resolution for satellite-derived air temperature estimation. *International Journal of Remote Sensing,* 29**,** 7213-7223.

Nichol, J. E., Fung, W. Y., Lam, K.-S. & Wong, M. S. 2009. Urban heat island diagnosis using ASTER satellite images and 'in situ' air temperature. *Atmospheric Research,* 94**,** 276-284.

Oke, P. R. 2002a. *Urban heat islands: an overview of the research and its implications* [Online]. Toronto, Canada: Urban Heat Island Summit. Available: www.city.toronto.on.ca/cleanairpartnership/uhis_summit.htm [Accessed].

Oke, P. R., Oke, T., Oke, T. & Oke, T. 2006. Initial guidance to obtain representative meteorological observations at urban sites.

Oke, T. 1995. The heat island of the urban boundary layer: characteristics, causes and effects. *Wind climate in cities*. Springer.

Oke, T. 1999. Observing urban weather and climate using'standard'stations. *EURASAP Newsletter,* 35.

Oke, T., Johnson, G., Steyn, D. & Watson, I. 1991. Simulation of surface urban heat islands under 'ideal'conditions at night part 2: Diagnosis of causation. *Boundary-Layer Meteorology,* 56**,** 339-358.

Oke, T. R. 1973. City size and the urban heat island. *Atmospheric Environment (1967),* 7**,** 769-779.

Oke, T. R. 1982. The energetic basis of the urban heat island. *Quarterly Journal of the Royal Meteorological Society,* 108**,** 1-24.

Oke, T. R. 1988a. Street design and urban canopy layer climate. *Energy and buildings,* 11**,** 103-113.

Oke, T. R. 1988b. The urban energy balance. *Progress in Physical geography,* 12**,** 471-508.

Oke, T. R. 2002b. *Boundary layer climates*, Routledge.

Oke, T. R. 2007. Siting and exposure of meteorological instruments at urban sites. *Air pollution modeling and its application XVII*. Springer.

Oke, T. R. & Fuggle, R. 1972. Comparison of urban/rural counter and net radiation at night. *Boundary-Layer Meteorology,* 2**,** 290-308.

Oke, T. R. & Maxwell, G. B. 1975. Urban heat island dynamics in Montreal and Vancouver. *Atmospheric Environment (1967),* 9**,** 191-200.

Oke, T. R., Mills, G., A, C. & Voogt, J. A. 2017. *Urban climates*, Cambridge University Press.

Oklahoma City Council. 2010. *Building Footprints 2010* [Online]. Open Data Portal. Available: https://data.okc.gov/portal/page/start/ [Accessed 2010].

Oklahoma City Council. 2020. *PlanOKC Land Use Typology Areas* [Online]. Open Data Portal. Available: https://data.okc.gov/portal/page/catalog [Accessed].

Ordnance Survey 2014. OS MasterMap Building Heights Layer [FileGeoDatabase geospatial data], Scale 1:2500. *EDINA Digimap Ordnance Survey Service*.

Parlow, E., Vogt, R. & Feigenwinter, C. 2014. The urban heat island of Basel–seen from different perspectives. *DIE ERDE–Journal of the Geographical Society of Berlin,* 145**,** 96-110.

Parry, M. 1987. The urban 'heat island'. *Proc 3rd Int Biometeorol Congress, Pau***,** 616-624.

Parton, G. a. W., Kate. 2015. *Met Office MIDAS Quick Start User Guide. Documentation* [Online]. Available: http://cedadocs.ceda.ac.uk/id/eprint/1437 [Accessed].

Pasquill, F. & Smith, F. B. 1983. *Atmospheric Diffusion Third Edition,* Chichester, Ellis Horwood Limited.

Patz, J. A., Campbell-Lendrum, D., Holloway, T. & Foley, J. A. 2005. Impact of regional climate change on human health. *Nature,* 438**,** 310-317.

Paulson, C. A. 1970. The mathematical representation of wind speed and temperature profiles in the unstable atmospheric surface layer. *Journal of Applied Meteorology,* 9**,** 857-861.

Peacock, J. 1983. Two-dimensional goodness-of-fit testing in astronomy. *Monthly Notices of the Royal Astronomical Society,* 202**,** 615-627.

Peng, S., Piao, S., Ciais, P., Friedlingstein, P., Ottle, C., BréOn, F. O.-M., Nan, H., Zhou, L. & Myneni, R. B. 2011. Surface urban heat island across 419 global big cities. *Environmental science & technology,* 46**,** 696-703.

Perry, E. M. & Moran, M. S. 1994. An evaluation of atmospheric corrections of radiometric surface temperatures for a semiarid rangeland watershed. *Water Resources Research,* 30**,** 1261-1269.

Petitcolin, F. & Vermote, E. 2002. Land surface reflectance, emissivity and temperature from MODIS middle and thermal infrared data. *Remote Sensing of Environment,* 83**,** 112-134.

Pfister, R. 2011. Gender effects in gaming research: a case for regression residuals? *Cyberpsychology, Behavior, and Social Networking,* 14**,** 603-606.

Pichierri, M., Bonafoni, S. & Biondi, R. 2012. Satellite air temperature estimation for monitoring the canopy layer heat island of Milan. *Remote Sensing of Environment,* 127**,** 130-138.

Pinker, R. 1990. Satellites and our understanding of the surface energy balance. *Global and Planetary Change,* 2**,** 321-342.

Poulos, G. S. & Burns, S. P. 2003. An evaluation of bulk Ri-based surface layer flux formulas for stable and very stable conditions with intermittent turbulence. *Journal of the atmospheric sciences,* 60**,** 2523-2537.

Prandtl, L. 1925. 7. Bericht über Untersuchungen zur ausgebildeten Turbulenz. *ZAMM-Journal of Applied Mathematics and Mechanics/Zeitschrift für Angewandte Mathematik und Mechanik,* 5**,** 136-139.

Prigent, C., Aires, F. & Rossow, W. B. 2003. Land surface skin temperatures from a combined analysis of microwave and infrared satellite observations for an all-weather evaluation of the differences between air and skin temperatures. *Journal of Geophysical Research: Atmospheres,* 108.

Rasul, A., Balzter, H. & Smith, C. 2016. Diurnal and Seasonal Variation of Surface Urban Cool and Heat Islands in the Semi-Arid City of Erbil, Iraq. *Climate,* 4.

Raupach, M., Thom, A. & Edwards, I. 1980. A wind-tunnel study of turbulent flow close to regularly arrayed rough surfaces. *Boundary-Layer Meteorology,* 18**,** 373-397.

Ren, C., Ng, E. Y. Y. & Katzschner, L. 2011. Urban climatic map studies: a review. *International journal of climatology,* 31**,** 2213-2233.

Richard, Y., Emery, J., Dudek, J., Pergaud, J., Chateau-Smith, C., Zito, S., Rega, M., Vairet, T., Castel, T. & Thévenin, T. 2018. How relevant are local climate zones and urban climate zones for urban climate research? Dijon (France) as a case study. *Urban climate,* 26**,** 258-274.

Rivard, B., Petroy, S. B. & Miller, J. R. 1993. Measured effects of desert varnish on the mid-infrared spectra of weathered rocks as an aid to TIMS imagery

interpretation. *IEEE Transactions on Geoscience and Remote Sensing,* 31**,** 284-291.

Rivera, E., Antonio-Nemiga, X., Origel-Gutierrez, G., Sarricolea, P. & Adame-Martinez, S. 2017. Spatiotemporal analysis of the atmospheric and surface urban heat islands of the Metropolitan Area of Toluca, Mexico. *Environmental Earth Sciences,* 76.

Rizwan, A. M., Dennis, L. Y. & Chunho, L. 2008. A review on the generation, determination and mitigation of Urban Heat Island. *Journal of Environmental Sciences,* 20**,** 120-128.

Roth, M., Oke, T. & Emery, W. 1989. Satellite-derived urban heat islands from three coastal cities and the utilization of such data in urban climatology. *International Journal of Remote Sensing,* 10**,** 1699-1720.

Runnalls, K. & Oke, T. 2000. Dynamics and controls of the near-surface heat island of Vancouver, British Columbia. *Physical Geography,* 21**,** 283-304.

Rutherford, A. 2001. *Introducing ANOVA and ANCOVA: a GLM approach*, Sage.

Schneider, A., Friedl, M. A. & Potere, D. 2009. A new map of global urban extent from MODIS satellite data. *Environmental research letters,* 4**,** 044003.

Schroeder, A. J., Basara, J. B. & Illston, B. G. 2010. Challenges associated with classifying urban meteorological stations: the Oklahoma City Micronet example. *The Open Atmospheric Science Journal,* 4.

Schwarz, N., Lautenbach, S. & Seppelt, R. 2011. Exploring indicators for quantifying surface urban heat islands of European cities with MODIS land surface temperatures. *Remote Sensing of Environment,* 115**,** 3175-3186.

Schwarz, N., Schlink, U., Franck, U. & Grossmann, K. 2012. Relationship of land surface and air temperatures and its implications for quantifying urban heat island indicators-An application for the city of Leipzig (Germany). *Ecological Indicators,* 18**,** 693-704.

Shao, Y., Molnar, L. F., Jung, Y., Kussmann, J., Ochsenfeld, C., Brown, S. T., Gilbert, A. T., Slipchenko, L. V., Levchenko, S. V. & O'neill, D. P. 2006. Advances in methods and algorithms in a modern quantum chemistry program package. *Physical Chemistry Chemical Physics,* 8**,** 3172-3191.

Sheng, Y., Liu, X., Yang, X., Xin, Q., Deng, C. & Li, X. 2017. Quantifying the spatial and temporal relationship between air and land surface temperatures of different land-cover types in Southeastern China. *International journal of remote sensing,* 38**,** 1114-1136.

Shiflett, S. A., Liang, L. L., Crum, S. M., Feyisa, G. L., Wang, J. & Jenerette, G. D. 2017. Variation in the urban vegetation, surface temperature, air temperature nexus. *Science of the Total Environment,* 579**,** 495-505.

Smith, C. L., Webb, A., Levermore, G., Lindley, S. & Beswick, K. 2011. Fine-scale spatial temperature patterns across a UK conurbation. *Climatic Change,* 109**,** 269-286.

Sohrabinia, M., Zawar-Reza, P. & Rack, W. 2015. Spatio-temporal analysis of the relationship between LST from MODIS and air temperature in New Zealand. *Theoretical and applied climatology,* 119**,** 567-583.

Song, B. & Park, K. 2019. Analysis of spatiotemporal urban temperature characteristics by urban spatial patterns in Changwon city, South Korea. *Sustainability,* 11**,** 3777.

Spruyt, V. 2014. How to draw a covariance error ellipse. April.

Stewart, I. D. 2011. A systematic review and scientific critique of methodology in modern urban heat island literature. *International Journal of Climatology,* 31**,** 200-217.

Stewart, I. D. & Oke, T. R. 2012. Local climate zones for urban temperature studies. *Bulletin of the American Meteorological Society,* 93**,** 1879-1900.

Stewart, I. D., Oke, T. R. & Krayenhoff, E. S. 2014. Evaluation of the 'local climate zone'scheme using temperature observations and model simulations. *International journal of climatology,* 34**,** 1062-1080.

Stone, B. & Rodgers, M. O. 2001. Urban form and thermal efficiency - How the design of cities influences the urban heat island effect. *Journal of the American Planning Association,* 67**,** 186-198.

Streutker, D. R. 2002. A remote sensing study of the urban heat island of Houston, Texas. *International Journal of Remote Sensing,* 23**,** 2595-2608.

Stull, R. B. 1988. Mean boundary layer characteristics. *An Introduction to Boundary Layer Meteorology*. Springer.

Stull, R. B. 2012. *An introduction to boundary layer meteorology*, Springer Science & Business Media.

Stull, R. B. & Ahrens, C. D. 1995. *Meteorology today for scientists and engineers*, West Pub.

Sun, H., Chen, Y. & Zhan, W. 2015. Comparing surface-and canopy-layer urban heat islands over Beijing using MODIS data. *International Journal of Remote Sensing,* 36**,** 5448-5465.

Sun, Y.-J., Wang, J.-F., Zhang, R.-H., Gillies, R., Xue, Y. & Bo, Y.-C. 2005. Air temperature retrieval from remote sensing data based on thermodynamics. *Theoretical and applied climatology,* 80**,** 37-48.

Tabachnick, B. G., Fidell, L. S. & Ullman, J. B. 2007. *Using multivariate statistics*, Pearson Boston, MA.

Taesler, R. 1980. *Studies of the development and thermal structure of the urban boundary layer in Uppsala*, Uppsala Universitetet.

Takahashi, M. 1959. RELATION BETWEEN THE AIR TEMPERATURE DISTRIBUTION AND TEH DENSITY OF HOUSES IN SMALL CITIES IN JAPAN. *Geographical Review of Japan,* 32**,** 305-313.

Taleghani, M. & Berardi, U. 2018. The effect of pavement characteristics on pedestrians' thermal comfort in Toronto. *Urban climate,* 24**,** 449-459.

Taskinen, A., Sirviö, H. & Vehviläinen, B. 2003. Interpolation of Daily Temperature in Finland: Paper presented at the Nordic Hydrological Conference (Røros, Norway, 4-7 August 2002). *Hydrology Research,* 34**,** 413-426.

Teegavarapu, R. S. & Chandramouli, V. 2005. Improved weighting methods, deterministic and stochastic data-driven models for estimation of missing precipitation records. *Journal of hydrology,* 312**,** 191-206.

Tomlinson, C., Chapman, L., Thornes, J. & Baker, C. 2012. Derivation of Birmingham's summer surface urban heat island from MODIS satellite images. *International Journal of Climatology,* 32**,** 214-224.

Tomlinson, C. J., Chapman, L., Thornes, J. E. & Baker, C. 2011a. Remote sensing land surface temperature for meteorology and climatology: a review. *Meteorological Applications,* 18**,** 296-306.

Tomlinson, C. J., Chapman, L., Thornes, J. E. & Baker, C. J. 2011b. Including the urban heat island in spatial heat health risk assessment strategies: a case study for Birmingham, UK. *International journal of health geographics,* 10**,** 42.

Turner, D. B. 1970. *Workbook of atmospheric dispersion estimates: an introduction to dispersion modeling*, CRC press.

Unger, J. 1996. Heat island intensity with different meteorological conditions in a medium-sized town: Szeged, Hungary. *Theoretical and Applied Climatology,* 54**,** 147-151.

Unger, J. 2004. Intra-urban relationship between surface geometry and urban heat island: review and new approach. *Climate research,* 27**,** 253-264.

Unger, J. 2009. Connection between urban heat island and sky view factor approximated by a software tool on a 3D urban database. *International Journal of Environment and Pollution,* 36**,** 59-80.

Unger, J., Bottyán, Z., Sümeghy, Z. & Gulyás, Á. 2004. Connection between urban heat island and surface parameters: measurements and modeling. *IDŐJÁRÁS/QUARTERLY JOURNAL OF THE HUNGARIAN METEOROLOGICAL SERVICE,* 108**,** 173-194.

United Nations, D. O. E. & Social Affairs, P. D. 2015. World population prospects: The 2015 revision. *key findings and advance tables. New York, USA*.

Van Hove, L., Jacobs, C., Heusinkveld, B., Elbers, J., Van Driel, B. & Holtslag, A. 2015. Temporal and spatial variability of urban heat island and thermal comfort within the Rotterdam agglomeration. *Building and Environment,* 83**,** 91-103.

Van Leeuwen, W. J., Huete, A. R. & Laing, T. W. 1999. MODIS vegetation index compositing approach: A prototype with AVHRR data. *Remote Sensing of Environment,* 69**,** 264-280.

Vancutsem, C., Ceccato, P., Dinku, T. & Connor, S. J. 2010. Evaluation of MODIS land surface temperature data to estimate air temperature in different ecosystems over Africa. *Remote Sensing of Environment,* 114**,** 449-465.

Voogt, J. A. & Oke, T. 1998. Effects of urban surface geometry on remotely-sensed surface temperature. *International Journal of Remote Sensing,* 19**,** 895-920.

Voogt, J. A. & Oke, T. R. 1997. Complete urban surface temperatures. *Journal of applied meteorology,* 36**,** 1117-1132.

Voogt, J. A. & Oke, T. R. 2003. Thermal remote sensing of urban climates. *Remote sensing of environment,* 86**,** 370-384.

Wan, Z. 2006. MODIS land surface temperature products users' guide. *Institute for Computational Earth System Science, University of California: Santa Barbara, CA, USA*.

Wan, Z. 2007. Collection-5 MODIS land surface temperature products users' guide. *ICESS, University of California, Santa Barbara*.

Wan, Z. 2008. New refinements and validation of the MODIS land-surface temperature/emissivity products. *Remote sensing of Environment,* 112**,** 59-74.

Wan, Z. & Dozier, J. 1989. Land-surface temperature measurement from space: Physical principles and inverse modeling. *IEEE Transactions on Geoscience and Remote Sensing,* 27**,** 268-278.

Wang, K., Liu, J., Zhou, X., Sparrow, M., Ma, M., Sun, Z. & Jiang, W. 2004. Validation of the MODIS global land surface albedo product using ground measurements in a semidesert region on the Tibetan Plateau. *Journal of Geophysical Research: Atmospheres,* 109.

Ward, K., Lauf, S., Kleinschmit, B. & Endlicher, W. 2016. Heat waves and urban heat islands in Europe: A review of relevant drivers. *Science of the Total Environment,* 569**,** 527-539.

Warren, E. L., Young, D. T., Chapman, L., Muller, C., Grimmond, C. & Cai, X.-M. 2016. The Birmingham Urban Climate Laboratory—A high density, urban meteorological dataset, from 2012–2014. *Scientific data,* 3**,** 1-8.

Wilby, R. L., Jones, P. D. & Lister, D. H. 2011. Decadal variations in the nocturnal heat island of London. *Weather,* 66**,** 59-64.

Wilmers, F. 1990. Effects of vegetation on urban climate and buildings. *Energy and buildings,* 15**,** 507-514.

Wilson, E. B. & Hilferty, M. M. 1931. The distribution of chi-square. *proceedings of the National Academy of Sciences of the United States of America,* 17**,** 684.

World Meteorological Organization 2007. WMO No.488 — Guide to the Global Observing System.

Wyngaard, J. C. 2010. *Turbulence in the Atmosphere*, Cambridge University Press.

Xu, Y. & Liu, Y. 2015. Monitoring the Near-surface Urban Heat Island in B eijing, C hina by Satellite Remote Sensing. *Geographical Research,* 53**,** 16-25.

Yang, X., Peng, L. L., Jiang, Z., Chen, Y., Yao, L., He, Y. & Xu, T. 2020. Impact of urban heat island on energy demand in buildings: Local climate zones in Nanjing. *Applied Energy,* 260**,** 114279.

Yao, R., Wang, L. C., Huang, X., Niu, Z. G., Liu, F. F. & Wang, Q. 2017. Temporal trends of surface urban heat islands and associated determinants in major Chinese cities. *Science of the Total Environment,* 609**,** 742-754.

Yuan, F. & Bauer, M. E. 2007. Comparison of impervious surface area and normalized difference vegetation index as indicators of surface urban heat island effects in Landsat imagery. *Remote Sensing of environment,* 106**,** 375-386.

Zhang, F., Cai, X. & Thornes, J. E. 2014. Birmingham's air and surface urban heat islands associated with Lamb weather types and cloudless anticyclonic conditions. *Progress in physical geography,* 38**,** 431-447.

Zhao, L., Lee, X., Smith, R. B. & Oleson, K. 2014. Strong contributions of local background climate to urban heat islands. *Nature,* 511**,** 216-219.

Zhou, B., Lauwaet, D., Hooyberghs, H., De Ridder, K., Kropp, J. P. & Rybski, D. 2016. Assessing seasonality in the surface urban heat island of London. *Journal of Applied Meteorology and Climatology,* 55**,** 493-505.

Zhou, B., Rybski, D. & Kropp, J. P. 2013. On the statistics of urban heat island intensity. *Geophysical research letters,* 40**,** 5486-5491.

Zhou, D., Zhao, S., Liu, S., Zhang, L. & Zhu, C. 2014. Surface urban heat island in China's 32 major cities: Spatial patterns and drivers. *Remote Sensing of Environment,* 152**,** 51-61.